Modeling of Manganese Removal from Groundwater by Filtration through Manganese Oxide Coated Media

A Thesis

by

Shakil Ahmed

MASTER OF SCIENCE IN CIVIL ENGNEERING (ENVIRONMENTAL)

Department of Civil Engineering

BANGLADESH UNIVERSITY OF ENGINEERING AND TECHNOLOGY

November, 2013

Modeling of Manganese Removal from Groundwater by Filtration through Manganese Oxide Coated Media

A Thesis

by

Shakil Ahmed

Submitted to the Department of Civil Engineering, Bangladesh University of Engineering and Technology (BUET), Dhaka in partial fulfillment of the requirements for the degree

of

MASTER OF SCIENCE IN CIVIL ENGNEERING (ENVIRONMENTAL)

November, 2013

Department of Civil Engineering

BANGLADESH UNIVERSITY OF ENGINEERING AND TECHNOLOGY

The thesis titled "Modeling of Manganese Removal from Groundwater by Filtration through Manganese Oxide Coated Media" submitted by Shakil Ahmed, Roll No.: 0411042113, Session: April, 2011 has been accepted as satisfactory in partial fulfillment of the requirement for the degree of Master of Science in Civil Engineering (Environmental) on 12th November, 2013.

BOARD OF EXAMINERS

1. _____
   Dr. M. Ashraf Ali — Chairman
   Professor — (Supervisor)
   Department of Civil Engineering, BUET

2. _____
   Dr. A.M.M.Taufiqul Anwar. — Member
   Professor and Head — (Ex-officio)
   Department of Civil Engineering, BUET

3. _____
   Dr. A.B.M. Badruzzaman — Member
   Professor — (Internal)
   Department of Civil Engineering, BUET

4. _____
   Dr. Md. Rezaul Karim — Member
   Professor — (External)
   Department of Civil and Environmental Engineering, IUT

DECLARATION

It is hereby declared that except for the contents where specific references have been made to the work of others, the studies contained in this thesis are the result of investigation carried out by the author. No part of this thesis has been submitted to any other University or other educational establishment for a Degree, Diploma or other qualification (except for publication).

_____

Shakil Ahmed

ACKNOWLEDGEMENT

First of all, I would like to express my heartiest gratitude to Almighty ALLAH for His graciousness and unlimited kindness, the blessings to Whom is always required for completion of any good work.

The author wishes to express his deepest gratitude to his supervisor Prof. Dr. M. Ashraf Ali, for his continuous guidance, invaluable constructive suggestions, encouragement, generous help and unfailing enthusiasm at every stage of this study.

The author also would like to thank Prof. Dr. A.M.M. Taufiqul Anwar. and Prof. Dr. A.B.M. Badruzzaman for their valuable comments, critical ideas and serving as members of examination committee. I am greatly indebted to Prof. Dr. Md. Rezaul Karim for kindly accepting to serve as External Examiner. His valuable advice, guidance and professional comments are highly appreciated.

I gratefully acknowledge Dr. John Little, whose idea was crucial to solve the model and write the model code in Statistical Software "R". I am also grateful to Mr. Kevin Bierlein for sharing his astute knowledge on numerical analysis and model development.

My special thanks to Mr. Ehosan Habib, whose continuous support and guidance assisted me to conduct laboratory experiments successfully. I would also like to thank Mr. Rashed Rakib and Ms. Baishakhi Bose for their helpful support in laboratory experiments.

I sincerely would like to thank all lab instructors and staffs of Environmental Engineering Laboratory in the Civil Engineering Department of BUET, Dhaka, which contributed in various ways to the completion of this thesis.

Finally, I would like to express my deepest gratitude to my parents and my wife whose support and love contributed in various ways for the completion of this research work.

Dedicated

to

my Family

ABSTRACT

High intake of manganese has shown to be toxic with adverse health impacts, and therefore, WHO (2004) recommended a health-based guideline value of 0.4 mg/l for drinking water. WHO **(**2011**)** eliminated the health-based guideline value noting that this value is well above the concentrations of Mn normally found in drinking-water. However, well water Mn concentration in many regions in Bangladesh exceeds 0.4 mg/l. Bangladesh, therefore, needs a low cost and efficient water treatment technology to remove Mn from groundwater. Adsorption of soluble manganese onto manganese oxide coated sand is one of the effective treatment methods for removal of Mn from drinking water. This research work focused on understanding the mechanism of Mn removal from water during filtration through Mn oxide coated media, and developing a model to simulate adsorption and surface oxidation of Mn during filtration.

Laboratory column experiments were carried out to assess the Mn removal by Mn-oxide coated filter media (commercially available green sand) under various water quality (e.g., different pH, initial Mn, Dissolved Oxygen, Bicarbonate) and system (e.g., flow rate) conditions. Experimental results suggest that in the absence of Bicarbonate in the influent water, the removal of Mn is characterized by only adsorption, and the system gradually approaches the breakthrough point since the adsorption sites on the media are exhausted with increasing filter run time. In the absence of Bicarbonate, effluent Mn concentration increased gradually from 13% to nearly 71% of influent Mn concentration (10.2 mg/l) during filter run time of up to 350 minutes. However, in the presence of Bicarbonate (200 mg/l) in the influent water, Mn removal efficiency of Mn-oxide coated media was found to increase significantly and the system did not approach the breakthrough point; effluent Mn concentration stabilizes at nearly 38% of influent Mn concentration. Results of laboratory column experiments suggest that the dominant mechanism for the removal of Mn(II) is continuous regeneration of Mn-oxide coated media, caused by the surface mediated oxidation of adsorbed Mn by DO in the presence of Bicarbonate, rather than $MnCO_3(s)$ precipitation. Results of multi-port column experiments also support the concept of regeneration of Mn-oxide coated media. Results of multi-port column experiments provided useful insights on the effects of flow rate, initial Mn concentration and pH on the removal of Mn within the filter media. Mn removal has been found to increase with decreasing flow rate (due to higher contact time), with increase in initial Mn concentration of the influent water (due to increase in linear driving force), and with increase in pH value of influent water (which promotes Mn oxidation). Under the experimental conditions, maximum removal efficiency of 98% was found for an initial Mn concentration of 4.2 mg/l at flow rate of 1 ml/min.cm^2.

A model developed by Zuravnsky (2006) was modified to predict the soluble Mn removal via adsorption and surface oxidation onto Mn-oxide coated media under continuous media regeneration by DO. A number of model parameters were estimated from laboratory batch

experiments and from empirical formulations. The model was calibrated (to find out the value of oxidation rate constant, k_r by curve fitting) using experimental data under various operating conditions (flow rate of 1-3 ml/min.cm^2, initial Mn concentration of 1.15-4.83 mg/l, and pH of 6-8 of influent water), and subsequently used to predict soluble Mn removal. The model was able to predict Mn removal reasonably well. The sensitivity analysis suggests that flow rate, Freundlich isotherm constants (K, n) and k_r have a significant effect on the model predicted bulk-water Mn concentration profile, while the effects of axial dispersion coefficient (D_L), mass transfer coefficient (k_f) and specific surface area of media (A_v) are not significant.

TABLE OF CONTENTS

LIST OF TABLES

LIST OF FIGURES

LIST OF ABBREVIATIONS

OCM	Oxide-coated media
IR	Intermittent regeneration
CR	Continuous regeneration
DO	Dissolved oxygen
TOC	Total organic carbon
F.M.	Fineness Modulus
AAS	Atomic Adsorption Spectrophotometer
WOC	Water-oxidizing complex
LDF	Linear driving force
HLR	Hydraulic loading rate
AWWA	American Water Works Association
DPHE	Department of Public Health Engineering
BGS	British Geological Survey
WHO	World Health Organization
PSII	Photosystem II

CHAPTER 1: INTRODUCTION

1.1 Background

Manganese is a mineral that is abundantly found in nature and a common water contaminant. A number of studies (BGS and DPHE, 2001; Hug et al., 2011) showed that apart from As, large numbers of wells exceed permissible limits for Fe and Mn in Bangladesh. The National Hydro-geochemical Survey (BGS and DPHE, 2001) found that half of the 3,534 wells surveyed in Bangladesh exceeded the drinking water standard (based on aesthetic concerns) for Fe (1 mg/l), and three quarters exceeded the standard for Mn (0.1 mg/l). High intakes of manganese through both inhalational exposures and drinking water have been shown to be toxic (Institute of Medicine Food and Nutrition Board, 2002). For Manganese having such adverse health impacts, WHO (2004) recommends a guideline value of 0.4 mg/l to protect against neurological damage and, WHO **(**2011**)** eliminated the health-based guideline value noting that "this health-based value is well above concentrations of Mn normally found in drinking-water". However, this logic is not valid for Bangladesh, since, about 40% of wells sampled in the BGS-DPHE survey in Bangladesh exceeded the WHO (2004) recommended health based guideline value of 0.4 mg/l for Mn. BGS and DPHE (2001) reveals that the people of central, north and south-east regions of Bangladesh is exposed to great health risk for presence of high concentration of Mn (>0.4 mg/l) in groundwater in this regions. According to BGS and DPHE (2001), nationwide about 32% of wells, which contain safe level of arsenic (i.e., < 0.05 mg/l) have been found to contain unsafe level of manganese (i.e., >0.4 mg/l). Therefore, this would significantly increase the population exposed to unsafe water, beyond that estimated for arsenic alone. Detection of high concentrations of manganese in groundwater has introduced a new dimension to the already difficult safe water supply scenario in Bangladesh. However, manganese issue has attracted relatively less attention so far in the water supply sector in Bangladesh. Due to widespread presence of manganese in groundwater in addition to arsenic and iron, it is important to raise awareness among the stakeholders about the manganese issue and develop Mn removal technologies from water.

One of the effective treatment methods available for removal of soluble Mn from drinking water is the adsorption of soluble manganese onto manganese oxide coated sand (e.g., green sand). Green sand is a purple-black granular filter medium processed from glauconite sand which is naturally or synthetically coated with a thin layer of manganese dioxide, MnO_2. This coating of manganese oxide adsorbs soluble manganese from water and, in the presence of an oxidant, these adsorbed Mn(II) are oxidized to solid Mn(IV) to create more available sites (Merkle et al., 1997). Currently, there is no other treatment alternative available that can remove soluble Mn with the high efficiency as Mn oxide coated sand (Zuravnsky, 2006; Subramaniam, 2010).

Oxide-coated media (OCM) perform a dual function in the Mn removal process, permitting two modes of operation for soluble Mn^{2+} removal (Merkle et al., 1997b). In the intermittent regeneration (IR) mode, the filter media bed absorbs Mn^{2+} in the absence of a strong oxidant. Sorption capacity is periodically regenerated by application of oxidant (e.g., chlorine, potassium permanganate). In the continuous regeneration (CR) mode, oxidant is continuously supplied to oxidize the adsorbed Mn^{2+} to insoluble MnOx(s) on the coated media surface, continuously regenerating sorption capacity and catalytic function. There are a number of parameters that affect the manganese removal performance of oxide coated media (OCM). Researchers have noted the significance of the type of oxidant applied, the pH of water applied to the bed, and the capacity of the media as related to the available surface sites on the oxide coating (Merkle et al., 1997b; Zuravnsky, 2006; Subramaniam, 2010).

Previous research developed analytical solutions for steady-state process operation for both intermittent and continuous regeneration modes. Merkle et al. (1997b) developed model for both intermittent and continuous regeneration modes to create an overall reaction for manganese adsorption and surface oxidation. Based on the Mass transfer and oxidation principles used to develop the previous dynamic model of Merkle *et al.* (1997b), a simplified CR model was developed by Zuravnsky (2006) (and later used by Subramaniam, 2010; Bierlein, 2012) on steady state and high flow conditions under continuous media regeneration via free chlorine addition.

The studies on Mn removal by Mn-oxide coated media discussed above have been performed with using strong oxidizing agent (e.g., $KMnO_4$, HOCl) to regenerate the coating by oxidizing the adsorbed Mn. However, recent study (ITN-BUET,2011) shows that formation of Mn-oxide coating (indicating the oxidation of adsorbed Mn) is possible while passing Mn containing groundwater through Sylhet sand (with and without acid wash) without addition of any oxidizing agent from external source (experimental pH value up to 8.3). At maturation (i.e., 100% removal of Mn within the filter media), the sand grains in different columns contained different quantity of Mn (up to 1384 mg Mn/kg sand). ITN-BUET (2011) also reported that a breakthrough point could not be found while removing Mn from groundwater (without involving any external oxidizing agent) by filtration through commercially available green sand; indicating possible regeneration of Mn oxide coating. This is a contradiction of the result found by Knocke et al. (1991), which showed no regeneration of active sites without the presence of any externally applied oxidant. The possible reason for regeneration of media in ITN-BUET (2011) study could be the role of certain parameters (possibly dissolved oxygen, DO, and bicarbonate) in groundwater that might promote oxidation of the Mn and therefore, regenerates the Mn-oxide coating. However, previous study (Morgan and Stumm, 1964, Weber, 1972) revealed that a solution pH of above 9.5 (which is much higher than the experiment conducted by ITN-BUET, 2011) is required to oxidize the soluble Mn by DO or air. Hence, to oxidize the Mn by DO in natural ground water pH (nearly 7), it is required to decrease the oxidation potential of Mn. Bicarbonate in natural groundwater

(which was around 265.5 mg/l in the study of ITN-BUET, 2011) could potentially reduce the oxidation potential of Mn and enable DO to oxidize Mn in near-neutral pH range. However, this potential mechanism of Mn oxidation needs to be investigated.

1.2 Objectives of the Present Research

The main objective of this study is to develop better understanding of the Mn removal mechanism from ground water during filtration through Mn oxide coated media, and develop a model to simulate adsorption and surface oxidation of Mn during filtration. The specific research objectives are stated below:

1) Conduct laboratory experiments to understand the key mechanisms (e.g., oxidation and adsorption) involved in Mn removal by Mn-coated filter media.
2) Conduct laboratory experiments to determine the isotherm constants for Mn adsorption onto Mn oxide coated media.
3) Develop a mathematical model (based on analyzed removal mechanism) to predict soluble Mn removal profiles across oxide-coated media bed**.**
4) Conduct laboratory experiments to generate data on Mn concentrations at different depths of filter media under various operational conditions (flow rate, initial Mn concentration and pH); and use the data for model calibration.
5) Perform sensitivity analysis, using the model, to identify the controlling factors in the removal process.

The proposed research work is expected to improve understanding of Mn removal mechanisms from ground water through filtration by Mn-oxide coated media. Based on the concept of the removal mechanism, a mathematical model is expected to be developed to predict Mn removal profile, which could eventually be used in the design of community scale treatment system.

1.3 Outline of Methodology

To achieve all the mentioned objectives, the following tasks were undertaken:

1) For evaluating the mechanism of Mn removal in Mn-oxide coated filter media, influent water of varying composition (with respect to Mn and other water parameters) were passed through a green sand (commercially available) filter column (made by glass burette) maintaining a specific flow rate and the effluent water was collected and analyzed for residual Mn. Influent water was prepared by deionized water containing 0.01 M KCl. Column experiments were carried out to assess the effects of dissolved oxygen (DO), initial Mn concentration and bicarbonate on the removal of Mn in green sand filter column. Primarily three types of influent water containing Mn (II) were passed through the filter column:

(a) influent water containing 0.01 M KCl (electrolyte), varying Mn concentration, and varying DO (dissolved oxygen);
(b) influent water containing 0.01 M KCl (electrolyte), varying Mn concentration; and
(c) influent water containing 0.01 M KCl (electrolyte), varying Mn concentration, and varying bicarbonate concentration.

2) Based on the removal mechanism revealed from analysis of the experimental results discussed above, an effort was made to modify a model (primarily developed by Zuravnsky, 2006) to predict Mn removal in green sand filter column. The "multi-port column" experiments have been carried out to evaluate the effects of different parameters (flow rate, initial Mn concentration, pH) on Mn removal, and to generate data for calibration and validation of the model. The contactor column consists of an acrylic glass column with x-sectional area of 26.4 cm^2, and total height of about 40 cm, fitted with sampling ports (for collection of pore-water) at 2, 4, 6 and 8 inches depth from the top of the 8 inches depth of green sand media contained in the multi-port column. Groundwater, collected from a deep tube well pump station at BUET with Manganese concentration of around 0.022 mg/L, was spiked with Manganese (II) stock solution to prepare influent water with different concentrations of Mn. In all experiments, pore-water water samples were collected from the multi-port column at depths of 2, 4, 6 and 8 inches from the top (through the sampling ports) of green sand filter media at filter run times of 90, 120 and 150 minutes. Various combinations of experimental conditions and water quality parameters were applied to study the effect of flow rate, initial Mn concentration, pH:
   a) In order to assess the effect of flow rate (or contact time) on Mn removal, the flow rate of the influent water through the multi-port filter column was varied from 1.0 to 4.0 ml/min.cm^2 while other parameters were kept unchanged.
   b) The effect of initial Mn concentration on Mn removal was assessed by varying initial Mn concentration from 1.15 mg/l to 11.2 mg/l in influent water, while keeping the flow rate fixed at 2 ml/min.cm^2.
   c) In order to analyze the effect of pH of influent water on Mn removal, column experiments similar to those described above were conducted where pH of the influent water was fixed at 6.0, 7.0, and 8.0(by adding dilute nitric acid or sodium hydroxide to water), keeping the flow rate fixed at 2 ml/min.cm^2.
3) Batch experiments were conducted to estimate the isotherm constants for describing adsorption of Mn on green sand. Several airtight containers containing groundwater with different initial Mn concentrations were prepared; to each container a different mass of Mn oxide coated sand were added. The suspension was then rotated and allowed to equilibrate; after filtering, Mn content of water was measured. The results were used to determine isotherm constants.

The developed model equations were solved for soluble Mn and oxidant concentrations using numerical analysis and assuming an initial value of oxidation rate constant (k_r). The solutions were then coded into Statistical Software R (Version 2.15.2).

4) The model data were then fitted with experimental data of Mn concentration at different filter column depths to determine k_r. A simple sensitivity analysis of the model with respect to various operational parameters was performed to identify the controlling factors in the removal process.

1.4 Organization of the Thesis

Apart from this chapter, the remainder of the thesis has been divided into five chapters. Chapter 2 presents an overview of manganese chemistry in water, water quality problems associated with presence of Mn in water including health effects, and common methods and techniques for removal of manganese from water. This chapter presents a detail discussion on previous research works conducted on removal of soluble manganese by adsorption onto manganese oxide coated media, and modeling efforts for describing Mn removal by adsorption and oxidation. The results of previous studies were analyzed to identify the needs for further experimental and modeling works for enhancement of knowledge in this area.

Chapter 3 describes the experimental setup and analytical methods used to carry out the laboratory experiments. It provides description on the experimental setup of the laboratory column experiments carried out to evaluate the removal of Mn from water during filtration through a green sand column, under different conditions (e.g., with respect to DO, pH, bicarbonate). It also describes the multi-port column design and experimental methods to generate data on dissolved Mn concentration at different depths in the green sand column during filtration; this data have been used to calibrate the mathematical model to predict Mn concentration profile. Finally, the Chapter describes the isotherm experiments conducted to determine Mn uptake capacity of green sand media, and analytical methods used for measurement of different parameters.

Chapter 4 demonstrates the experimental results obtained from various tests of Mn removal during filtration through Mn-oxide coated sand (green sand). In the first part of this chapter, results of the column experiments have been presented based on which removal mechanism of Mn in Mn-oxide coated filter media have been discussed. Results of multi-port column experiments presented in this Chapter show effects of various water quality and operational parameters on removal of Mn, and provides useful insight into the removal mechanism of Mn in Mn-oxide coated filter media.

Chapter 5 describes the model developed in this study for describing removal of Mn in Mn-oxide coated filter media, based on the removal mechanism identified in chapter 4. The validation and application of the model to predict soluble Mn removal profile via adsorption and oxidation onto Mn-oxide coated media has been discussed. The first part of this Chapter presents the model, which has been developed by modifying the model developed by

Zuravnsky (2006), and discusses the numerical solution of the model with required model input parameter estimation. In later part, the modified model was used to simulate Mn removal in a Mn-oxide coated column with various input parameters determined from appropriate correlations and experiments conducted under different conditions. This Chapter also presents model calibration, model predictions and sensitivity analysis under different conditions to assess the applicability of the developed model.

Finally, Chapter 6 presents major conclusions of the study and provides recommendations for future direction of study.

CHAPTER 2: LITERATURE REVIEW

2.1 Introduction

The main objective of this study was to develop better understanding of the Mn removal mechanism from water during filtration through Mn oxide coated media, and develop a model to simulate adsorption and surface oxidation of Mn during filtration. This Chapter presents an overview of manganese chemistry in water, water quality problems associated with presence of Mn in water including health effects, and common methods and techniques for removal of manganese from water. This chapter presents a detail discussion on previous research works conducted on removal of soluble manganese by adsorption onto manganese oxide coated media, and modeling efforts for describing Mn removal by adsorption and oxidation. The results of previous studies were analyzed to identify the needs for further experimental and modeling works for enhancement of knowledge in this area.

2.2 Manganese Chemistry

Manganese is a mineral that is abundantly found in nature and occurs in rocks and soil, and is normal constituent of the human diet. It is a transition metal which has numerous oxidation states between 0 and +7. The most commonly encountered states are Mn(II), Mn(III), Mn(IV), and Mn(VII). The reduced Mn (II) is generally found as the soluble Mn^{2+} cation. The highly oxidized Mn(VII) is widely known as permanganate and found in the form of the soluble MnO^{4-} anion. The insoluble oxides of manganese are formed from Mn(III) and Mn(IV) and are often found as MnOOH(s) and MnO_2(s), respectively. Mixed oxides also exist in the form of MnOx, where x varies from 1.1 to 1.8 (Morgan and Stumm, 1964). Manganese is distributed mainly in manganese oxides of which pyrolusite (MnO_2) is the most common. Manganese also occurs as an impurity in iron oxides, some silicates and carbonates. It occurs more rarely as a major constituent of rhodocrosite ($MnCO_3$). The structure and compositions of manganese oxides is complex due to variable oxidation states and to their ion-exchange properties. These properties are important in soils and aquifers as they can play a significant role in trace-metal adsorption. In sediments, manganese oxides also typically occur as fine-grained and poorly-crystalline forms which are easily dissolved under favorable conditions.

The principal controls on manganese concentration in groundwater are pH (acidity) and redox (oxidation-reduction) condition. Calculation of the solubilities and stabilities of the ion to oxidation can be used to create an Eh-pH diagram for the Mn-O_2-H_2O system (Bricker, 1965) which reveals that manganese is stable under reducing conditions up to pH 10. Increasing the pH under reducing conditions produces hydroxides of Mn.

Eh-pH diagram for the Mn-O_2-H_2O system indicates that solubility of Mn is lowered in water which is well oxygenated. As the system becomes more oxidizing, the aqueous Mn(II) is converted directly to various solid manganese forms, Mn_3O_4 (Hausmannite), Mn_2O_3 (manganite or Feitknechtite) and MnO_2. Birnessite and feitknechtite are the most commonly found solid forms (Murray et. al., 1985).The direct conversion of Mn(II) to solid oxide forms in water apparently does not occur without the presence of hydroxide (Hem, 1981; Coughlin and Matsui 976). In fact the rate of oxidation depends on the oxygen concentration and the square of the hydroxide concentration, suggesting that although the oxides are stable versus dissolution at moderate pH, the creation of the oxides proceeds through a manganese hydroxide intermediate form. Manganese removal is catalyzed by solids, including Mn oxides (autocatalysis) (Coughlin and Matsui, 1976; Kessick and Morgan, 1975); the presence of small amounts of solid through sludge recycling or due to turbidity may increase the rate of Mn oxidation.

In pH-neutral conditions, the mobility of manganese is determined by ambient redox conditions. Under aerobic conditions typical of many shallow aquifers and surface waters, manganese is stable in its oxidized form, $Mn(IV)O_2$ which is highly insoluble. Hence, concentrations of manganese in aerobic water are usually low and commonly below analytical detection limits. Under anaerobic conditions, manganese is reduced to the more soluble form, Mn (II), which is released from minerals. Mn^{2+} is the soluble form in most waters. As a result, much higher manganese concentrations can be found in anaerobic groundwater. As dissolved oxygen concentrations in groundwater tend to decrease with well depth, anaerobic conditions and hence high manganese concentrations tend to occur more commonly in deep wells. Under strongly reducing conditions in the presence of dissolved sulphide, manganese can be immobilized by the formation of insoluble manganese sulphide (MnS), although this is usually only important at high pH (>8). As anaerobic conditions occur commonly in aquifers, problems with iron and manganese in groundwater are relatively widespread, though the concentrations attained vary widely (USEPA, 2004).

As groundwater infiltrate through soils and aquifers, their compositions typically evolve from aerobic to anaerobic, the rates of change depending on the rates of diffusion of oxygen and other oxidants in the system. Reduction reactions in aquifers and soils follow a sequence as the conditions become progressively more reducing. Typically the first compound to be removed from the system is oxygen, followed by nitrate and thereafter manganese. Progressively more reducing conditions lead to reduction of iron followed by sulphate.

Manganese is dissolved in anoxic and acid water. Homogeneous precipitation of Mn(II) as an oxide phase does not occur below pH 8, but Mn(II) oxidation does occur in the presence of different mineral surface and /or via bacterial process between pH 6 and 8. it is also known that bacterial mediated oxidation of dissolved manganese (Davidson et. al., 1989).

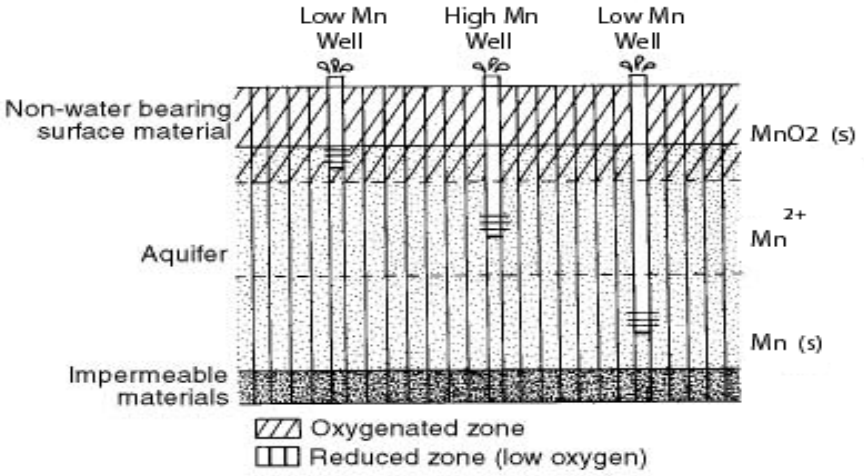

Figure 2.1: Dissolve manganese concentration with variation in depth of well (Source: Seelig et al., 1992).

Manganese problems are most likely to develop in water from wells with high carbonate and low oxygen. Problems occur when this type of water is pumped to the surface. The chemical equilibrium is changed upon exposure to the atmosphere. The end result is precipitation of manganese compounds in plumbing, on fixtures, and on clothing, dishes and utensils. As shown in Figure 2.1, the amount of manganese dissolved in water often follows a trend of low to high back to low again as depth of the well increase (Seelig et. al., 1992).

The mobilization of manganese is increased in organic-rich waters through complexation with organic acids (humic or fulvic acids). Such conditions occur for example in peaty soil waters and upland lakes associated with them. They also occur in some strongly reducing aquifers. Waters with high concentrations of organic acids typically have a brown coloration (not caused by particulate matter) and may develop a surface froth.

Some forms of bacteria gain energy by oxidation of soluble Mn in water and can produce notable surface slimes where concentrations of manganese are high. Bacteria can accelerate the oxidation process and may also exacerbate staining problems.

2.3 Water Quality Problems Related to Manganese

In Bangladesh, Manganese is a common natural contaminant of groundwater. A number of studies **(**BGS and DPHE, 2001**;** Hug et. al., 2011**)** showed that apart from arsenic (As), large numbers of wells exceed permissible limits for iron (Fe) and manganese (Mn) in Bangladesh. This is true for shallow tube wells, and also to some extent for deep tube wells and ring-wells, which are common water supply options in As-affected areas. The National Hydro-geochemical Survey (BGS and DPHE, 2001) found that half of the 3,534 wells surveyed in 61 out of 64 districts exceeded the Bangladesh drinking water standard (1 mg/l) for iron (Fe), and three quarters exceeded the permissible limit (0.1 mg/l) for manganese (Mn). Both of these limits are based on aesthetic concerns; above these levels, people may be unwilling to

drink the water, and turn instead to a better-tasting, but microbiologically less safe water sources. Some of the reported Fe and Mn concentrations (BGS and DPHE, 2001) are very high, over ten times the permissible limit. Iron and manganese concentrations as high as 25 mg/l and 10 mg/l, respectively have been reported. Average Fe concentration in the surveyed wells has been reported to be 3 mg/l (median 1 mg/l) and average Mn concentration 0.5 mg/l (median 0.3 mg/l) (BGS and WaterAid, 2001).

High concentrations are found in most areas, but particular high-manganese areas are seen in the current Brahmaputra and Ganges floodplains. The distribution generally does not correspond with that of arsenic. This means that groundwater with acceptable concentrations of arsenic may not have acceptable concentrations of manganese. It is notable that groundwater from the deep aquifer (>150 m) contain relatively low concentrations of both arsenic and manganese.

Figure 2.2 represents manganese concentration in groundwater of Bangladesh measured between <0.002 mg/l and 10 mg/l (BGS and DPHE, 2001). Medians of the concentrations in the shallow and deep aquifers were 0.34 mg/L and 0.03 mg/L respectively. This highlights the large difference in concentrations between the shallow and deep aquifers. This figure indicates that the central, north and south-east regions of Bangladesh have higher concentrations of manganese.

Figure 2.3 shows distribution of Mn in well water of Bangladesh, based water quality data obtained from the National Hydro-chemical Survey (BGS and DPHE, 2001). It shows that about 27% of the surveyed tube wells have manganese concentrations within the Bangladesh drinking water standard of 0.1 mg/L. About 32% of groundwater samples have manganese concentration between 0.1 and 0.4 mg/L, and about 25% have concentration between 0.4 and 1.0 mg/L. About 17% of samples have manganese concentration exceeding 1.0 mg/L; only 10 samples have concentration exceeding 5 mg/L.

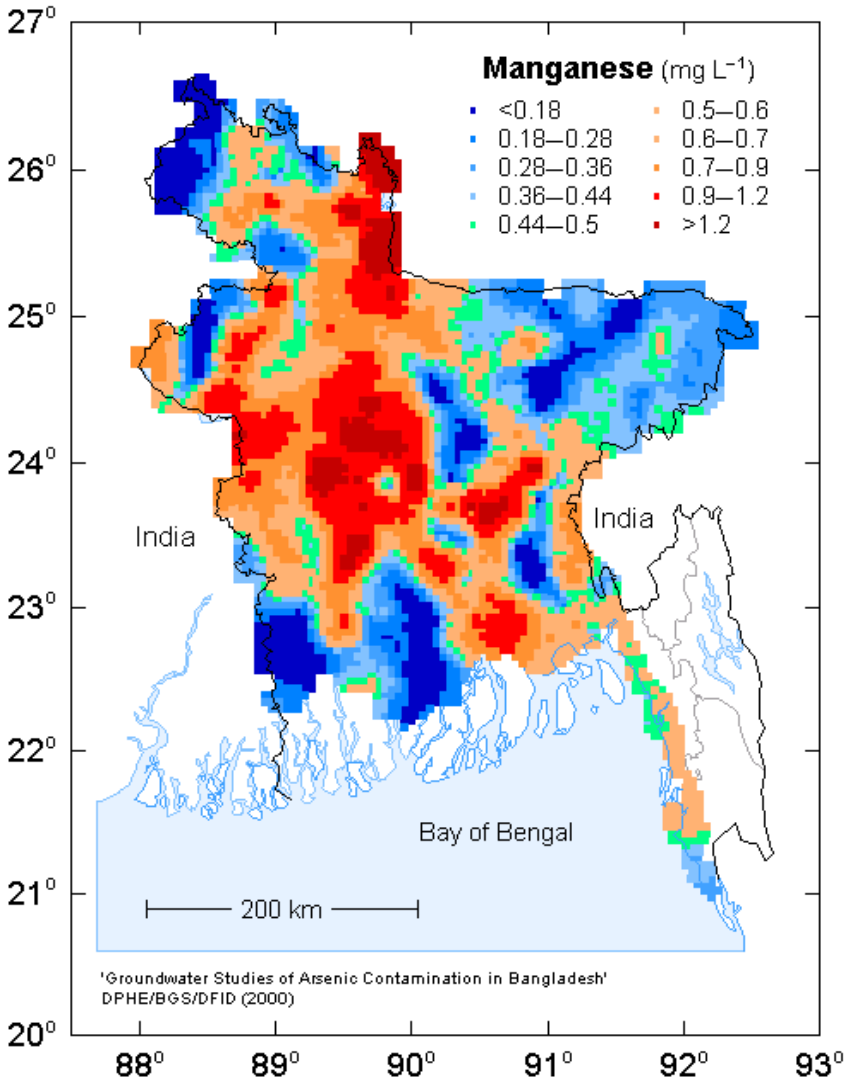

Figure 2.2: Distribution of manganese in groundwater of Bangladesh (Source: BGS and DPHE, 2001)

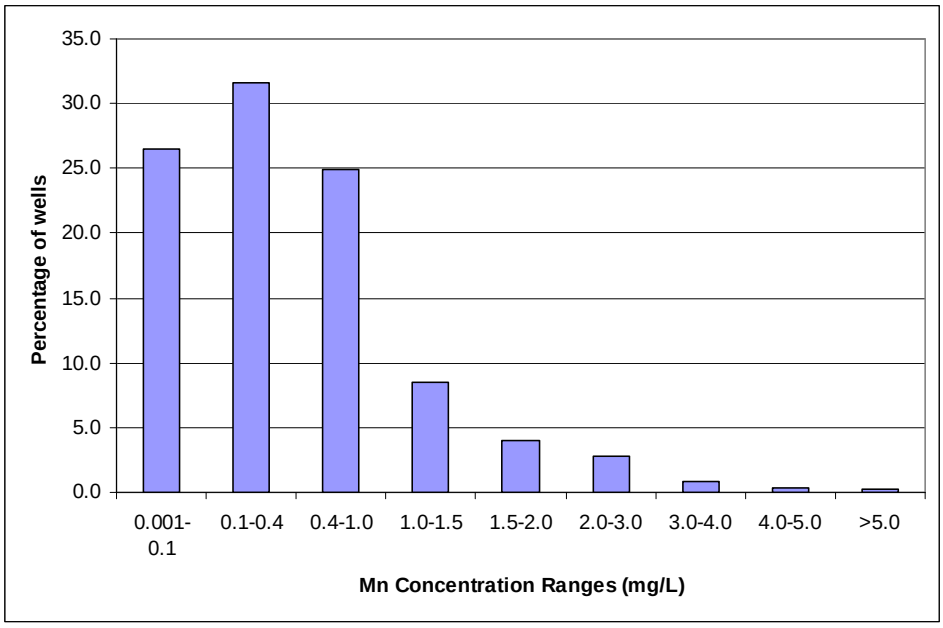

Figure 2.3: Wells with different ranges of manganese concentrations (Source: Hasan and Ali, 2010)

Water with a high concentration of manganese may cause the staining of plumbing fixtures or laundry. Manganese solids may form deposits within pipes and break off as black particles that give water an unpleasant appearance and taste. High intakes of manganese through both inhalational exposures and drinking water have been shown to be toxic (Institute of Medicine Food and Nutrition Board, 2002). Manganese is best characterized as a neurotoxin; occupational exposures are associated with a characteristic syndrome called manganism, which involves both psychiatric symptoms and Parkinsonian features (Yamada et. al. 1986; Calne et. al., 1994; Dobson et. al., 2004). For Manganese having such adverse health impacts, WHO (2004) recommends a guideline value of 0.4 mg/l to protect against neurological damage and, WHO **(**2011**)** eliminated the health-based guideline value noting that "this health-based value is well above concentrations of Mn normally found in drinking-water". However, this logic is not valid for Bangladesh, since, about 40% of wells sampled in the BGS-DPHE survey in Bangladesh exceeded the WHO (2004) recommended health based guideline value of 0.4 mg/l for Mn. As shown in Figure 2.2, the people of central, north and south-east regions of Bangladesh is exposed to great health risk for presence of high concentration of Mn (>0.4 mg/l) in groundwater in this regions. According to BGS and DPHE (2001), nationwide about 32% of wells, which contain safe level of arsenic (i.e., < 0.05 mg/l) have been found to contain unsafe level of manganese (i.e., >0.4 mg/l). Therefore, this would significantly increase the population exposed to unsafe water, beyond that estimated for arsenic alone. Detection of high concentrations of manganese in groundwater has introduced a new dimension to the already difficult safe water supply scenario in Bangladesh. However, manganese issue has attracted relatively less attention so far in the

water supply sector in Bangladesh. Due to widespread presence of manganese in groundwater in addition to arsenic and iron, it is important to raise awareness among the stakeholders about the manganese issue and develop Mn removal technologies from water.

2.4 Common Treatment Options for Removal of Mn from Water

There are a number of removal technologies used to remove manganese from water. The most common removal technologies are chemical oxidation, sequestration, and adsorption. Adsorption using oxide coated media is discussed in more detail in the following section.

The soluble manganese can be removed by the physical process of aeration. Burns (1998) had investigated source reduction of manganese levels by using bubble aerators to mix deep water reservoirs and reduce the effect of thermal stratification. Both groundwater and surface water can be aerated using various techniques during treatment. However, the rate of reaction between manganese and oxygen is slow and a retention tank with several hours of detention time is recommended to allow adequate conversion (Wong, 1984). Alkaline pH (> 9.0) is generally required to oxidize the soluble manganese in this way within the duration of water treatment (Morgan and Stumm, 1964). Filtration is then applied for the removal of the solid manganese oxide particles. Aeration is not often used for large plants or water high levels of manganese. The slow reaction time and capital cost involved in construction of large retention basins do not promote widespread usage.

Manganese removal has been accomplished by the addition of various types of chemical oxidants, including free chlorine, chlorine dioxide, potassium permanganate and ozone. Knocke et al. (1987) revealed that alkaline conditions (pH > 8) are required for adequate manganese removal by chlorine addition. Low temperatures (< 5°C) were also shown to hinder the process. Since traditional coagulation-flocculation treatment benefits from acidic pH conditions, the only use of chlorine as an oxidant for manganese removal is not recommended. Chlorine is the oxidant preferred to enhance removal via oxide coated media by regenerating the media while oxidizing the soluble Mn.

Knocke et. al. (1987) used chlorine dioxide (ClO_2) for removal of Mn from water. The theoretical stoichiometric amount of chlorine dioxide needed for manganese oxidation is 2.45 mg/mg Mn^{2+}. Laboratory testing showed that twice the theoretical amount could be required for effective soluble manganese removal (Knocke et al., 1987). The concentration of organic material in the water significantly affects the dosage of chlorine dioxide required. At low total organic carbon (TOC) concentrations (< 2.5 mg/L), chlorine dioxide dose between 1.0–1.5 mg/L was effective across a large range of pH values. However, water with higher organic demands (8-10 mg/L TOC) required doses of over 3 mg/L of ClO_2 for similar removal. Due to health concerns of chlorite and chlorate presence in drinking water, most regulatory agencies do not permit dosage of chlorine dioxide outside the range of 0.5-2.0 mg/L. Hence, chlorine dioxide is an effective oxidant for manganese removal but should be

used in conjunction with another oxidant when high concentrations of organic material and/or high initial soluble manganese levels are present.

Soluble manganese oxidation has been performed conventionally by Potassium permanganate ($KMnO_4$). Also affected by organic concentrations, the permanganate dosage increases to much higher than the theoretical stoichiometric amount when the TOC levels increase above 3 mg/L (Knocke et al., 1987). The chemical cost per unit of potassium permanganate is higher than the cost per unit required for oxidation by free chlorine (Knocke et al., 1987).

A strong and rapid-acting oxidant Ozone (O_3) has become a widely accepted disinfectant in water treatment since it do not produce disinfection by-products, except when bromide is present in the water. Reckhow et al. (1991) conducted a study to determine the stoichiometry and kinetic rates of the oxidation reaction between ozone and manganese under both low and moderate organic concentration conditions. The study found that the reaction rate increased with increasing pH; further, at a pH of 8.0 the required dose was practically equal to the theoretical stoichiometry. However, with the addition of organics, between 2-5 times the stoichiometric dose was required to oxidize the manganese. Bicarbonate was added to minimize the formation of unproductive radicals and hence, reduce the dose of ozone required. Therefore, Ozone use is more often recommended for oxidizing manganese in water with low organic concentration.

Most of the removal methods discussed above chemically or physically oxidize manganese to its solid form. These oxide particles are then required to be physical removed. This is often accomplished by traditional treatment methods consisting of coagulation, flocculation, clarification, and filtration to remove the oxides along with other water impurities. However, oxidized manganese often forms particles in the colloidal range which are not efficiently removed when applied directly to filtration media (Knocke et al., 1988). Therefore, research on membrane filtration as a viable method for removing oxidized manganese particulate has also been conducted (Suzuki et al., 1998; Rahman et al., 2000).

Sequestration of manganese is another limited used method of controlling manganese oxidation. The addition of polyphosphates or a combination of sodium silicate and chlorine has been shown to sequester the inorganic with various degrees of success. However, limited research has been found in developing this treatment method (Trace Inorganic Substances Committee, 1987).

2.5 Adsorption and Oxidation of Mn onto Filter Media

There are a number of technologies available to remove manganese from water such as aeration, chemical oxidation, sequestration, and adsorption. The focus of this research is the adsorption of soluble manganese onto manganese oxide coated sand (green sand). Green sand is a purple-black granular filter medium processed from glauconite sand which is

naturally or synthetically coated with a thin layer of manganese dioxide, MnO_2. This coating of manganese oxide adsorbs soluble manganese from water and, in the presence of an oxidant, these adsorbed Mn(II) are then oxidized to solid Mn(IV) to create more available sites (Merkle et al., 1997). Various oxidizing agents can be used to change the oxidation state of Mn so that it can be removed from water. Table 2.1 shows the Mn oxidation reactions for oxidants typically used in drinking water treatment, listing ideal or theoretical stoichiometric ratio of oxidant to Mn for each reaction.

Table 2.1: Theoretical reaction stoichiometry for manganese (II)

Oxidant	Reaction	Stoichiometric ratio, mg oxidant : mg Mn metal
O_2	$Mn^{2+} + ½\ O_2 + H_2O \Rightarrow MnO_2(s) + 2H^+$	0.29 : 1
HOCl	$Mn^{2+} + HOCl + H_2O \Rightarrow MnO_2(s) + Cl^- + 3H^+$	1.30 : 1
MnO_4	$3Mn^{2+} + 2\ KMnO_4 + 2H_2O \Rightarrow 5\ MnO_2(s) + 2K^+ + 4H^+$	1.92 : 1
O_3(aq.)	$Mn^{2+} + O_3 + H_2O \Rightarrow MnO_2(s) + O_2 + 2H^+$	0.88 : 1
ClO_2	$Mn^{2+} + 2ClO_2 + 2H_2O \Rightarrow MnO_2(s) + 2ClO_2^- + 4H^+$	2.45 : 1

Source: Adapted from Sommerfeld (1999)

The technology of manganese removal through sorption and oxidation on manganese greensand has been applied for decades, primarily in treating groundwater with elevated soluble manganese levels. Manganese oxide coatings formed on media acts as good adsorbents for Mn and also play a role in its oxidation by autocatalysis (Kessick and Morgan, 1975; Eley et. al., 1993; AWWA, 1994; Merkle, et. al., 1997b; Zuravnsky, 2006; Subramaniam, 2010; Tasneem, 2010). Oxide-coated media (OCM) perform a dual function in the Mn removal process, permitting two modes of operation for soluble Mn^{2+} removal (Merkle et al., 1997b). In the intermittent regeneration (IR) mode, the filter media bed absorbs Mn^{2+} in the absence of a strong oxidant. Sorption capacity is periodically regenerated by application of oxidant (e.g., chlorine, potassium permanganate). In the continuous regeneration (CR) mode, oxidant is continuously supplied to oxidize the sorbed Mn^{2+} to insoluble MnOx(s) on the coated media surface, continuously regenerating sorption capacity and catalytic function. There are a number of parameters that affect the manganese removal performance of oxide coated media (OCM). Researchers have noted the significance of the type of oxidant applied, the pH of water applied to the bed, and the capacity of the media as related to the available surface sites on the oxide coating.

Knocke et al. (1988) analyzed the use of four different oxidants to promote manganese removal across the OCM filter bed. Oxidants were applied to the water prior to passage through the filter bed. Strong oxidants such as permanganate, chlorine dioxide, and ozone oxidized the soluble manganese almost immediately in the bulk solution. On the other hand,

the addition of free chlorine prior to the filtration through OCM filter bed did not oxidize the manganese in the bulk solution. Instead, the majority of the manganese reaching the filter bed was in the soluble form. In this case, the removal mechanism was determined to be direct sorption of soluble manganese onto the media surface. The chlorine residual provided the necessary oxidant to regenerate the active adsorbent sites on the media. The capacity of the media in combination with the regenerative properties of the free chlorine caused the necessary manganese removal at both low and high loading rate conditions. The results indicated that the presence of free chlorine at a concentration of >1-2 mg/L was sufficient for rapid soluble manganese removal (Knocke et al., 1988). The study revealed that continuous removal of manganese can occur with the application of free chlorine, while without free chlorine, the capacity of the media is eventually exhausted. Zuravnsky (2006) found a free chlorine concentration of greater than 1.0 mg/L was required for effective soluble Mn removal; furthermore, increased free chlorine concentrations generally improved the soluble Mn removal profile.

Knocke et al. (1991) used shallow bed depths (5-6 in) and high influent manganese concentrations (1.0 mg/L) to promote rapid exhaustion of the available sorption sites to evaluate the effects of the absence of chlorine on manganese removal. There was no evidence of auto oxidation found and no active sites were being regenerated without the presence of an oxidant. The media was found to start being exhausted (breakthrough point) after passing of 25 liter water without the presence of HOCl at pH = 7.8

A number of studies have shown significant effects related to the pH of the applied water on oxide-coated filter media performance (Knocke *et al.,* 1988; Knocke *et al.,* 1990; Zuravnsky, 2006). In the absence of free chlorine, the effect of pH on the media capacity was observed and, the detrimental effects of acidic pH on the media manganese adsorption capacity and the benefits of alkaline conditions for effective removal have been found. A slightly alkaline bulk solution pH (7.0-8.0) provided a greater percentage of soluble Mn removal across the contactor depth than a mildly acidic pH (6.3-6.7) (Zuravnsky, 2006).

Research has been conducted to find the relationship between removal efficiency and the amount of extractable manganese oxide present on the media (Bouchard, 2005). The capacity of the media to remove manganese was found to increase as the extractable manganese oxide amount increased. In research, the correlation between extractable coating and manganese adsorption capacity has been evaluated more directly by Bouchard (2005). A 4-hour capacity test was developed to determine the manganese absorptive capacity of the media. This test was used to evaluate media capacity as related to bed depth in an active surface water treatment plant. The capacity results were also compared to the amount of extracted manganese oxide. The plot of absorptive capacity versus extractable manganese indicates that uptake capacity increases with increasing MnOx coating until approximately 12 mg coating per gm of media. Beyond this point the capacity does not seem to increase with an

increase in extractable coating, suggesting that layering of MnOx coatings covers previously available adsorption sites, making them inaccessible.

The result of this study agrees with the kinetic studies conducted by Morgan and Stumm (1964), where different kinetic rates of manganese adsorption were found between colloidal and flocculated manganese dioxide particles. The colloidal suspensions were found to react more rapidly than the flocculated suspensions. It was suggested that the reaction between soluble manganese and manganese dioxide is a surface related phenomena and the colloidal sites were more available, allowing for a faster reaction (Morgan and Stumm, 1964). Together, these findings indicate a sorption reaction that is surface related.

Since the process of adsorption and oxidation adds layers of manganese oxide to the filter media grains, research was conducted to determine the effect of oxide coatings on the physical properties of the media. No significant changes in the physical size or density of the media (Knocke *et al.*, 1990) were found, and therefore, no significant changes in the hydraulic properties in the media bed should be expected.

Zuravnsky (2006) investigated the effect of initial soluble Mn concentrations on the removal efficiency of OCM. Increasing the initial soluble Mn concentration was found to have a slightly positive effect on the soluble Mn removal profile. This is because an increased soluble Mn concentration in solution provides a slightly larger driving force between the bulk solution concentration and concentration at the surface of the media. The accumulation of manganese oxide coating is often found to be concentrated in the upper portions of the filter bed. This phenomenon has been observed in both operating utilities (Bouchard, 2005; ITN-BUET, 2011) and pilot-scale experiments (Hargette and Knocke, 2001).

The studies on Mn removal by Mn-oxide coated media discussed above have been performed with using strong oxidizing agent (e.g., $KMnO_4$, HOCl) to regenerate the coating by oxidizing the adsorbed Mn. However, recent study (ITN-BUET,2011) shows that formation of Mn-oxide coating (indicating the oxidation of adsorbed Mn) is possible while passing Mn containing groundwater through Sylhet sand (with and without acid wash) without addition of any oxidizing agent from external source. The research was conducted using groundwater with initial Mn concentration of 0.5-5.0 mg/L with no effort to adjust the pH of the influent water (which was found to increase during the test from nearly 7 up to 8.3). At maturation (i.e., 100% removal of Mn within the filter media), the sand grains in different columns contained different quantity of Mn. Figure 2.4 shows retention of total Mn by the sand filter media as a function of bed volume (volume of water passed divided by the volume of the sand filter media) of water passed through the media for different initial Mn concentrations. The average quantity of Mn retained by sand expressed as mg Mn/g sand varies from about 149 mg Mn/kg sand (for the column with initial Mn = 0.5 mg/L) to 1384 mg Mn/kg sand (for the column with initial Mn = 5.0 mg/L).

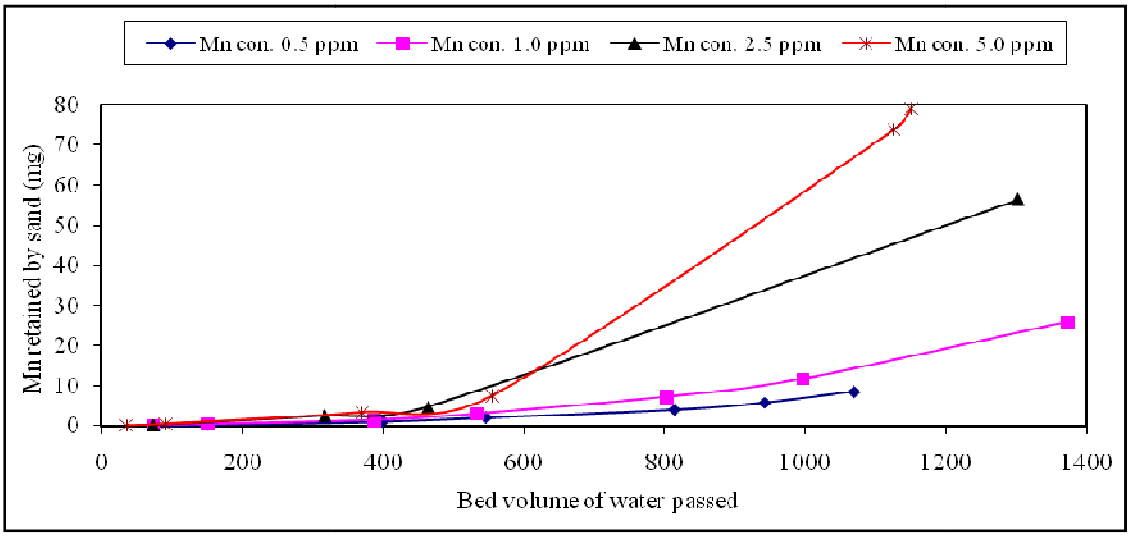

Figure 2.4: Amount of Manganese retained by sand in each column up to maturation as a function of bed volume of water passed (ITN-BUET, 2011)

ITN-BUET (2011) also reported that a breakthrough point could not be found while removing Mn from groundwater (having initial Mn concentration of 0.5-5.0 mg/l, pH range of 7-8.3 and without involving any external oxidizing agent) by filtration through green sand; indicating possible regeneration of Mn oxide coating. The amount of water passed during this study was more than 50 L. This is a contradiction of the result found by Knocke et al. (1991), as discussed earlier in this section, which showed no regeneration of active sites without the presence of any externally applied oxidant. The possible reason for regeneration of media in ITN-BUET (2011) study could be the role of certain parameters (possibly dissolved oxygen, DO) in groundwater that might promote oxidation of the Mn and therefore, regenerates the Mn-oxide coating. However, previous study (Morgan and Stumm, 1964, Weber, 1972) revealed that a solution pH of above 9.5 (alkaline condition) is required to oxidize the soluble Mn by DO or air. Hence, to oxidize the Mn by DO in natural ground water pH (nearly 7), it is required to decrease the oxidation potential of Mn. The findings of the studies by Kozlov et. al. (2004) and Tang et. al. (2009) suggest that Mn(II) oxidation is favored in the presence of Bicarbonate in water. Tang et.al. (2009) investigated the effect of Bicarbonate on the binding and oxidation of divalent Manganese in bacterial reaction centers, and revealed that Bicarbonate is able to facilitate the binding and oxidation of the Manganese (II) ion between pH 6 and 8 in center where the tight binding in their absence could not otherwise be established. Kozlov et. al. (2004) studied oxidation potentials of Mn(II) in aqueous solutions of Bicarbonate and found that Bicarbonate stimulates the electron transfer from Mn(II) to Mn-depleted water-oxidizing complex of photosystem II (apo-WOC-PSII). Therefore, Bicarbonate in natural groundwater (which was around 265.5 mg/l in the study of ITN-BUET, 2011) could potentially reduce the oxidation potential of Mn and enable DO to

oxidize Mn in near-neutral pH range. However, this potential mechanism of Mn oxidation needs to be investigated.

2.6 Modeling of Adsorption and Oxidation of Mn on Filter Media

The primary phenomena of Mn removal by oxide coated sand have been identified as Mn^{2+} sorption and surface oxidation (Zapffe, 1933; Edwards and McCall, 1946; Griffin, 1960; Cleasby, 1975; Knocke et al., 1988). Previous research developed analytical solutions for steady-state process operation for both intermittent and continuous regeneration modes. Coffey (1993) modeled the steady-state cases for Mn sorption and oxidation by free chlorine at the oxide surface after the method of Nakanishi (1967)

$$Mn^{+2} + MnO(OH)_2(s) = MnO_2MnO(s) + 2\ H^+ \qquad \text{(reversible sorption)} \qquad (2.1)$$

$$MnO_2MnO(s) + HOCl = 2\ MnO_2(s) + H^+ + Cl^- \qquad \text{(oxidation)} \qquad (2.2)$$

An implicit assumption in Equation 2.1 and 2.2 is the regeneration of one surface site as $MnO(OH)_2(s)$ and incorporation of MnO_2 into the oxide phase. The overall reaction described by Coffey (1993) is

$$Mn^{+2} + MnO(OH)_2(s) + HOCl + H_2O = MnO_2(s) + MnO(OH)_2(s) + 3H^+ + Cl^- \qquad (2.3)$$

Merkle et. al. (1997b) developed model for both intermittent and continuous regeneration modes. The model was based on a simplified version of Equation 2.3 to create an overall reaction for manganese adsorption and surface oxidation. Since a detailed knowledge of the sorption site structure and Mn^{2+} oxidation product stoichiometry was lacking, a simplified form of Equation 2.3 was used as shown in Equation 2.4

$$Mn^{+2} + SITE + HOCl = MnO_x(s) + SITE \qquad (2.4)$$

This reaction states that the bulk-water soluble manganese first adsorbs to a site, and then it is oxidized to replace and regenerate the previous oxide site. The reacting species of Equation 2.4 are assumed to be located in the immediate region of the oxide surface. This assumes that the total number of sites is independent of any oxide accumulation, an assumption that may not be valid over extended periods of filter operation. Any near-surface pH change (and local changes in pH dependent site density that affect catalysis rates), due to Mn^{2+} sorption and oxidation reactions along with incorporation of other inorganic species, are neglected.

The intermittent regeneration (IR) mode is a special case of the model with no oxidant present, in which the media bed performs as a filter-absorber unit. For IR mode, a linear driving force (LDF) approximation was used to predict the sorption process. However, LDF did not agree with desorption data and consistently over-predicted the effluent soluble manganese concentration. The continuous regeneration (CR) model was developed as an

adaptation of the intermittent model by including the surface oxidation reaction. The oxidation was assumed to be limited to the surface of the media because the oxidant ($HOCl/OCl^-$) is not considered to diffuse past the surface to interior sites. It is assumed that the reactants reach the surface sites by turbulent and molecular diffusion, but once there, they do not equally participate in surface diffusion to interior Mn^{2+} sorption sites. Once an oxidant molecule encounters a surface site, it is most likely to encounter a sorbed Mn^{2+} and react. However, the sorbed Mn^{2+} is free to surface diffusion into the interior of the coating to sorption sites kinetically inaccessible to the oxidant, for which intrapore transport is relatively hindered (Merkle et. al., 1997b).

The calibration parameter used in both models was referred to as the kinetically available fraction of sorption capacity (AFR). The value determined for AFR was related to the sites available through surface diffusion. The continuous regeneration model included another fitted parameter, the mass transport coefficient (k_f) of Mn from the bulk fluid to the particle surface. The model predictions were valid under conditions generally found in water treatment. The model did not agree with the data when subjected to high flows at low manganese adsorption capacity.

Based on the Mass transfer and oxidation principles used to develop the dynamic model of Merkle *et al.* (1997b), a simplified CR model was developed by Zuravnsky (2006) on steady state and high flow conditions under continuous media regeneration via free chlorine addition. The model was simplified version of the previous model since the concept of unavailable adsorption sites developed by Merkle et. al. (1997b) was not included in this model. In the later part of this thesis, the steady state equations those were used in this model and derivation of these equations have been discussed in detail.

2.7 Summary

Among several Mn removal technologies, adsorption and oxidation of Mn on filter media has been found very effective. Several studies have been performed to investigate the simultaneous adsorptive removal of Mn and regeneration of the Mn oxide coating onto filter media by using strong oxidizing agent. However, recent study reveals that the naturally present DO and other constituents (e.g., bicarbonate) in water could promote removal of Mn in a filter media (by sorption and oxidation) without the addition of an oxidant. This phenomenon needs to be investigated in more detail, through laboratory experiments. A model needs to be developed incorporating this possible mechanism that needs to be calibrated and validated with experimental results.

CHAPTER 3: EXPERIMENTAL METHODS AND MATERIALS

3.1 Introduction

The main objective of this study was to develop better understanding of the Mn removal mechanism during filtration through Mn oxide coated media through laboratory study and model development. This chapter describes the experimental setup and analytical methods used to carry out the laboratory experiments. It describes (Section 3.2) the experimental setup of the laboratory column experiments carried out to evaluate the removal of Mn from water during filtration through a green sand column, under different conditions (e.g., with respect to DO, pH, bicarbonate). It also describes the multi-port column design and experimental methods aimed at measuring the dissolved Mn concentration at different depths in the green sand column during filtration (Section 3.3). The results from the contractor column experiments have been used to calibrate the model developed to simulate Mn removal in the sand column. Finally, the Chapter describes the isotherm experiments conducted to determine Mn uptake capacity of commercially available green sand media (Section 3.4), and analytical methods used for measurement of different parameters.

3.2 Column Experiments

For evaluating the mechanism of Mn removal in Mn coated filter media, influent water of varying composition (with respect to Mn and other water parameters) were passed through a green sand (commercially available) filter column maintaining a specific flow rate and the effluent water was collected and analyzed for residual Mn. Filter beds were prepared with green sand using glass burette (50 ml) with a cross sectional area of 1 cm^2. The Fineness Modulus (F.M.) and unit weight of the green sand used as filter media were determined as 4.6 and 2.33 g/cm^3(measured from apparent specific gravity), respectively. Fractional pore volume (porosity) of green sand was measured as 0.44. The initial average Mn-content of the green sand was determined (by ITN-BUET, 2011) after selectively leaching Mn from the sand media using hydroxylamine hydrochloride, following the method reported in Eley and Nicholson (1993), and was found to be about 14,400 mg Mn/kg green sand. Total depth of filter media in the filter column was 50 cm, consisting of top 48 cm green sand and bottom 2 cm gravel (to avoid clogging of burette outlet by finer particle).

The experimental set up consisted of a bucket and an acrylic glass column (x-sectional area of 26.4 cm^2 and depth 45 cm) for holding raw water, green sand filter beds in glass burette, a dosing pump (Type: CNPA0705PVT209/A01, ProMinent, Germany), collector buckets and flow control (manual valve) arrangements (see Figure 3.1). Raw influent water was first stored in a bucket and thereafter, it was pumped from the bucket to the acrylic glass column. A constant head of the influent water had to be maintained in the acrylic glass column (to maintain a fixed effluent flow rate) which was accomplished by providing an outlet point near the top (8 cm from top) of the acrylic glass column to flow out the excess influent water

back to the raw water bucket. Influent water in acrylic glass column was allowed to flow by a pipe (1.12 cm outer diameter) through the green sand column in glass burette with a constant flow rate. Effluent water was then collected in a collector bucket. It should be noted that the surface of the influent water stored in the bucket and acrylic glass column was in contact with atmosphere during experiment.

Column experiments were carried out to assess the effects of dissolved oxygen (DO), initial Mn concentration and bicarbonate on the removal of Mn in green sand filter column. Primarily three types of influent water containing Mn (II) were passed through the filter column:

(a) influent water containing 0.01 M KCl (electrolyte), varying Mn concentration, and varying DO (dissolved oxygen);
(b) influent water containing 0.01 M KCl (electrolyte), varying Mn concentration; and
(c) influent water containing 0.01 M KCl (electrolyte), varying Mn concentration, and varying bicarbonate concentration.

For column experiments deionized water containing 0.01 M KCl was prepared, which was spiked with Mn(II) and Bicarbonate stock solutions to attain desired concentrations of Mn and bicarbonate concentration. Mn(II) stock solution was prepared by dissolving manganese salt $MnCl_2.4H_2O$ in distilled water; while Bicarbonate stock solution was being prepared using sodium bicarbonate ($NaHCO_3$). Addition of bicarbonate increased pH of influent water above 8.0 which was adjusted to about 7.0 by adding dilute nitric acid. Influent Mn(II) concentration was varied from 7.21 mg/l to 10.24 mg/l; while bicarbonate concentration was varied from about 200 mg/l to 443 mg/l.

To assess the effect of dissolved DO, at first, efforts were made to remove DO from natural groundwater by passing argon gas through water contained in a gallon and covered with flexible polymer film to avoid contact with air. It was possible to reduce DO level to about 0.2 mg/l (with continuous passage of nitrogen/argon). However, during passage of argon, the pH of groundwater increased significantly up to about 10.0 (due to continued loss of carbon-di-oxide). At the high pH, Mn(II) was oxidized to Mn(IV) and precipitated out of the bulk solution. Effort to control pH by addition of dilute nitric acid was not successful. Subsequently, experiments to assess the effect of DO was carried out using influent water prepared from deionized water containing 0.01 M KCl and desired concentration of Mn. Argon gas was passed through this solution to drive off DO, and with continuous passage of argon, a DO level of about 2.0 mg/l could be maintained throughout the column experiment; the DO level could not be reduced below this value under the experimental conditions used in this study.

Influent water was passed through the prepared green sand column, and surface overflow rate or flow rate (ml/min divided by x-area) was kept fixed at approximately 6 ml/min.cm^2. pH was found to increase with filter run time for the influent water containing bicarbonate. Hence, pH was adjusted (nearly 7) by applying dilute nitric acid to the raw influent water (when required during the test); however, it did not decrease the applied bicarbonate concentration significantly (up to 5%). Effluent water sample was collected to determine Mn concentration; DO and pH of influent water were measured at different filter run times (up to 350 minutes). New green sand media was used for each individual column experiment.

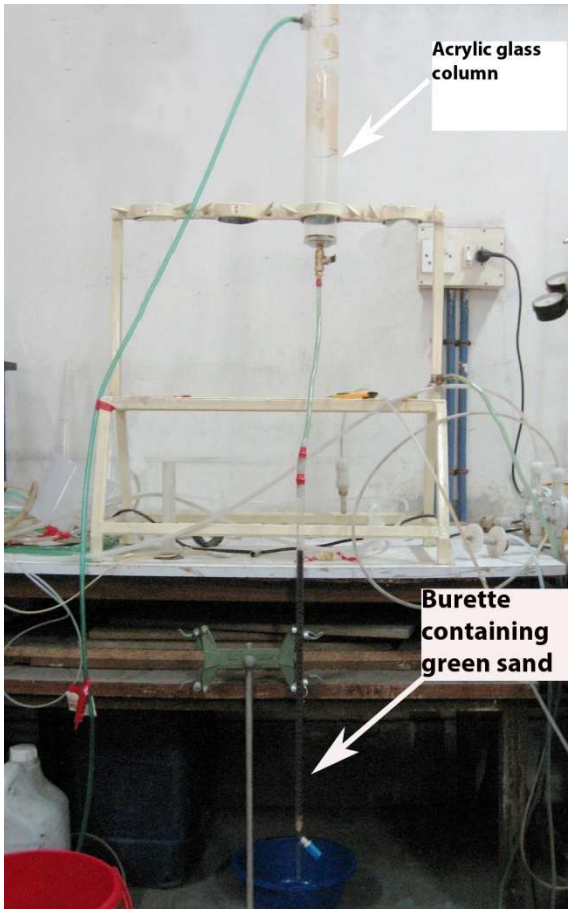

Figure 3.1: Experimental set up for Mn removal mechanism study

3.3 Multi-port Column Experiments

As a part of this research, a mathematical model has been developed (see Section 5.2.1) to predict Mn removal in green sand filter column. The model predicts concentration of Mn in bulkwater (i.e., pore water) along the depth of the filter column. The "multi-port column" experiments have been carried out to evaluate the effects of different parameters (flow rate, initial Mn concentration, pH) on Mn removal, and to generate data for calibration and validation of the model. The multi-port column consists of an acrylic glass column with x-sectional area of 26.4 cm^2, and total height of about 40 cm; with containing 8 inches of depth

of green sand media.The multi-port column was fitted with sampling ports (for collection of pore-water) at 2, 4, 6 and 8 inches depth from the top of the of green sand media (shown in Figure 3.2). The unit weight, F.M., porosity, and initial Mn content of the green sand were 2.33 g/cm^3 (measured from apparent specific gravity), 4.60, 0.44, and 14,400 mg Mn/kg, respectively. The experimental set ups consisted of green sand filter beds in the multi-port column (shown in Figure 3.2), flow control arrangements, a pump and collector buckets.

Groundwater, collected from a deep tube well pump station at BUET with Manganese concentration of around 0.022 mg/L, was spiked with Manganese (II) stock solution to prepare influent water with different concentrations of Mn. Table 3.1 provides a detailed characterization of ground water used in all of the multi-port column experiments.

Table 3.1: Detailed characterization of ground water used in laboratory experiments

Parameter	Unit	Concentration
pH	--	7±0.1
Alkalinity as $CaCO_3$	mg/L	254±5 mg/l
DO	mg/L	7.5±0.1 at 28^0 C
Chloride	mg/L	55
Iron	mg/L	0.01
Manganese	mg/L	0.022
Arsenic	µg/L	<1

In order to assess the effect of flow rate (or contact time) on Mn removal, the flow rate of the influent water through the multi-port filter column was varied from 1.0 to 4.0 ml/min.cm^2 (i.e., 26.4 to 105.6 ml/min), while other parameters were kept unchanged. Initial pH of influent water was close to the pH of natural groundwater (7±0.1) and was found to vary slightly (7.2±0.1) with the filter run time (up to 150 minutes); no effort was made to adjust the pH.

The effect of initial Mn concentration on Mn removal was assessed by varying initial Mn concentration from 1.15 mg/l to 11.2 mg/l in influent water, while keeping the flow rate fixed at 2 ml/min.cm^2. The concentrations of Mn in the influent water were set considering Mn concentration in well water in Bangladesh (BGS and DPHE, 2001). As before, initial pH of influent water was close to 7± 0.1, which changed slightly (7.2±0.1) with the filter run time (up to 150 minutes); no effort was made to adjust the pH.

In order to analyze the effect of pH of influent water on Mn removal, column experiments similar to those described above were conducted where pH of the influent water was fixed at 6.0, 7.0, and 8.0 (by adding dilute nitric acid or sodium hydroxide to water), keeping the flow rate fixed at 2 ml/min.cm^2. The pH values for influent water were set at the neutral range (6 to 8) considering the pH value of natural groundwater in Bangladesh. The pH of influent water was found to vary slightly (6.0±0.2, 7.2±0.1 and 8.0±0.1 for influent water with initial pH of 7.0, 6.0 and 8.0, respectively) with the filter run time (up to 150 minutes); no effort

was made to adjust the pH during filter run. In all experiments, pore-water samples were collected from the multi-port column at depths of 2, 4, 6 and 8 inches from the top (through the sampling ports) of green sand filter media at filter run times of 90, 120 and 150 minutes.

It should be noted that the effect of the presence of other ions (e.g., Fe, As) was not considered in this study, because in typical treatment systems, Fe and As are removed prior to filtration of water by aeration followed by precipitation and often roughing filtration.

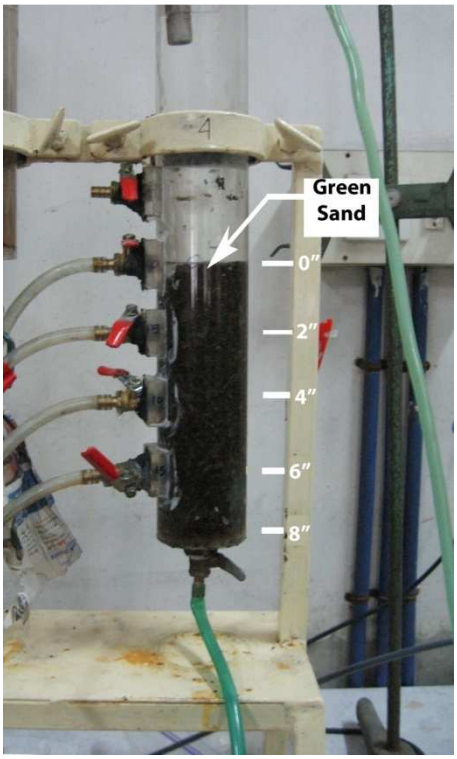

Figure 3.2: Multi-port column for model calibration

3.4 Isotherm Experiments

Batch experiments were conducted to estimate the isotherm constants for describing adsorption of Mn on green sand. Freundlich isotherm constants (K, n) and Langmuir Isotherm constant (Q, b) were calculated using data from batch experiments in which Mn uptake of green sand at pH of 7.2±0.1 and temperature of 28^{o}C was measured. Several airtight containers (50 ml) containing groundwater with different initial Mn concentrations (3.40-12.9 mg/L) were prepared; to each container a different masses (0.4-1.0 gm) of green sand were added. The suspensions were then continuously rotated (up to 52 hours) using a tilted rotator (shown in Figure 3.3), allowed to equilibrate and filtered with normal filter paper (0.80 μm). For each set of experiment, three tests were conducted with equilibrations time of 48, 50 and 52 hours, and thereafter, concentrations of Mn in the filtrate were measured. The uptake capacity (q) is calculated as shown in Equation 3.1. The results (data tabulated in Appendix B) were used to determine Freundlich isotherm constants and

Langmuir Isotherm constants for green sand media. The equation for a linear trend line fitted to this plot is analogous to the linearized form of the Freundlich isotherm equation (Equation 3.2), which allows the values of K and n to be determined. Freundlich Isotherm constants were verified by plotting the isotherm relationship along with the experimental data. Similarly, Langmuir Isotherm constants were determined using the linear form of equation as shown in Equation 3.3. It should be noted that theisotherm constants determined by batch experiment could be slightly different than that exist in column experiment since the linear driving force (caused by the difference between the adsorbate concentration in the bulk solution and the concentration at the external surface of media) gets reduced with treatment time in batch experiment, while it remains fixed in column experiment.

$$q = \frac{V\,(Ci - Cf)}{M} \tag{3.1}$$

$$\ln(q) = \ln(K) + (1/n)\ln(C_f) \tag{3.2}$$

where:

C_i = Initial soluble Mn concentration (mg/L)
C_f = Final soluble Mn concentration (mg/L)
M = Mass of media (green sand) in column (gm)
q = Mn uptake capacity of media (mg Mn/gm media)
V = Volume of solution in reservoir (L)

$$\frac{C_f}{q} = \frac{1}{bQ} + \frac{C_f}{Q} \tag{3.3}$$

Where:

Q = maximum number of Mn adsorbed/adsorbent mass when surface sites are saturated
b = empirical constant

Figure 3.3: Tilted rotator used for batch experiment to determine Mn uptake capacity of green sand media.

3.5 Reagents and Analytical Methods

All chemicals used in this research work are of reagent grade. Mn(II) and bicarbonate stock solution was prepared by dissolving manganese salt $MnCl_2.4H_2O$ and sodium bicarbonate ($NaHCO_3$) in deionized water, respectively.

The pH of water samples was measured using a pH meter (3400i, WTW 82362 Weilheim, Germany). DO was measured using a DO meter (Multiline P4, WTW 82362 Weilheim, Germany).

Samples collected for soluble Mn concentration determination were acidified with the addition of 0.1% concentrated nitric acid for sample preservation. Manganese concentrations were measured using an Atomic Adsorption Spectrophotometer (Shimadzu, AA-6800; Flame-AAS). All other water quality parameters were measured following the Standard Methods (AWWA, APHA).

CHAPTER 4: EXPERIMENTAL RESULTS AND DISCUSSIONS

4.1 Introduction

The main objective of this study was to develop better understanding of the Mn removal mechanism during filtration through Mn oxide coated media through laboratory study and model development. This chapter presents the experimental results obtained from various tests of Mn removal during filtration through Mn-oxide coated sand (green sand). In the first part (Section 4.2) of this chapter, results of the column experiments have been presented based on which removal mechanism of Mn in Mn-oxide coated filter media have been discussed. Results of multi-port column experiments presented in this Chapter (Section 4.3) show effects of various water quality and operational parameters on removal of Mn, and provides useful insight into the removal mechanism of Mn in Mn-oxide coated filter media.

4.2 Results of Column Experiments

Several studies (Merkle et al., 1997; Zuravnsky, 2006; Subramaniam, 2010; Bierlein, 2012) have been performed on Mn removal by filtration through Mn-oxide coated media where strong oxidizing agents (e.g., $KMnO_4$, HOCl) have been used to regenerate the Mn-oxide coating by oxidizing the adsorbed Mn. However, ITN-BUET (2011) shows that formation of Mn-oxide coating (indicating the oxidation of adsorbed Mn) on filter media is possible without addition of any oxidizing agent (detailed description provided in Chapter 2). For evaluating the mechanism of Mn removal in Mn coated filter media, column experiments have been carried out in this study where influent water of varying composition (with respect to Mn and other water parameters) were passed through a green sand filter column maintaining a specific flow rate and the effluent water was collected and analyzed for residual Mn.

Figure 4.1 and Figure 4.2 show the removal of Mn in green sand filter column under similar conditions, with the exception of DO concentration in influent water. These two sets of experiments were carried out to assess the effect of DO on removal of Mn in the filter media. The figures also show concentrations of Mn, DO and pH of influent water as a function of filter run time. Figure 4.1 shows that effluent Mn concentration increased gradually from nearly 4% (i.e., about 0.44 mg/l at 60 minutes of filter run time) to nearly 35% of influent Mn concentration (i.e., about 3.82 mg/l at 200 minutes of filter run time), indicating significant decrease in removal efficiency and possibly indicating an approach to the breakthrough point (i.e., where influent and effluent Mn concentration would be the same). The influent pH, DO and Mn concentration remained more or less unchanged throughout the experiment.

Figure 4.2 shows results of column experiments under similar conditions, except at a higher DO concentration of the influent water. This experiment was conducted to assess the possible effect to DO on removal of Mn in the filter media. Figure 4.2 shows a trend of Mn removal

similar to that observed in Fig. 4.1; Mn removal efficiency decreases with increasing filter run time, and the system appears to approach a breakthrough point. The influent pH, DO and Mn concentration did not change significantly during the course of the experiment.

Both Fig. 4.1 and Fig. 4.2 show that the system approaches the breakthrough point as filter run time increases. Fig. 4.2 shows effluent Mn concentration increased gradually from nearly 13% (i.e., about 1.33 mg/l at 10 minutes of filter run time) to nearly 71% of influent Mn concentration (i.e., about 7.24 mg/l at 350 minutes of filter run time), and the system appears to approach a breakthrough point. This indicates that the removal of Mn is characterized by only adsorption, and the removal capacity decreases as the adsorption sites on the media are exhausted with increasing filter run time. These figures also indicate absence of regeneration of Mn-oxide coating on the filter media (e.g., by oxidation of adsorbed Mn on filter media); such regeneration would increase Mn removal by continuously creating new adsorption sites, which is not apparent from the experimental results. Thus, it appears that DO alone cannot regenerate the media by oxidizing Mn(II) under experimental condition applied in this study.

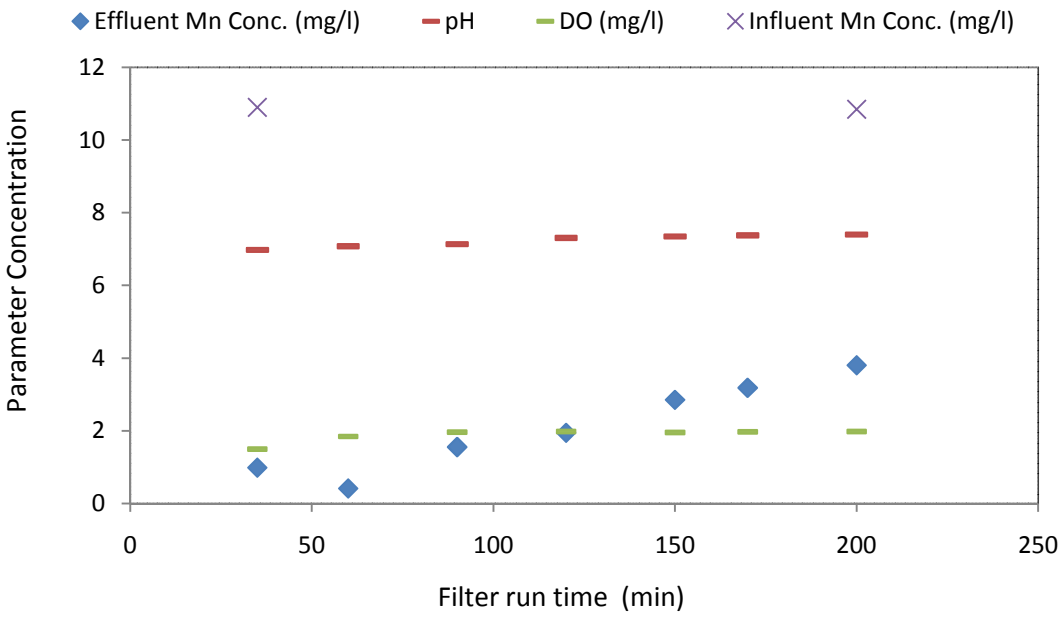

Figure 4.1: Effluent Mn concentration as a function of filter run time in column experiment carried out with reduced DO (~2mg/l) (Influent water prepared with deionized water containing 0.01 M KCl and 10.9 mg/l Mn(II); hydraulic loading rate, HLR= 6 ml/min.cm^2, Temp=28 °C)

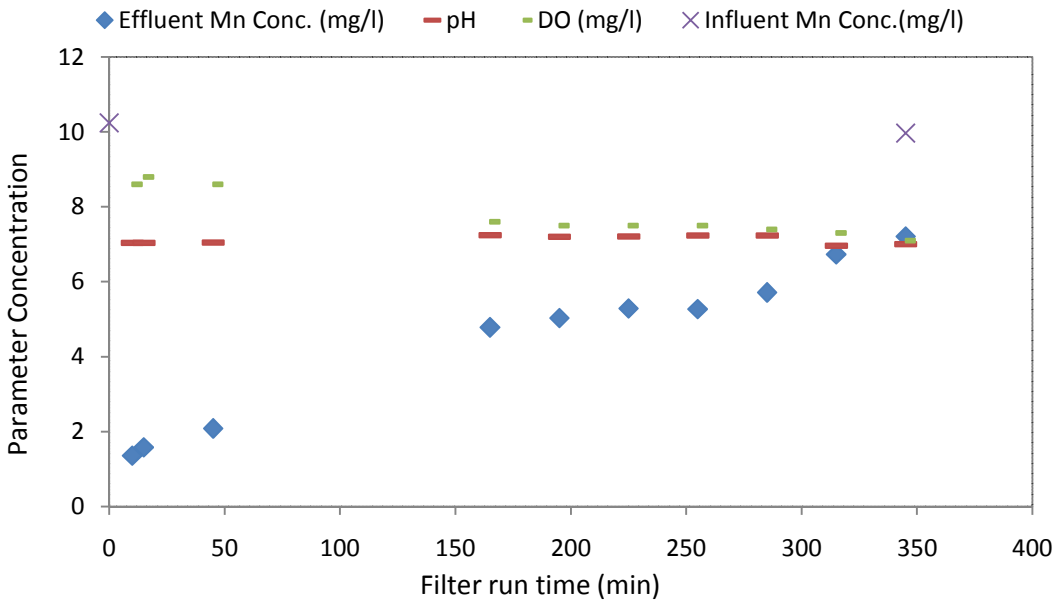

Figure 4.2: Effluent Mn concentration as a function of filter run time in column experiment carried out with higher DO (~8 mg/l) (Influent water prepared with deionized water containing 0.01 M KCl and 10.2 mg/l Mn(II); hydraulic loading rate, HLR= 6 ml/min.cm^2, Temp=28 °C)

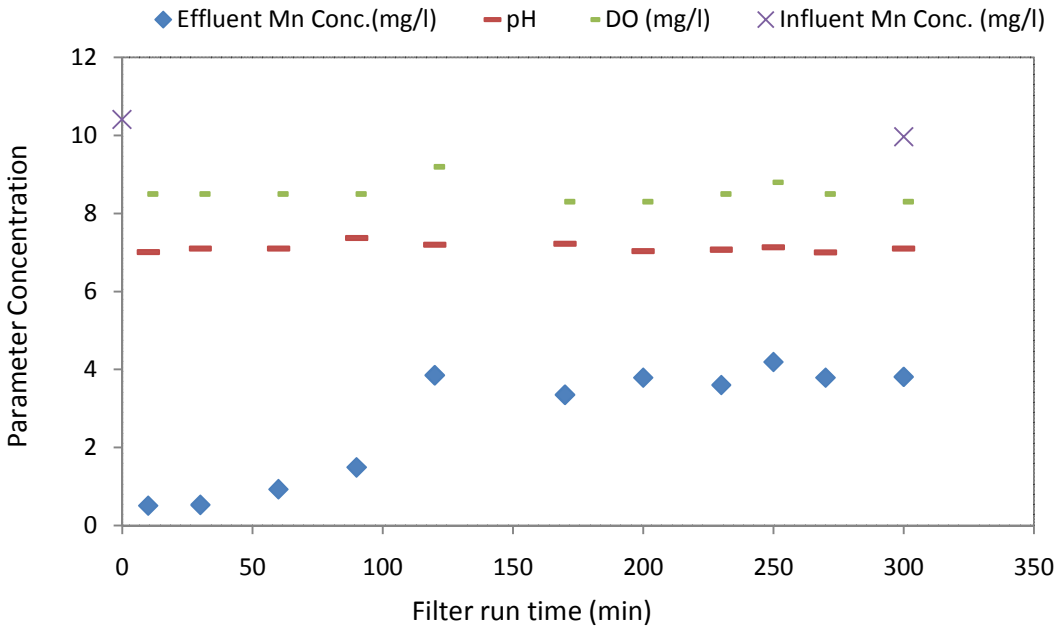

Figure 4.3: Effluent Mn concentration as a function of filter run time in the present of Bicarbonate in influent water (Influent water prepared with deionized water containing

0.01 M KCl, 10.4 mg/l Mn(II), and 200 mg/l Bicarbonate; hydraulic flow rate, HLR= 6 ml/min.cm^2, Temp=28 °C, influent water DO+~8.0 mg/l)

As discussed in Chapter 2, bicarbonate can play a role in catalyzing the oxidation of Mn. Bicarbonate could also promote formation of $MnCO_3$(s) solids within the filter media, which would also promote removal of Mn by precipitation (and possibly by creating additional adsorption sites). In order to evaluate these possible mechanisms, column experiments were conducted under conditions similar to those discussed above, but with addition of bicarbonate in the influent water. Figure 4.3 shows removal of Mn in the green sand filter column as a function of filter run time in the presence of 200 mg/l Bicarbonate. It shows that effluent Mn concentration gradually increased up to 38% of influent Mn concentration (4 mg/l effluent Mn concentration after 120 minutes of filter run time), but thereafter it did not increase further during the remaining filter run time (up to 300 minutes), showing possible stabilization of effluent Mn concentration (equilibrium condition).

Comparing the results of the two similar experiments presented in Figure 4.2 (without Bicarbonate in influent water) and Figure 4.3 (with Bicarbonate in influent water), it is obvious that Mn removal efficiency is increased in the presence of bicarbonate and the system does not approach the breakthrough point. There are two possible reasons for this phenomenon:

(1) Possible surface mediated oxidation (at the surfaces of Mn-oxide coated filter media) of adsorbed Mn by DO in the presence of Bicarbonate, which produces insoluble Mn-oxide and regenerates the exhausted media.
(2) Possible formation of insoluble $MnCO_3$(s) in the presence of Bicarbonate which increases removal efficiency by removing Mn within the filter media by precipitation.

To investigate the dominant mechanism among these two possible mechanisms, efforts have been made to invoke fundamental concept of solid precipitation and dissolution. Equation 4.1 and Eq. 4.2 show formation/dissolution of $MnCO_3$(s) and the mass law expression for formation/dissolution of $MnCO_3$(s). Equation 4.2 shows that at equilibrium the product of the molar concentrations of Mn^{+2} and CO_3^{-2} ions will always be equal to the solubility product, K_{sp}. If precipitation of $MnCO_3$(s) is the dominant mechanism in presence of Bicarbonate, then the change in aqueous concentration of any one of the ions (Mn^{+2} and CO_3^{-2}) would cause change in the concentration of the other ion accordingly so that the value of K_{sp} remains constant.

$$MnCO_3\,(s) \leftrightarrow Mn^{+2} + CO_3^{-2} \tag{4.1}$$

$$K_{sp} = [Mn^{+2}]\,[CO_3^{-2}] = [Mn^{+2}]\,[\alpha_2 C_T] \tag{4.2}$$

where:

$[Mn^{+2}]$ = molar concentration of Mn^{+2} ion in equilibrium
$[CO_3^{-2}]$ = molar concentration of CO_3^{-2} ion in equilibrium
K_{sp} = solubility product
α_2 = distribution coefficient, is a function of pH only
C_T = Total concentration of dissolved inorganic carbon= $[H_2CO_3] + [HCO_3^-] + [CO_3^{-2}]$

According to Equation 4.2, if Bicarbonate concentration is increased at a particular pH (i.e., by changing the total concentration of inorganic carbon, C_T, in water), more CO_3^{2-} will be available in solution, and a lower concentration of Mn^{2+} would cause precipitation of $MnCO_3$(s).

To investigate this issue, two sets of experiments were conducted; one with increased Bicarbonate concentration (442.9 mg/l) and other with decreased influent Mn concentration (7.21 mg/l), keeping the other water quality and operational parameters (e.g., flow rate) unchanged.

Figure 4.4 shows effluent Mn concentration as a function of filter run time for the column experiment with an increased bicarbonate concentration of 442.9 mg/l and initial Mn(II) concentration of 10.8 mg/l. Therefore, Figure 4.3 and Fig. 4.4 show removal of Mn under similar conditions, except for the difference in Bicarbonate concentration. Figure 4.4 shows that effluent Mn concentration increases gradually from nearly 1.5 mg/l (at 70 minutes of filter run time) to nearly 4 mg/l (at 220 minutes of filter run time), where it gets stable and does not increase further during the rest of the filter run time (up to 320 minutes), indicating an equilibrium condition. If $MnCO_3$(s) precipitation was the dominant mechanism then according to Equation 4.2, effluent Mn concentration would have been lower in this experiment than that of the experiment corresponding to Figure 4.3, since higher Bicarbonate concentration (and hence C_T) had been used in this test.

Figure 4.5 shows results of a similar experiment where Mn(II) and Bicarbonate concentration in the influent water were 7.2 mg/l and 200 mg/l, respectively. As shown in Figure 4.5, effluent Mn concentration increases up to 1 mg/l (at filter run time of 100 minutes) and thereafter, and does not increase further during the rest of filter run time (up to 280 minutes), indicating an equilibrium condition. If $MnCO_3$(s) precipitation was the dominant mechanism then according to Equation 4.2, effluent Mn concentration at equilibrium would have been similar to that of the experiment corresponding to Figure 4.3, since in both of these tests Bicarbonate concentration (and hence, C_T) was similar. On the other hand, this experimental result agrees well with the concept of surface mediated oxidation of adsorbed Mn by DO in the presence of bicarbonate, since under continuous regeneration and adsorption, equilibrium concentration of adsorbate is proportional to its initial concentration.

Analysis of the results shown in Figures 4.3 through Figure 4.5 suggest that the dominant mechanism for the removal of Mn(II) is continuous regeneration of Mn-oxide coated media (caused by the surface mediated oxidation of adsorbed Mn by DO in the presence of Bicarbonate) rather than $MnCO_3$(s) precipitation. This result is supported by the findings of a previous study (Kozlov et. al., 2004; Tang et. al., 2009) which shows that Mn(II) oxidation is favored in the presence of Bicarbonate in water. Tang et.al. (2009) investigated the effect of bicarbonate on the binding and oxidation of divalent Manganese in bacterial reaction centers, and revealed that Bicarbonate is able to facilitate the binding and oxidation of the Manganese (II) ion between pH 6 and 8 in center where the tight binding in their absence could not otherwise be established. Kozlov et. al. (2004) studied oxidation potentials of Mn(II) in aqueous solutions of bicarbonate and found that bicarbonate stimulates the electron transfer from Mn(II) to Mn-depleted water-oxidizing complex of photosystem II (apo-WOC-PSII).

Based on the results of laboratory experiments, a continuous regeneration mode of model (by oxidation of Mn by DO) has been developed for describing the removal of Mn from groundwater during filtration through a green sand column.

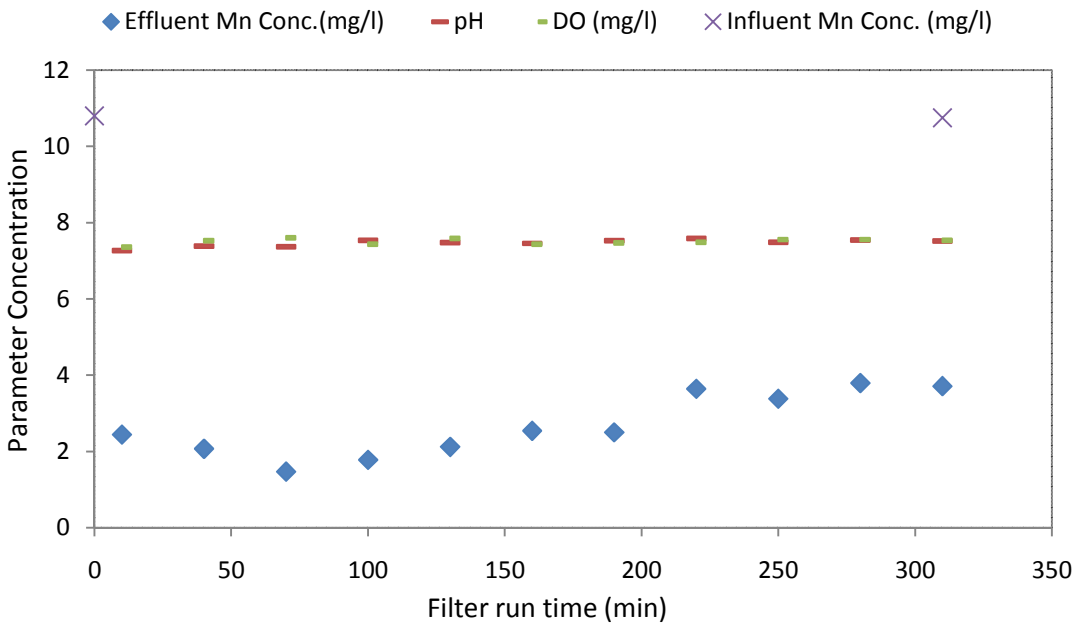

Figure 4.4: Effluent Mn removal as a function of filter run time in the presence of Bicarbonate in influent water (Influent water prepared with deionized water containing 0.01 M KCl, 10.8 mg/l Mn(II), and 442.9 mg/l Bicarbonate; hydraulic flow rate, HLR= 6 ml/min.cm^2, Temp=28 °C, influent water DO+~8.0 mg/l)

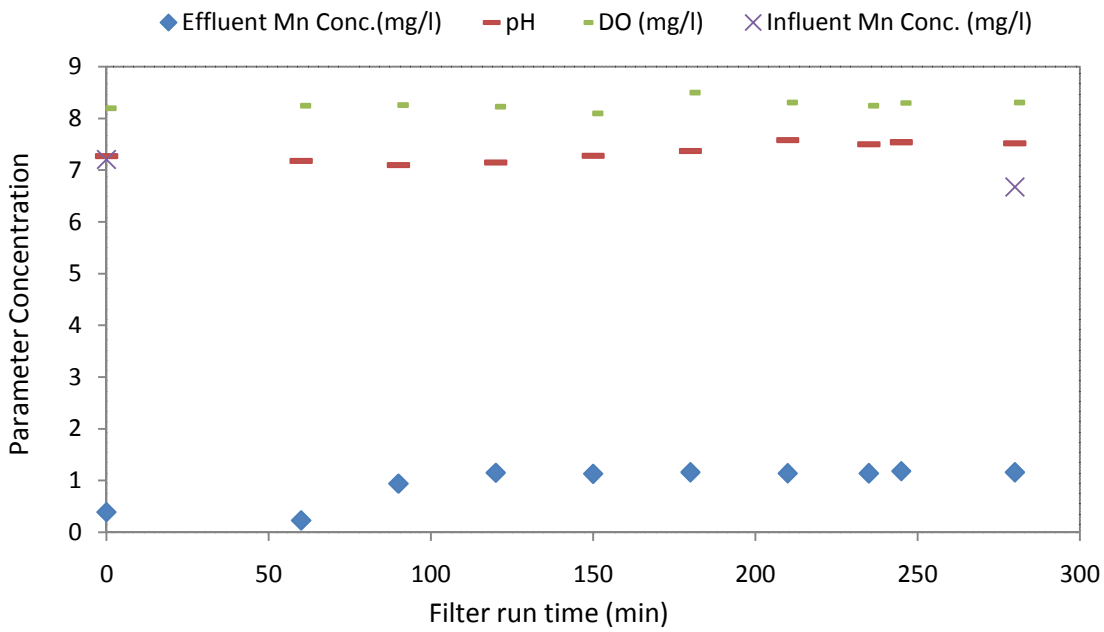

Figure 4.5: Effluent Mn concentration as a function of filter run time in the presence of Bicarbonate in influent water (Influent water prepared with deionized water containing 0.01 M KCl, 7.2 mg/l Mn(II), and 200 mg/l Bicarbonate; hydraulic flow rate, HLR= 6 ml/min.cm^2, Temp=28 °C, influent water DO+~8.0 mg/l)

4.3 Results of Multi-port Column Experiments

As noted above, a mathematical model has been developed (see Section 5.2.1) to predict Mn removal in green sand filter column, based on the mechanism of continuous regeneration of Mn-oxide coating on filter media by oxidation of Mn(II) by DO in the presence of Bicarbonate. The model predicts concentration of Mn in bulk-water along the depth of the filter column. The "multi-port column" experiments have been carried out to evaluate the effects of various parameters (flow rate, initial Mn concentration, pH) on removal of Mn, and to generate data for calibration and validation of the model. Soluble Mn concentration profiles in bulk-water were generated through measurements of pore-water Mn concentration at four depths (2, 4, 6 and 8 inches from the top of the green sand media) in the filter column (as described in Chapter 3); the Mn concentrations measurements were carried out after 90, 120 and 150 minutes of filter run time. Various combinations of experimental conditions were applied to evaluate the effects of different parameters on Mn removal. Results from these experiments were used for model calibration and validation.

4.3.1 Manganese removal: Effect of flow rate/contact time

In order to assess the effect of flow rate (or contact time) on Mn removal, flow rate (ml/min divided by column x-area) of the influent water was varied from 1.0 to 4.0 ml/min.cm^2 (26.4 to 105.6 ml/min) through the multi-port column keeping the other applied water conditions nearly similar. Groundwater collected from a deep tube well pump station at BUET, was

spiked with Manganese (II) stock solution to prepare the influent water. Initial pH of influent water was 7±0.1 and was found to vary slightly (7.2±0.1) during the filter run time (up to 150 minutes); Table 4.1 provides characterization of influent water used in multi-port column experiments at different flow rate conditions.

Table 4.1: Characteristics of influent water used in multi-port column experiments at different flow rate conditions

Parameter	Parameter value
Flow rate (ml/min.cm^2)	1
Influent water Mn concentration (mg/l)	4.2
pH during filter run (up to 150 minutes)	7.2±0.1
Alkalinity as $CaCO_3$ (mg/l)	254±5
DO (mg/l)	7.5±0.1 at 28 ^oC
Temperature (^{o} C)	28
Flow rate (ml/min.cm^2)	2
Influent water Mn concentration (mg/l)	4.83
pH during filter run (up to 150 minutes)	7.2±0.1
Alkalinity as $CaCO_3$ (mg/l)	254±5
DO (mg/l)	7.5±0.1 at 28 ^oC
Temperature (^{o} C)	28
Flow rate (ml/min.cm^2)	3
Influent water Mn concentration (mg/l)	4.5
pH during filter run (up to 150 minutes)	7.2±0.1
Alkalinity as $CaCO_3$ (mg/l)	254±5
DO (mg/l)	7.5±0.1 at 28 ^oC
Temperature (^{o} C)	28
Flow rate (ml/min.cm^2)	4
Influent water Mn concentration (mg/l)	4.23
pH during filter run (up to 150 minutes)	7.2±0.1
Alkalinity as $CaCO_3$ (mg/l)	254±5
DO (mg/l)	7.5±0.1 at 28 ^oC
Temperature (^{o} C)	28

Figures 4.6, 4.7, 4.8 and 4.9 present data from multi-port column experiments conducted with flow rate of 1, 2, 3 and 4 ml/min.cm^2, respectively, under nearly similar operation conditions (noted in Table 4.1). Figures 4.6(a), 4.7(a), 4.8(a), 4.9(a) show bulk-water Mn concentration profiles in the multi-port column at various filter run times. Manganese concentration at depth "0" inch indicates influent concentration, while Mn concentration at 8 inch depth indicates effluent concentration. Figure 4.6(b), 4.7(b), 4.8(b), 4.9(b) show bulk-water Mn concentration as a function of filter run time at various depths of multi-port column. It is clear from the figures that in all cases, Mn concentration profiles did not vary

significantly with filter run time between 120 and 150 minutes. Therefore, in later data analysis, the stable profiles at filter run time of 150 minutes were presented as a single profile for ease of comparison (Fig. 4.10).

The multi-port column containing green sand provided effective Mn removal under experimental conditions. The removal profiles observed in Figures 4.6(a), 4.7(a), 4.8(a) and 4.9(a) show a rapid initial removal as the water moved through the media. Under all flow rate conditions, Mn removal at the upper depths of the media was higher than at the lower depths. The possible reason could be the linear driving force (LDF), caused by the difference between the adsorbate concentration in the bulk solution and the concentration at the external surface of media, that helps adsorption by film diffusion; the driving force gets reduced as the water moves through the media depth. In all four sets of experiments, the dissolve Mn profile within the filter column did not change appreciably with time (from 90 to 150 minutes). If the removal of Mn within the filter media were governed by adsorption alone, then the capacity of of the media, specially at the top layers, would have decreased with time (i.e., with passage of Mn bearing water), and bulk-water Mn concentration would have increased with time. However, no significant increase in bulk-water Mn concentration with time indicates that exhaustion of adsorption sites is accompanied by regeneration of new sites (possibly by oxidation of Mn by DO in the presence of Bicarbonate, as explained above), thereby keeping the Mn removal capacity virtually unaffected with passage of time. Thus, results of multi-port column experiments also suggest regeneration of Mn-oxide coated media in the presence of bicarbonate.

The initial Mn concentrations for the four sets of experiments varied from 4.2 to 4.83 mg/l; hence, to compare the effect of flow rate on Mn removal, the normalized Mn concentration profiles as a function of depth have been plotted in Figure 4.10 for various flow rates. Figure 4.10 shows that flow rate has a significant effect on the removal capacity of media. Lower flow rate increases the contact time between soluble Mn and media, and therefore, increases removal capacity. The result agreed with the findings of the experiment of Subramaniam (2010), where high flow rates (16-24 gpm/ft^2) were applied for water with low initial Mn concentration (0.06-0.07 mg/l) and with free chlorine (1.1-1.2 mg/l) as oxidant. In the current study, as shown in Figure 4.10, maximum removal of soluble Mn (at the bottom of the filter column) have been found as 98%, 83%, 74% and 64% for flow rate of 1, 2, 3 and 4 ml/min.cm^2, respectively. Thus, depending on influent Mn concentration, flow rate and depth of filter media, almost complete removal of Mn is possible within Mn-oxide coated filter media.

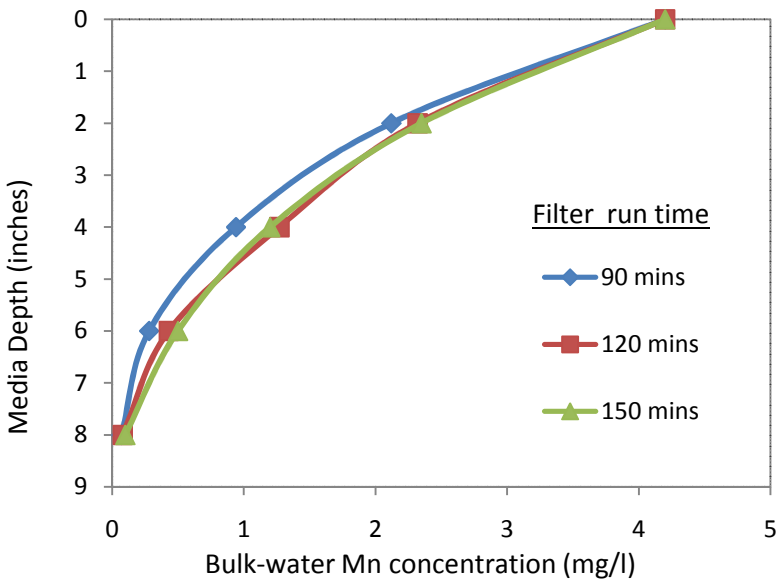

Figure 4.6 (a): Bulk water Mn concentration profiles in green sand media at various filter run time at a flow rate of 1 ml/min.cm^2

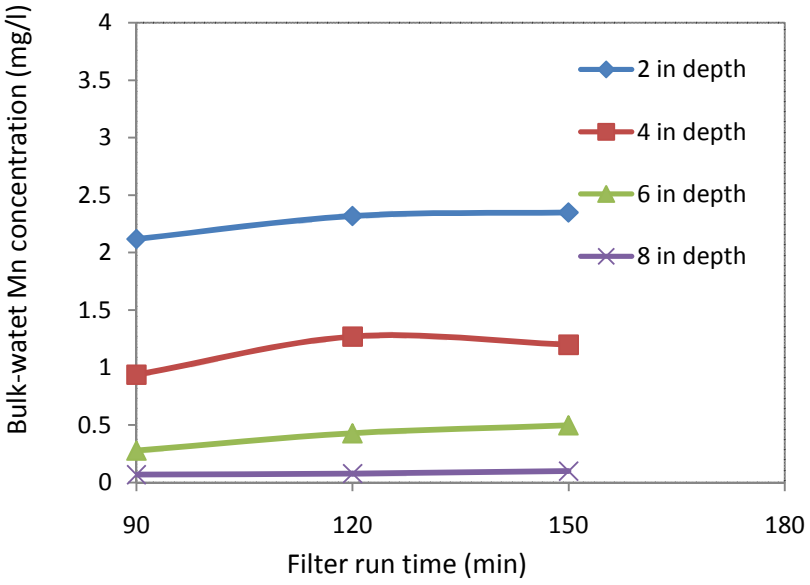

Figure 4.6 (b): Bulk water Mn concentration as a function of filter run time at various depths of green sand media at a flow rate of 1 ml/min.cm^2.

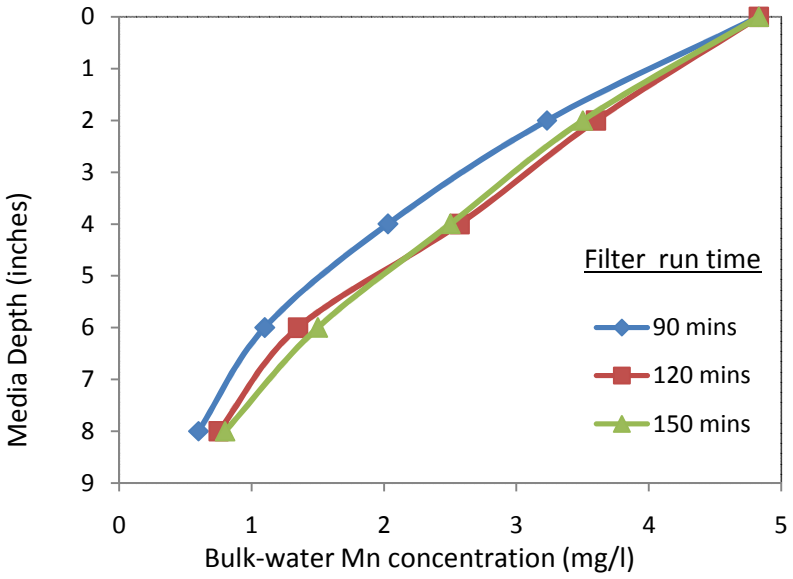

Figure 4.7 (a): Bulk water Mn profiles in of green sand media at various filter run time at a flow rate of 2 ml/min.cm^2

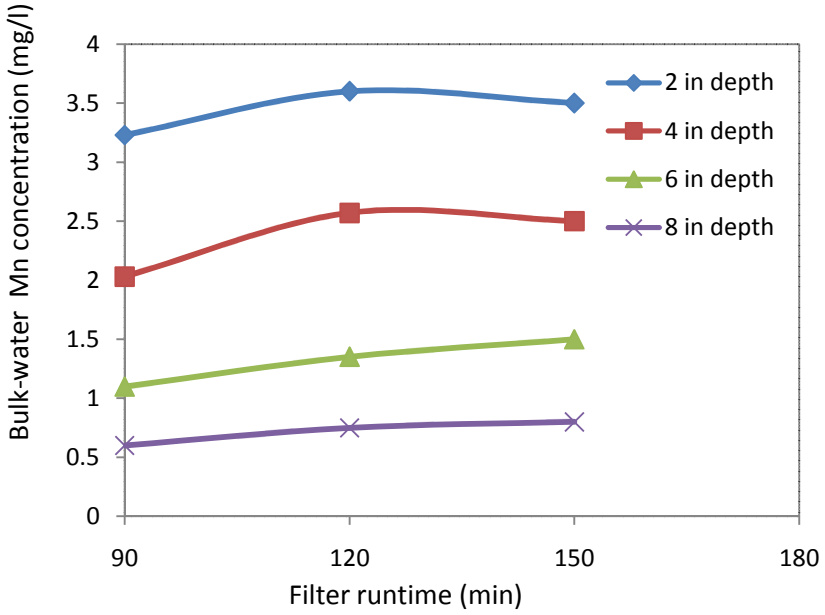

Figure 4.7 (b): Bulk water Mn concentration as a function of filter run time at various depths of green sand media at a flow rate of 2 ml/min.cm^2

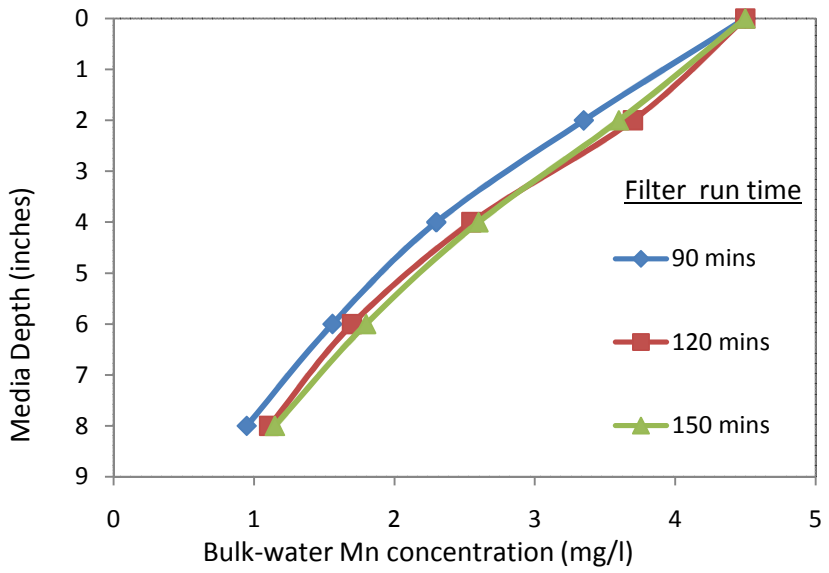

Figure 4.8 (a): Bulk water Mn concentration profiles in green sand media at various filter run time at a flow rate of 3 ml/min.cm^2

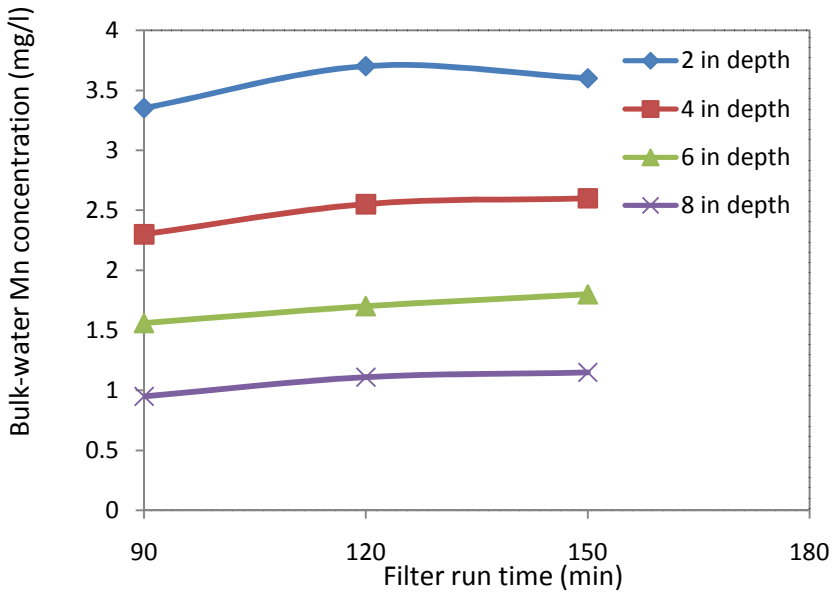

Figure 4.8 (b): Bulk water Mn concentration as a function of filter run time at various depths of green sand media at a flow rate of 3 ml/min.cm^2

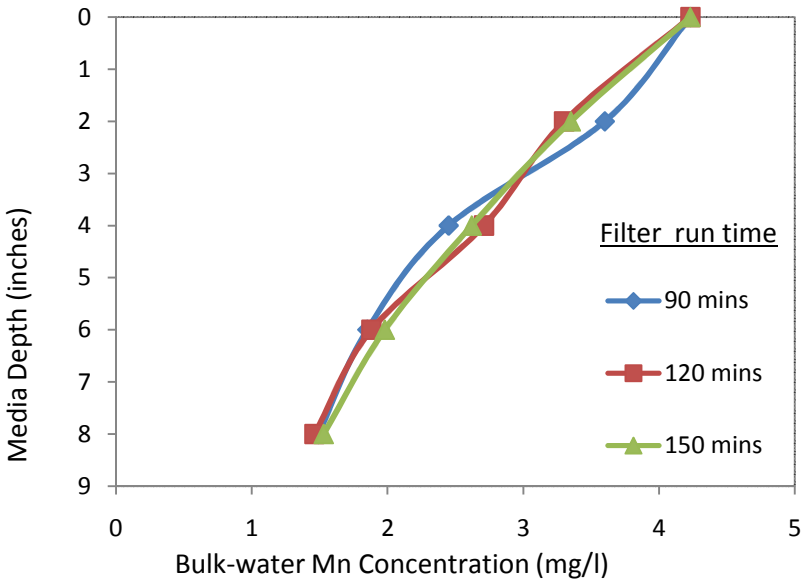

Figure 4.9 (a): Bulk water Mn concentration profiles in green sand media at various filter run time at a flow rate of 4 ml/min.cm^2

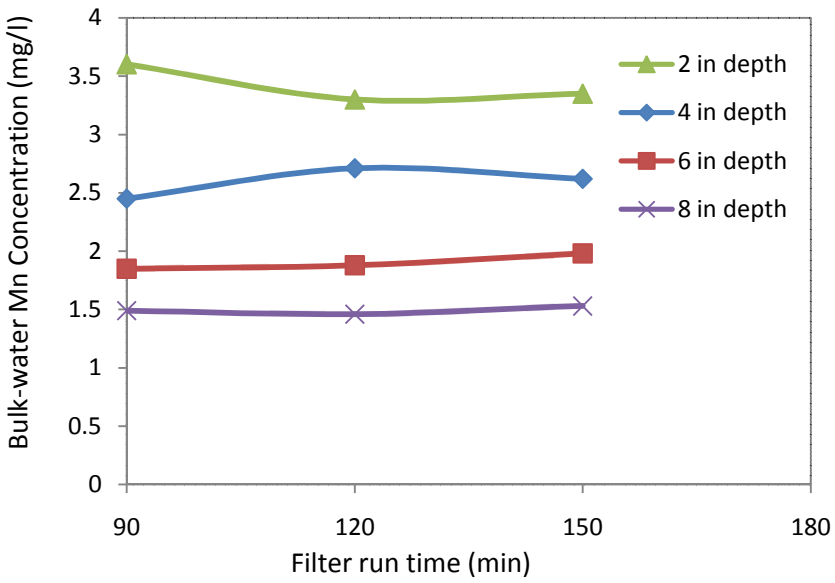

Figure 4.9 (b): Bulk water Mn concentration as a function of filter run time at various depths of green sand media at a flow rate of 4 ml/min.cm^2

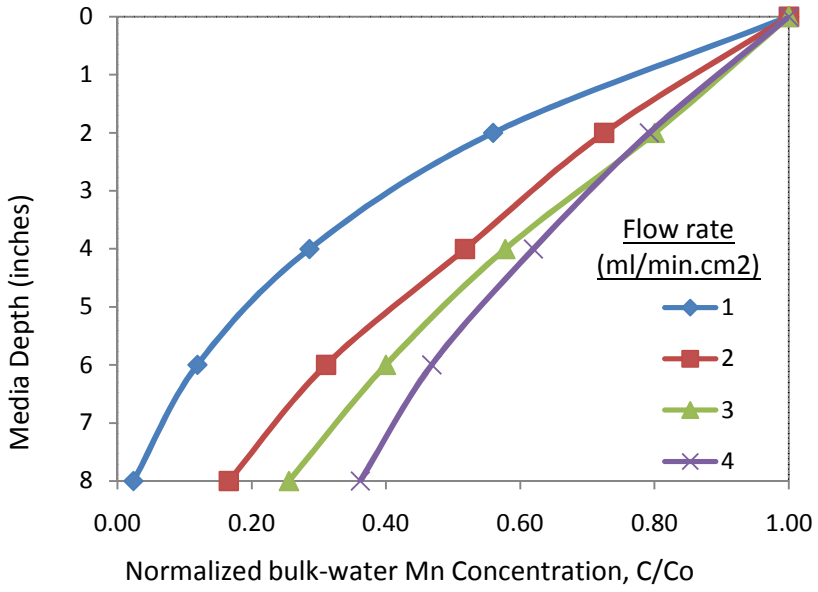

Figure 4.10: Normalized bulk water Mn concentration profiles in green sand media at various flow rates

4.3.2 Manganese removal: Effect of initial Mn concentration

In order to assess the effect of initial (influent) Mn concentration on Mn removal, experiments were conducted by varying the initial Mn concentration of the influent water from 1.15 to 11.2 mg/l; flow rate was fixed at 2 ml/min.cm^2. Initial pH of influent water was 7± 0.1 and was found to vary slightly (7.2±0.1) during the filter run time (up to 150 minutes). Table 4.2 shows the characterization of influent water used in multi-port column experiments at different initial Mn concentrations.

Table 4.2: Characteristics of influent water used in multi-port column experiments at different initial Mn concentrations

Parameter	Parameter value
Influent water Mn concentration (mg/l)	1.15
Flow rate (ml/min.cm^2)	2
pH during filter run (up to 150 minutes)	7.2±0.1
Alkalinity as $CaCO_3$ (mg/l)	254±5
DO (mg/l)	7.5±0.1 at 28 ^oC
Temperature (^{o} C)	28
Influent water Mn concentration (mg/l)	2.31 mg/l
Flow rate (ml/min.cm^2)	2
pH during filter run (up to 150 minutes)	7.2±0.1
Alkalinity as $CaCO_3$ (mg/l)	254±5
DO (mg/l)	7.5±0.1 at 28 ^oC
Temperature (^{o} C)	28
Influent water Mn concentration (mg/l)	4.83 mg/l

Flow rate (ml/min.cm^2)	2
pH during filter run (up to 150 minutes)	7.2±0.1
Alkalinity as $CaCO_3$ (mg/l)	254±5
DO (mg/l)	7.5±0.1 at 28 ^oC
Temperature (^{o} C)	28
Influent water Mn concentration (mg/l)	11.2
Flow rate (ml/min.cm^2)	2
pH during filter run (up to 150 minutes)	7.2±0.1
Alkalinity as $CaCO_3$ (mg/l)	254±5
DO (mg/l)	7.5±0.1 at 28 ^oC
Temperature (^{o} C)	28

Figures 4.11, 4.12, 4.7 (discussed earlier) and 4.13 present results of the column experiments conducted with initial Mn concentrations of 1.15, 2.31, 4.83, 11.2 mg/l, respectively, under nearly similar operation conditions (noted in Table 4.2). Figures 4.11(a), 4.12(a), 4.7(a) and 4.13(a) show bulk-water Mn profiles in the multi-port column at various filter run time. As before, concentration at "0" inch depth indicate influent concentration, while concentration at 8 inch depth indicates effluent concentration. Figure 4.11(b), 4.12(b), 4.7(b), 4. 13(b) show bulk-water Mn concentration as a function of filter run time at various depths of multi-port column. It is clear from the figures that, bulk-water Mn concentration profiles did not vary significantly with filter run time between 120 and 150 minutes. Therefore, in later data analysis, the stable profiles at filter run time of 150 minutes were displayed as a single profile for ease of comparison (Fig. 4.14).

The trends of Mn profile in the multi-port column obtained from these experiments are similar to those presented above (Figs. 4.6 to 4.9). To compare the effect of initial Mn concentration on Mn profile, the normalized Mn concentration profiles have been plotted in Figure 4.14 for influent water with various initial Mn concentrations. Figure 4.14 shows that Mn removal capacity of the media increases with increase in initial Mn concentration of the influent water. This is possibly due to the fact that higher initial Mn concentration increases the linear driving forced (LDF), which increases the bulk-water Mn mass transfer through the liquid film and hence removal capacity of the media increases. The result agreed with the findings of the experiment Zuravnsky (2006). Under experimental conditions, maximum removal of bulk-water Mn (at the bottom of the filter media) have been found as 56%, 74%, 83% and 79% for influent water with initial Mn concentrations of 1.15, 2.31, 4.83, 11.2 mg/l, respectively.

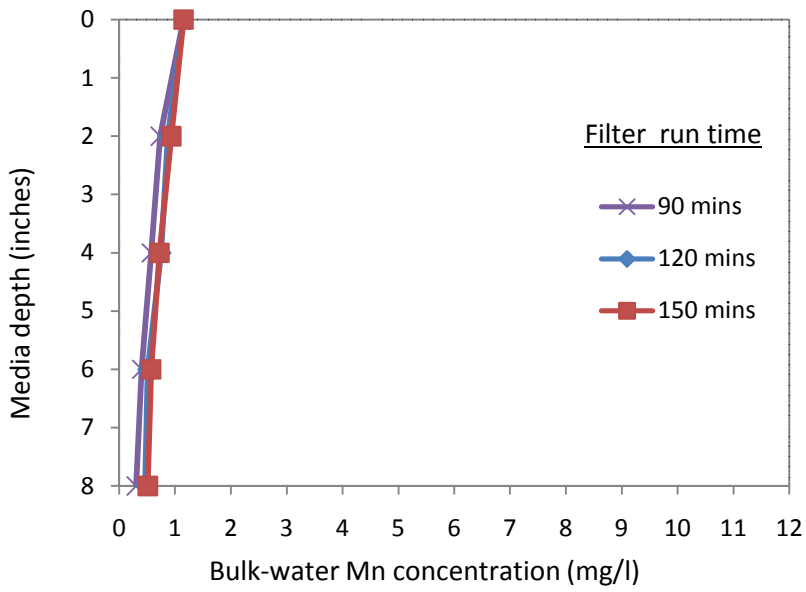

Figure 4.11 (a): Bulk water Mn profiles in green sand media at various filter run time with Initial Mn concentration of 1.15 mg/l

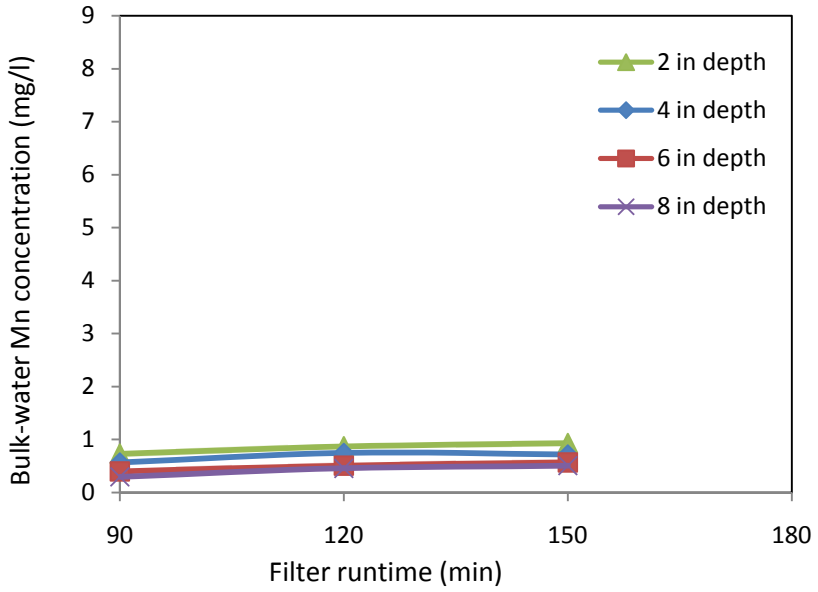

Figure 4.11 (b): Bulk water Mn concentration as a function of filter run time at various depths of green sand media with initial Mn concentration= 1.15 mg/l.

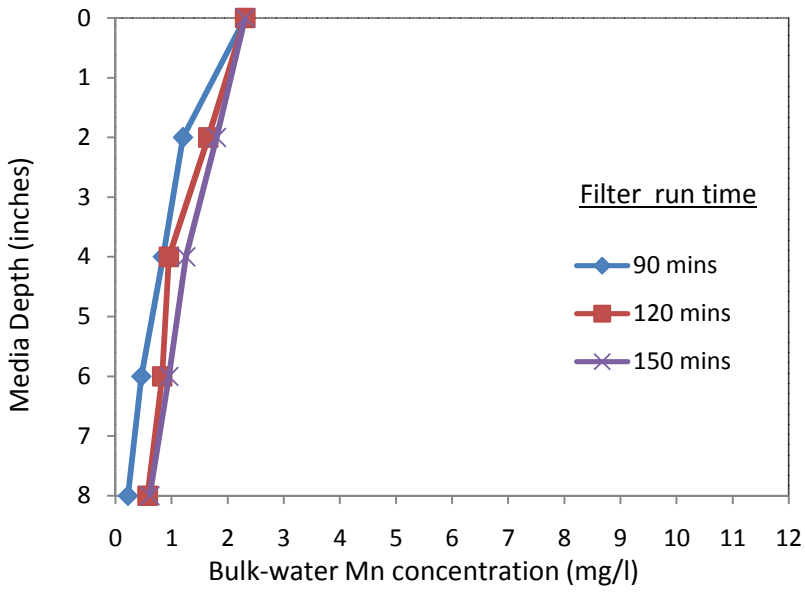

Figure 4.12 (a) Bulk water Mn profiles in green sand media at various filter run time with initial Mn concentration of 2.31 mg/l

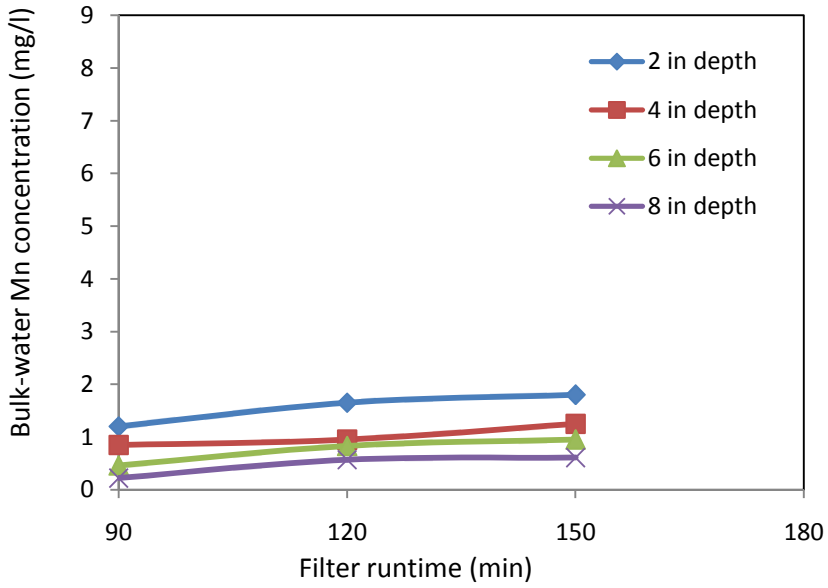

Figure 4.12 (b): Bulk water Mn concentration as a function of filter run time at various depths of green sand media with initial Mn concentration= 2.31 mg/l.

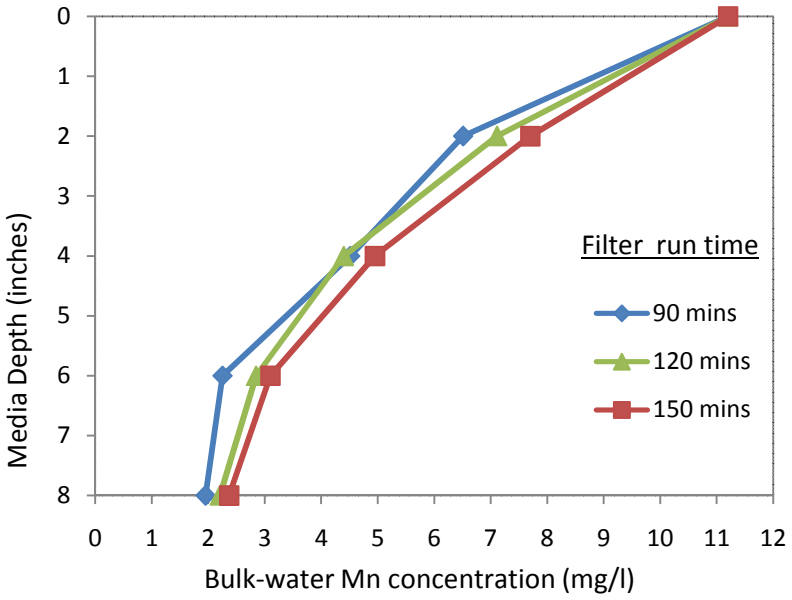

Figure 4.13 (a): Bulk water Mn profiles as in green sand media at various filter run time with initial Mn concentration of 11.2 mg/l

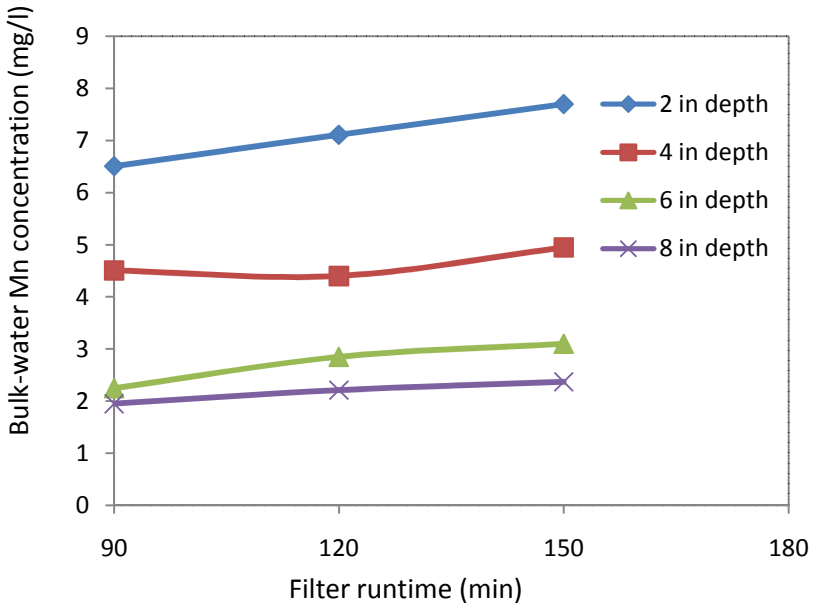

Figure 4.13 (b): Bulk water Mn concentration as a function of filter run time at various depths of green sand media with initial Mn concentration= 11.2 mg/l.

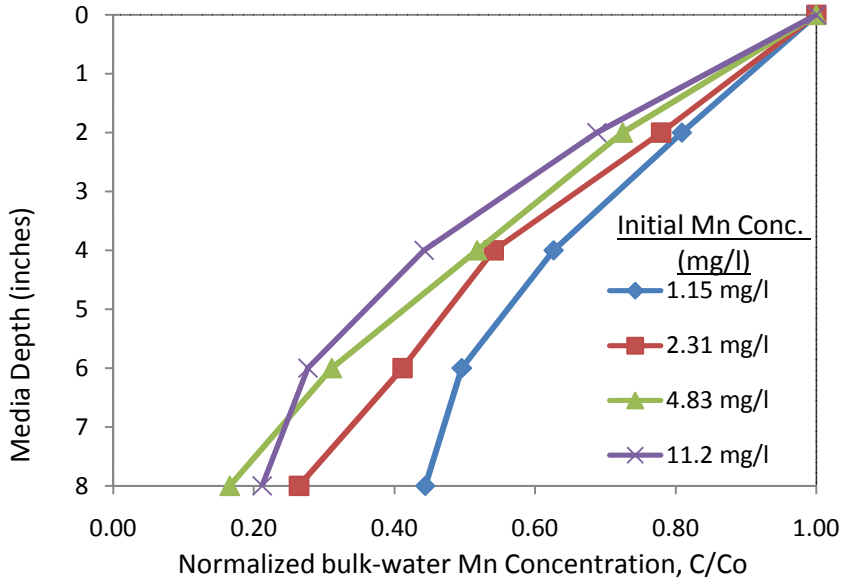

Figure 4.14: Normalized bulk-water Mn concentration profiles in green sand media for various initial Mn concentrations

4.3.3 Manganese removal: Effect of pH

In order to analyze the effect of influent water pH on Mn removal, column experiments similar to those described above were conducted where pH of the influent water was varied from 6.0 to 8.0, keeping the flow rate fixed at 2 ml/min.cm^2. Table 4.3 shows detail characteristics of influent water used in the experiments.

Table 4.3: Detail characteristics of influent water used in multi-port column experiments at different pH conditions

Parameter	Parameter value
Initial pH of influent water	6.0
pH during filter run (up to 150 minutes)	6.0±0.2
Influent Mn concentration (mg/l)	5.14
Alkalinity as $CaCO_3$ (mg/l)	200±5
DO (mg/l)	7.5±0.1 at 28 ^oC
Temperature (^{o} C)	28
Initial pH of influent water	7.0
pH during filter run (up to 150 minutes)	7.2±0.1
Influent water Mn concentration (mg/l)	4.83
Alkalinity as $CaCO_3$ (mg/l)	254±5
DO (mg/l)	7.5±0.1 at 28 ^oC
Temperature (^{o} C)	28
Initial pH of influent water	8.0
pH during filter run (up to 150 minutes)	8.0±0.1
Influent water Mn concentration (mg/l)	4.88
Alkalinity as $CaCO_3$ (mg/l)	300±5
DO (mg/l)	7.5±0.1 at 28 ^oC
Temperature (^{o} C)	28

Figures 4.15, 4.7 (discussed earlier) and 4.16 present results of the experiments carried out at various pH conditions of influent water, under nearly similar operating conditions (noted in Table 4.3). Figures 4.15(a), 4.7(a) and 4.16(a) show bulk-water Mn profile in the multi-port column at various filter run times. Figure 4.15(b), 4.7(b) and 4.16(b) show bulk-water Mn concentration as a function of filter run time at various depths of multi-port column. It is clear from the figures that, bulk-water Mn concentration profiles did not vary significantly with filter run time between 120 and 150 minutes. Therefore, in later data analysis, the stable profiles at filter run time of 150 minutes were displayed as a single profile for ease of comparison (Fig. 4.17).

To evaluate the effect of pH on Mn profile, the normalized Mn concentration profiles have been plotted in Figure 4.17 for various pH values of influent water. Figure 4.17 shows that pH has very significant effect on the removal capacity of media. It is observed that removal capacity of the media increases with increase in pH value of influent water. This was expected since it is well established that Mn oxidation is favored in higher pH range. This observation is in agreement with the results reported by Subramaniam (2010), Zuravnsky (2006) and Morgan and Stumm (1964), where alkaline pH conditions have been found to promote Mn adsorption by increasing the amount of available Mn adsorption sites on Mn oxide coated media. Under experimental conditions, maximum removal of bulk-water Mn (at

the bottom of the filter column) have been found as 66%, 83% and 90% for influent water pH of 6, 7 and 8, respectively.

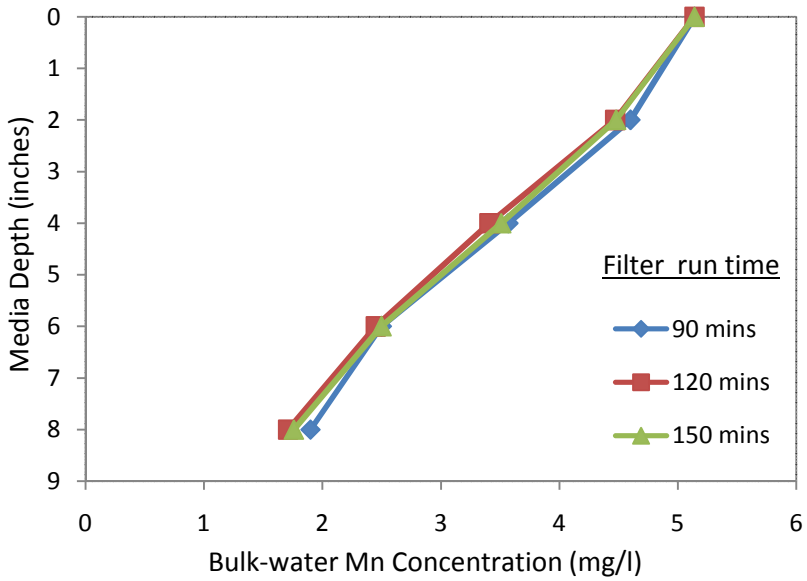

Figure 4.15 (a): Bulk water Mn profiles in green sand media at various filter run time with influent water pH= 6.0±0.2

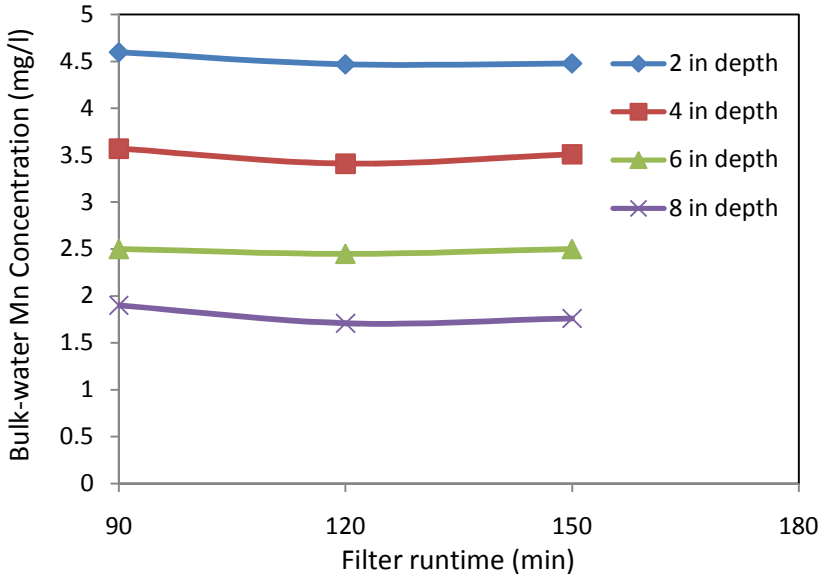

Figure 4.15 (b): Bulk water Mn concentration profiles as a function of filter run time at various depths of green sand media with influent water pH= 6.0±0.2.

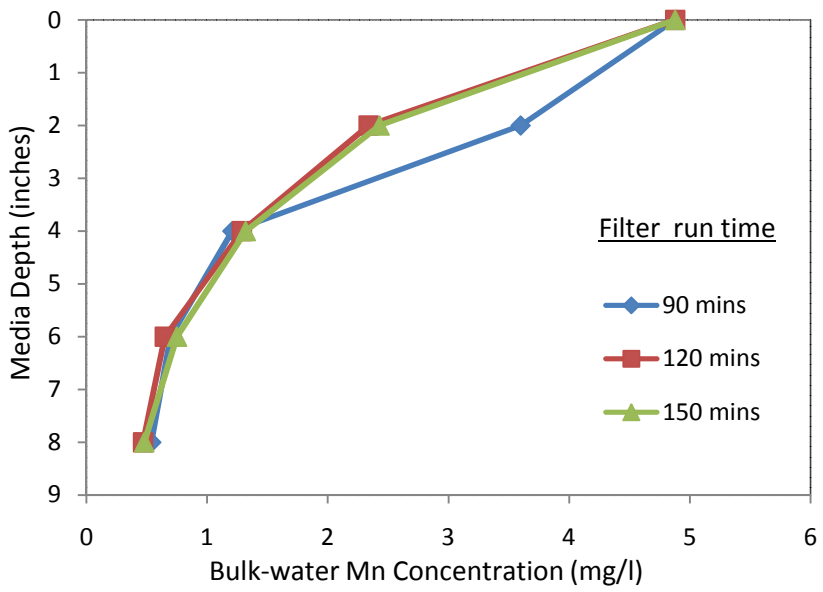

Figure 4.16 (a): Bulk water Mn profiles in green sand media at various filter run time with influent water pH= 8.0±0.1

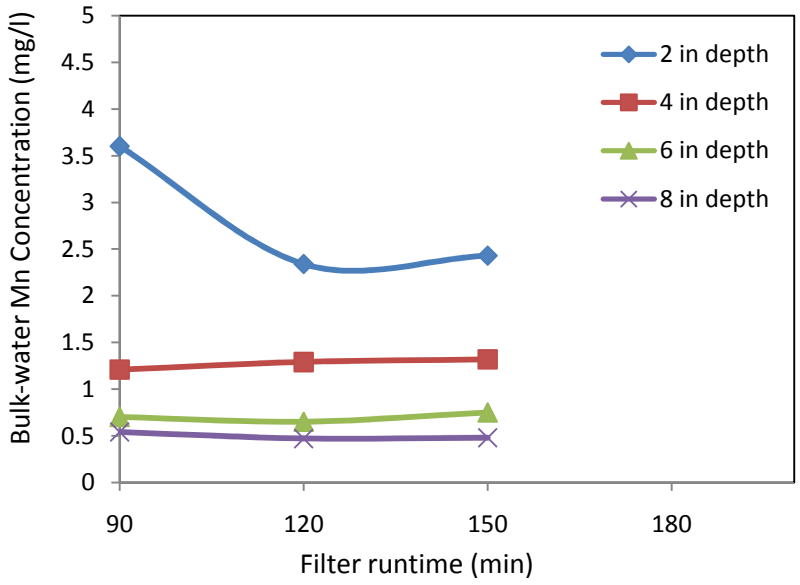

Figure 4.16 (b): Bulk water Mn concentration profiles as a function of filter run time at various depths of green sand media with influent water pH= 8.0±0.1.

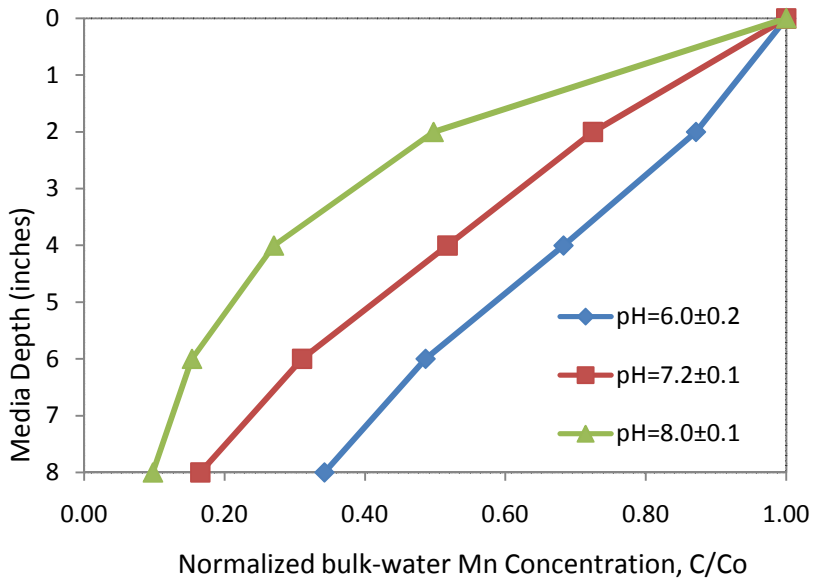

Figure 4.17: Normalized bulk-water Mn concentration profiles in green sand media for various pH values of influent water

4.4 Summary of Findings from Laboratory Experiments

Results from laboratory suggest in the absence of bicarbonate in the influent water, the removal of Mn during filtration through a Mn-oxide coated media is characterized by adsorption, and the system gradually approaches toward the breakthrough point (when effluent Mn concentration becomes equal to the influent Mn concentration). The removal capacity of the media, under such conditions, decreases as the adsorption sites on the media are exhausted with increasing filter run time.

In the presence of Bicarbonate in the influent water, Mn removal efficiency of Mn-oxide coated media increases significantly and the system does not approach the breakthrough point. There are two possible reasons for this phenomenon:

(1) Possible surface mediated oxidation (at the surfaces of Mn-oxide coated filter media) of adsorbed Mn by DO in the presence of Bicarbonate, which produces insoluble Mn-oxide and regenerates the exhausted media.

(2) Possible formation of insoluble $MnCO_3(s)$ in the presence of Bicarbonate which increases removal efficiency by removing Mn within the filter media by precipitation.

Results of laboratory column experiments carried out by varying Mn and Bicarbonate concentration of influent water reveal that the dominant mechanism for the removal of Mn(II) is continuous regeneration of Mn-oxide coated media, caused by the surface mediated oxidation of adsorbed Mn by DO in the presence of Bicarbonate, rather than $MnCO_3(s)$

precipitation. Results of multi-port column experiments also support the concept of regeneration of Mn-oxide coated media.

Results of laboratory multi-port column experiments provided useful insights on the effects of flow rate, initial Mn concentration and pH on the removal of Mn within the filter media. Mn removal has been found to increase with decreasing flow rate, which promote longer contact time between the filter media and water. Mn removal capacity of the media has been found to increase with increase in initial Mn concentration of the influent water. This is possibly due to the fact that higher initial Mn concentration increases the linear driving forced (LDF), which increases the bulk-water Mn mass transfer through the liquid film and hence, removal capacity of the media increases. The Mn removal capacity has also been found to increase with increase in pH value of influent water; it is well established that Mn oxidation is favored in higher pH range. The results of the multi-port column experiments have been used for calibration and validation of the model developed for describing Mn removal in Mn-oxide coated filter media (see Chapter 5).

CHAPTER 5: MODEL DEVELOPMENT AND VALIDATION

5.1 Introduction

This Chapter presents the model developed in this study for describing removal of Mn in Mn-oxide coated filter media, based on the removal mechanism identified in this study (Section 4.2). This Chapter describes the validation and application of the model to predict soluble Mn removal profile via adsorption and oxidation onto Mn-oxide coated media. The first part of this Chapter presents the model, which has been developed by modifying the model developed by Zuravnsky (2006), and discusses the numerical solution of the model with required model input parameter estimation. In later part, the modified model was used to simulate Mn removal in a Mn-oxide coated column with various input parameters determined from appropriate correlations and experiments conducted under different conditions. This Chapter also presents model calibration, model predictions and sensitivity analysis under different conditions to assess the applicability of the developed model.

5.2 Model Development

5.2.1 Model equations

As described in Section 4.2, experimental results suggest that, Mn removal from water by filtration through green sand media involves adsorption on the filter media, and regeneration of the media by the oxidation of Mn by DO in presence of bicarbonate. Hence, a continuous regeneration model previously developed by Zuravnsky (2006) was used in this study with modifications (using DO as oxidant to regenerate the green sand media). The model was developed to predict the soluble Mn removal via adsorption and surface oxidation (by DO) and subsequent deposition onto Mn-oxide coated media for steady state conditions. The development of the model begins with the application of first principles to a mass balance of soluble Mn across an incremental bed depth (as shown conceptually in Figure 5.1). The model simulates the manganese transport process by advection and dispersion within the multi-port column, followed by mass transfer through the boundary layer surrounding the media grains, and then adsorption and surface oxidation.

At steady state, the mass of soluble Mn entering the system is equal to the sum of the mass of soluble Mn removed by adsorption and the mass soluble Mn leaving the system (as shown in Equation 5.1). The soluble Mn flux was assumed to be driven by a linear driving force as described by Merkle *et al.* (1997b)

$$Q\, C_{1b(z)} = k_f\,(C_{1b} - C_{1s})\, Av\, (1 - \varepsilon_B)\, A\, \Delta z + Q\, C_{1b(z+\Delta z)} \qquad (5.1)$$

where : Q = volumetric water flow rate (m^3/s)

C_{1b} = bulk aqueous-phase Mn concentration (mol/m^3)

k_f = liquid to solid mass transfer coefficient (m/s)
C_{1s} = aqueous-phase Mn concentration at the liquid-solid interface (mol/m^3)
Av = specific surface of media (m^2 media/m^3 media)
ε_B = fractional pore volume (m^3 water/m^3 bed)
A = cross sectional area of bed (m^2)

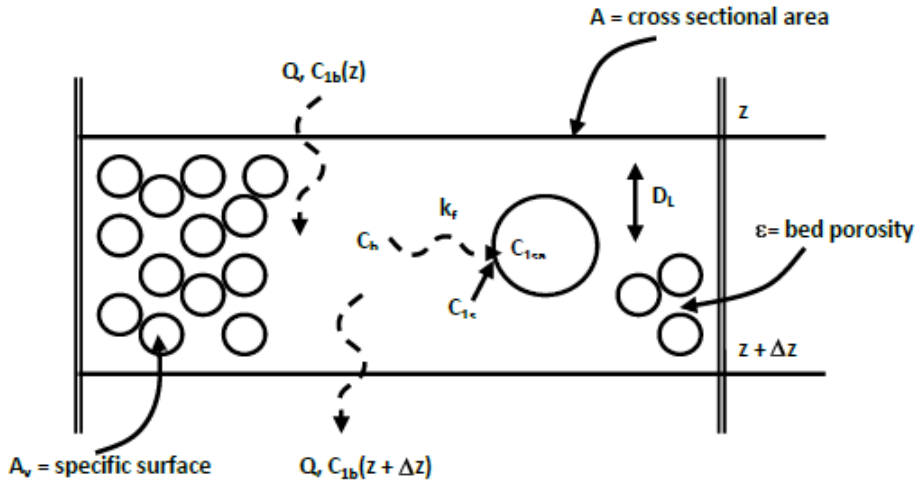

Figure 5.1: Representation of the flow of Mn across an incremental depth of media (Zuravnsky, 2006).

Manipulation of the soluble Mn mass balance equation provided a group of three solvable steady state equations as shown in Equations 5.2-5.4. In addition, an overall balance yields Equation 5.5 (Subramaniam, 2010). Detailed derivations of the equations are provided in Appendix A. The change in soluble Mn concentration over depth is shown in Equation 5.2. The change in oxidant concentration over depth can also be described by a mass balance approach and was manipulated into the form shown in Equations 5.3-5.4.

$$0 = -U\frac{\partial C_{1B}}{\partial z} + D_L\frac{\partial^2 C_{1B}}{\partial z^2} - k_f A_v \frac{(1-\varepsilon_B)}{\varepsilon_B}(C_{1b} - [\frac{C_{1sa}}{K}]^n) \quad (5.2)$$

$$0 = -U\frac{\partial C_{2B}}{\partial z} + D_L\frac{\partial^2 C_{2B}}{\partial z^2} - \rho_b k_r C_{1sa} C_{2b} \quad (5.3)$$

$$0 = \frac{k_f A_v}{\rho_b}(1-\varepsilon_B)(C_{1b} - [\frac{C_{1sa}}{K}]^n) - k_r \varepsilon_B C_{1sa} C_{2b} \quad (5.4)$$

$$C_{1b(in)} - C_{1b(out)} = C_{2b(in)} - C_{2b(out)} \quad (5.5)$$

where: C_{2b} = bulk aqueous-phase oxidant (DO in this study) concentration (mol/m^3)
ρ_b = bulk density of media (kg media/m^3 bed)
U = pore water velocity (= Q/Aε) (m/s)
D_L = axial dispersion coefficient (m^2/s)
k_r = Oxidation rate constant (m^3bed/mol*s)

C_{1sa} = adsorbed-phase Mn concentration on the media surface (=$K*C_{1s}^{1/n}$) (mol/kg)
K, n = Freundlich isotherm constants

Equations 5.2-5.4 agreed with the group of equations developed by Merkle *et al.* (1997b). However, this model is a simplification of Merkle's model, since it ignores the available fraction of sorption capacity (AFR), with adsorption and surface oxidation assumed to occur on the external surface of the media grains. Moreover, it is assumed that no additional species are present that might interfere with adsorption or oxidation, and that there is no increase in media grain diameter or adsorption capacity due to deposited MnOx(s). Because oxidant is usually present in excess, it is further assumed that the concentration of oxidant in the boundary layer surrounding the granular media is equal to the oxidant concentration in the bulk-water, rather than explicitly accounting for mass transfer of oxidant to the media surface. Thus, in the terms that account for the removal of Mn via oxidation on the right-hand side of Equations 5.3 and 5.4, the oxidant concentration is given by C_{2b}, which is the concentration in the bulk-water. If the experimental conditions were such that oxidant was not present in excess, mass transfer of oxidant from the bulk-water to the media surface would need to be taken into account.

5.2.2 Numerical solution of the model equations

The model equations discussed in 5.2.1 were solved for the soluble Mn concentration and DO concentration per unit depth, using numerical methods. As described in 5.2.1, the three solvable steady-state equations involve a second order derivative; four boundary conditions were required to solve the steady-state equations. The known values of influent Mn and DO concentrations accounted for two of the boundary conditions and the other two conditions are as shown in Equations 5.6 and 5.7.

$$C_{1b(n)} = C_{1b(n-1)} \tag{5.6}$$

$$C_{2b(n)} = C_{2b(n-1)} \tag{5.7}$$

Where
C_{1b} = bulk aqueous-phase manganese concentration (mol/m^3)
C_{2b} = bulk aqueous-phase free chlorine concentration (mol/m^3)
n = representative point of depth in the multi-port

To solve the model steady-state equations by numerical method, at first, an initial guess value of 0.001 mg/L was assigned for the soluble Mn concentration (C_{1b}) at the bottom of the multi-port and hence, the DO concentration (C_{2b}) at the same depth was then calculated using Equation 5.5. Then corresponding C_{1sa} was calculated by iterative process from Equation 5.4. Thereafter, soluble Mn concentration at different depths was calculated from Equation 5.2 with the help of the boundary conditions (Equations 5.6 and 5.7) and following approximations shown in Equation 5.8 and Equation 5.9.

$$\frac{C_{1B}}{\partial z} = \frac{C_{1B(i+1)-} C_{1B(i-1)}}{2\Delta z} \quad (5.8)$$

$$\frac{\partial^2 C_{1B}}{\partial z^2} = \frac{C_{1B(i+1)-} 2C_{1B(i)} + C_{1B(i-1)}}{\Delta z^2} \quad (5.9)$$

The error between the influent Mn concentration (corresponding to the media depth of 0") obtained by the above calculation and the actual influent Mn concentration for the particular experimental scenario was calculated and accordingly the initial guess value for the Mn concentration at the bottom of the multi-port was adjusted. The numerical iteration process was then repeated till the error between the calculated influent Mn concentration and the actual influent Mn concentration was eliminated. After solution of the steady-state equations, soluble Mn concentration profile with depth of the multi-port column was obtained. The DO concentrations along the media depth were calculated from Equation 5.3 using the same procedure.

With the exception of the oxidation rate constant (k_r) all parameters required to simulate the model were calculated as described in 5.2.3 or determined from experimental measurements as described in 5.2.3. The k_r was the only unknown parameter in this model which was determined by fitting the soluble Mn removal profiles derived from model output with experimental data from the multi-port column study as a base line. Best-fit values for k_r were determined using a Levenberg-Marquardt nonlinear regression algorithm with initial guess value of 0.00002 m^3/(mol.sec) (detailed description in section 5.2.3). The model was coded using an open-source statistical software called "R" (Version 2.15.2, The R Foundation for Statistical Computing ISBN 3-900051-07-0).

The major input parameters used in the model coding are the sampling depths, the observed Mn concentration at each of these depths, initial Mn concentration, initial DO concentration, HLR, Freundlich isotherm constants, media particle diameter and porosity. Based on the HLR, media particle diameter and porosity which are used as input, the code will appropriately use the relevant values for the other parameters such as pore-water velocity, mass transfer coefficient and axial dispersion coefficient under laminar flow region, since applied water condition in this study was in laminar flow region (i.e., Reynolds number (Re) <100).

5. 3 Estimation of model parameters

The input parameters for the model were determined for individual experiments since they were affected by applied water conditions and media characteristics. The influent Mn and DO concentrations were known for each experimental scenario. Characteristic parameters for green sand media measured in the laboratory and used in the experiment are presented in Table 5.1. Model input parameters for various hydraulic loading rates are provided in Table 5.2.

Table 5.1: Characteristic parameters for green sand media used in the experiment

Parameter name	Parameter value	Reference
Fractional pore volume, ε_B (m^3 water/m^3 bed)	0.44	Lab. experiment
Bulk density of media, ρ_b (kg media/m^3 bed)	1305	Lab. experiment
Specific surface of media, A_v (m^2 media/m^3 media)	5489	Merkle *et al.*, 1997b
Particle diameter (m)	0.0028	Lab. experiment
Media depth (inches)	8	Lab. experiment

Table 5.2: Input parameters in the model for green sand media used in the experiment

Parameter name	Hydraulic loading rate HLR, ml/(min.cm^2)	Parameter value	Reference
Pore water velocity, U (m/s)	1	3.7891×10^{-4}	Lab. experiment
Axial dispersion coefficient, D_L (m^2/s)		7.0730×10^{-07}	Suzuki (1990)
Liquid to solid mass transfer coefficient, k_f (m/s)		1.5905×10^{-05}	Suzuki (1990)
Pore water velocity, U (m/s)	2	7.5782×10^{-4}	Lab. experiment
Axial dispersion coefficient, D_L (m^2/s)		1.4146×10^{-06}	Suzuki (1990)
Liquid to solid mass transfer coefficient, k_f (m/s)		2.0039×10^{-05}	Suzuki (1990)
Pore water velocity, U (m/s)	3	11.3673×10^{-4}	Lab.experiment
Axial dispersion coefficient, D_L (m^2/s)		2.1219×10^{-06}	Suzuki (1990)
Liquid to solid mass transfer coefficient, k_f (m/s)		2.2939×10^{-05}	Suzuki (1990)
Pore water velocity, U (m/s)	4	15.1565×10^{-4}	Lab. experiment
Axial dispersion coefficient, D_L (m^2/s)		2.8292×10^{-06}	Suzuki (1990)
Liquid to solid mass transfer coefficient, k_f (m/s)		2.5247×10^{-05}	Suzuki (1990)

Fractional pore volume (ε_B) was measured as the volume of water that could be contained in a known volume of media bed. The density of the media (kg media/m^3 media) was measured by multiplying apparent specific gravity of the media with unit weight of water. This measurement was converted to bulk density of media (kg media/m^3 bed) by multiplying the media density by the fractional volume of media bed ($1-\varepsilon_B$). Particle diameter was determined as d_{50} from the sieve analysis result of green sand.

Specific surface area of the media (A_v) was calculated using known relationship of area to volume (as shows in Equation 5.10) with a fractal surface structure correction. The fractal surface correction was used because the assumption of a spherical surface structure often underestimates the specific surface area of oxide coated media (Merkle *et al.*, 1997b).

$$A_v = 6/d_p^{1.16} \quad (5.10)$$

where:
d_p = particle diameter (m)
A_v= Specific surface area of the media (m^2 media/m^3 media)

Solution characteristics were measured for each individual experiment. Initial bulk aqueous-phase soluble Mn concentration (mol/m^3) and initial DO concentration (mol/m^3) were measured with each soluble Mn profile collected experimentally. HLR was determined by dividing the volume of water passed per unit time by the cross sectional bed area of multi-port column. Pore water velocities (m/s) were calculated as the HLR divided by the fractional pore volume (ε_B). Axial dispersion coefficients, D_L (m^2/s) were calculated using Equation 5.11 as developed by Suzuki (1990), which uses Peclet number (dimensionless) to calculate D_L. Since the experimental study was under laminar flow regime (Reynolds number, Re < 100), Peclet number was determined as 1~2 for $d_p \geq 2$ mm, and $1.2d_p$ (mm) for dp < 2 mm (Suzuki, 1990). The units were then converted for use in the model.

$$D_L = (d_p.U)/P_e \quad (5.11)$$

Where
d_p = particle diameter (m)
P_e= Peclet number (dimensionless)
U=Pore water velocity (m/s)
D_L= Axial dispersion coefficient (m^2/s)

5.3.1 Isotherm constants

Isotherm constants were calculated using results of batch experiments where Mn uptake capacity of green sand was estimated under pH range of 7.2±0.1 and temperature of 28^{o}C. Several airtight containers (50 ml) containing groundwater with different initial Mn concentrations (3.39-12.91 mg/L) were prepared; to each container a different mass (0.4-1.0 gm) of green sand were added. The suspensions were then rotated and allowed to equilibrate; after filtering, Mn concentrations of the water samples were measured. The results (data tabulated in Appendix B) were used to determine Freundlich isotherm constants for green sand media from a log-log plot (as shown in Figure 5.2) of the uptake capacity data. Freundlich isotherm constants were verified by plotting the isotherm relationship along with the experimental data as shown in Figure B8 of Appendix B. The numerical values for the Freundlich isotherm constants are as follows:

Freundlich isotherm constant, K [(mol/kg)/(mol/m^3)^(1/n)] = 0.049

Freundlich isotherm constant, n [dimensionless] = 2.358

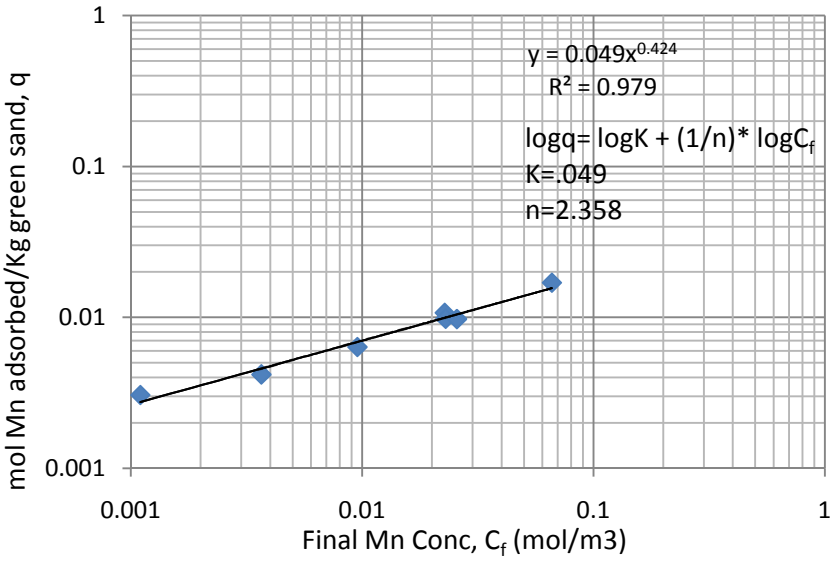

Figure 5.2: Log-log plot of green sand uptake capacity data at pH=7.2±0.1 to determine Freundlich isotherm constants

To determine the Langmuir isotherm constant, C_f/q is plotted against C_f(Figure 5.3). As shown in the figure, a linear fit to the data yields the vaules of the parameters for the Langmuir equation (Equation 3.3). The values of the Langmuir isotherm constants are as follows:

Langmuir isotherm constant: Q=0.01961 mol/kg

Langmuir isotherm constants: b=59.573 m^3/mol

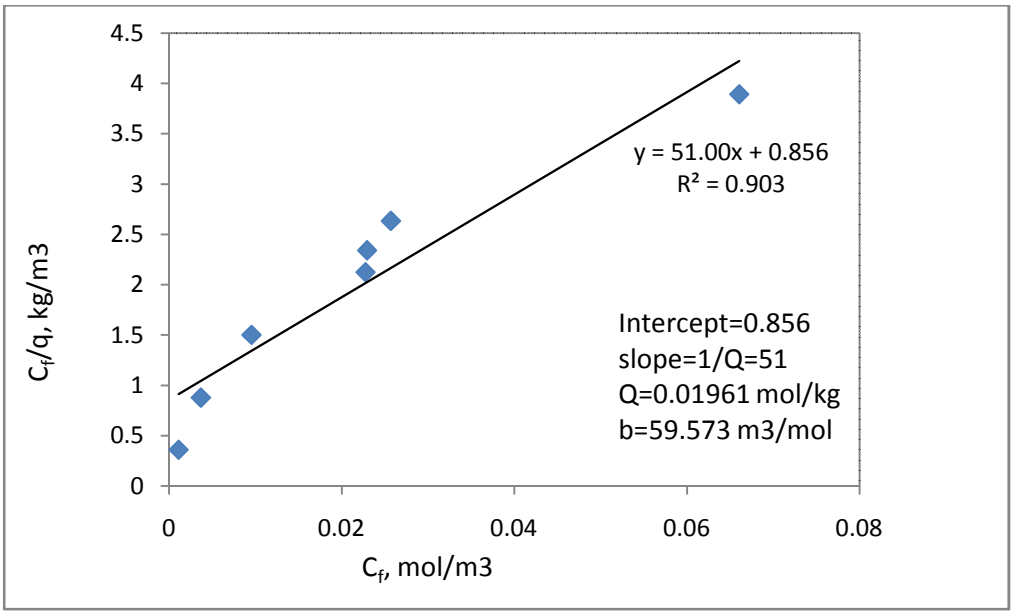

Figure 5.3: C_f/q against C_f plot to determine the parameters of Langmuir equation

Comparing Fig. 5.2 and Fig. 5.3, it is obvious that the Freundlich equation better fits the experimental Mn uptake data than the Langmuir equation. Therefore, Frendlich isotherm parameters have been incorporated in the model equations.

5.3.2 k_f (liquid to solid mass transfer coefficient)

The value of k_f was calculated by using correlations developed for various water flow conditions proposed by Suzuki (1990) which uses the Sherwood number (S_h). The appropriate criteria condition was determined by calculating Schmidt number (Sc= kinematic viscosity of water divided by the bulk liquid diffusivity ($D_{L,diff}$) at particular temperature). Suzuki (1990) developed various equations to calculate Sherwood number at various flow regimes as shown in Equation 5.12 and Equation 5.13. Since, the experimental study was under laminar flow regime (Re<100), S_h was determined using Equation 5.12. Thereafter, calculated S_h was used to determine k_f using Equation 5.14 (Suzuki, 1990).

$$S_h=(1.09/\varepsilon_B)\, Sc^{1/3}\, R^{1/3} \quad [\text{for } 0.0015<Re<100] \tag{5.12}$$

$$S_h=1.1\, Sc^{1/3}\, R^{0.6} \quad [\text{for } Re>100] \tag{5.13}$$

$$S_h=(k_f/d_p)/\, D_{L,diff} \tag{5.14}$$

Where

k_f = Liquid to solid mass transfer coefficient (m/s)
d_p = particle diameter (m)

$D_{L,diff}$ = bulk liquid diffusivity (m^2/s) = $2.34x10^{-9}$ m^2/s at 28°C temperature of water.

S_h = Sherwood number (dimensionless)
Re = Reynolds number (= Udp/ ν)
ν = kinematic viscosity of water (m^2/s) = $0.8372x10^{-6}$ m^2/s at 28°C temperature of water

5.3.3 k_r (Oxidation rate constant)

Estimated Freundlich isotherm constants for Mn uptake onto the green sand media under experimental condition was the key to the modeling efforts. With the K and 1/n values available and other model parameters being directly provided as input or calculated (e.g., k_f calculated by Suzuki, 1990 correlations) the only unknown parameter in the model was k_r, which is related to the rate of surface oxidation of Mn by DO. Therefore, it was possible to calculate the appropriate value of k_r by fitting the bulk-water Mn removal profiles generated from the laboratory multi-port column studies (conducted under various experimental conditions of HLR, pH, initial influent Mn concentration) and the model output.

The main objective to develop the model was to predict the soluble Mn removal along the depth of Mn-oxide coated column under different conditions. However, the model had to be calibrated to find out the value of k_r by curve fitting in various operating conditions to predict soluble Mn removal. The experimental data collected from the multi-port column study served as a good baseline for the model calibration.

The steady-state model equations (Equations 5.2-5.4) were coded into anopen source statistical software called "R". In the model, the soluble Mn concentration was found to be non-linearly dependent on the unknown parameter k_r. Hence, the best-fit parameter was determined by the process of minimization of the least square vector ($\chi 2$) returned by the function which predicted the soluble Mn concentration at various depths of the multi-port column. However, the minimization had to proceed iteratively since the non-linear dependence, i.e., trial value (0.00002 $m^3/(mol.sec)$) was initially given for the unknown parameter k_r and then a procedure was applied that improved the trial solution. The procedure was then repeated until $\chi 2$ value effectively stopped decreasing. The procedure used for solving the non-linear model was a variation of the Levenberg-Marquardt method (Press *et al.*, 2002). The best-fit estimate of k_r obtained was the one which resulted in a close match between the actual Mn removal profiles (plotted from experimental data) and the model predicted Mn removal profiles across the multi-port column depth. The k_r values obtained under different flow rates, pH values, and initial Mn concentrations were compared to identify the trend.

5.3.3.1 k_r at various flow rate conditions

Figures 5.4, 5.5, and 5.6 show model fit to experimental data of bulk-water Mn profile in green sand media at different flow rates (experimental results described earlier in Section 4.3.1), keeping the other conditions (noted in Table 4.1) nearly similar. In all of the figures

"bulk Mn removal profile (experimental data)" refers to the actual data of bulk-water Mn profile obtained from the experiment and "bulk Mn removal profile (model output)" refers to the model output of bulk water Mn profile obtained by fitting the model with experimental data. All of the figures show that the model fitted experimental Mn removal profile well. The results for the best-fit k_r obtained from the model fitting for the above conditions are tabulated in Table 5.3. Based on these results, it was observed that under experimental conditions, the k_r values increased with an increase in flow rate. This is because higher flow rate increases the availability of soluble Mn per unit time (by increasing linear driving force) to be adsorbed and finally be oxidized. This result agrees well with the findings of Merkle et. al. (1997b), where a higher flow rate (2.5-10 gpm/ft^2) and lower influent Mn concentration (0.15-0.7 mg/l) with hypochlorous acid (HOCl) as oxidizing agent had been used. Figure 5.7 illustrates the variation of k_r as a function of flow rate under experimental condition. The figure presents that under experimental condition, a power equation ($y=6x10^{-05}x^{0.444}$) trend line well predicts the relationship between k_r and flow rate with R^2 value of 0.997.

Table 5.3: Model fit k_r values at various flow rate conditions

Flow rate ml/(min.cm^2)	Initial Mn concentration (mg/l)	Alkalinity as $CaCO_3$ (mg/l)	pH	DO (mg/L)	Temperature (^{o}C)	Best fit kr estimated by the model (m^3/(mol.sec)	Standard error
1	4.2	254±5	7.2±0.1	7.5±0.1	28	$6.030x10^{-5}$	$1.102x10^{-06}$
2	4.83	254±5	7.2±0.1	7.5±0.1	28	$8.373x10^{-5}$	$2.589x10^{-06}$
3	4.5	254±5	7.2±0.1	7.5±0.1	28	$9.790x10^{-5}$	$3.525x10^{-06}$

To check the robustness of the model and validity of the established relationship, the value of k_r was calculated by using the established correlation ($y=6E-05x^{0.444}$) at flow rate of 4 ml/(min.cm^2) to generate data for plotting bulk-water Mn profile predicted by model (as shown in figure 5.8). Another bulk-water Mn removal profile was drawn in the same figure generated by the experimental data (as shown in Fig. 4.9(a)) conducted at similar operating conditions used to generate the model data. Figure 5.8 shows that under experimental conditions, both of the soluble Mn removal profiles (model predicted and experimental) fits very well, indicating that the established relationship of k_r and flow rate could be effectively used to predict Mn removal profile under experimental condition. However, the applied water conditions studied here were in laminar flow region (Reynolds number, Re< 100); hence, more tests should be run at higher flow rate to validate this relationship in turbulent flow region.

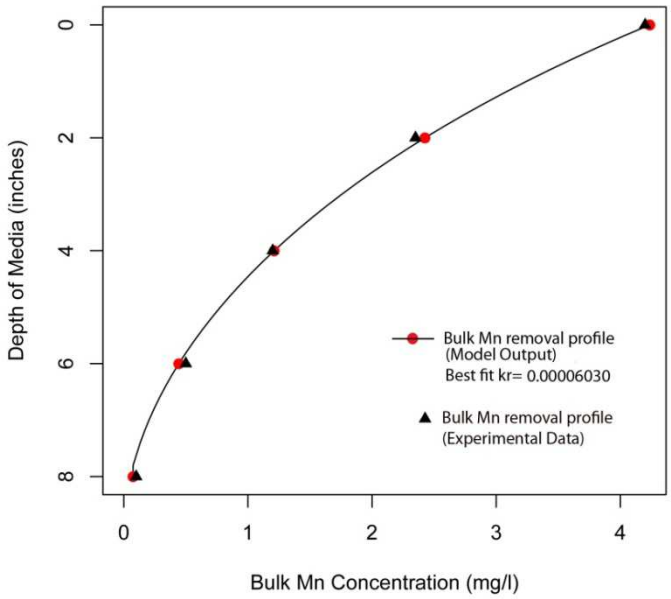

Figure 5.4: Model fit to experimental data of bulk-water Mn profiles in green sand media at a flow rate of 1 ml/min.cm^2

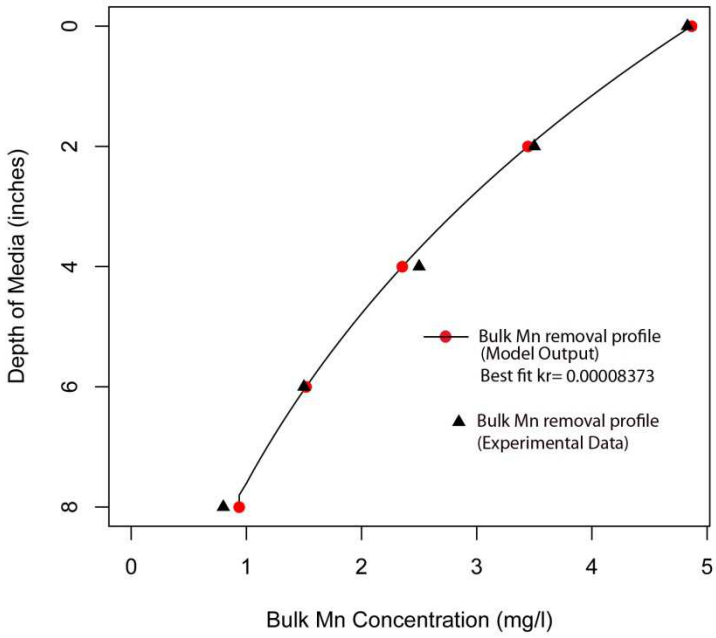

Figure 5.5: Model fit to experimental data of bulk-water Mn profiles in green sand media at a flow rate of 2 ml/min.cm^2

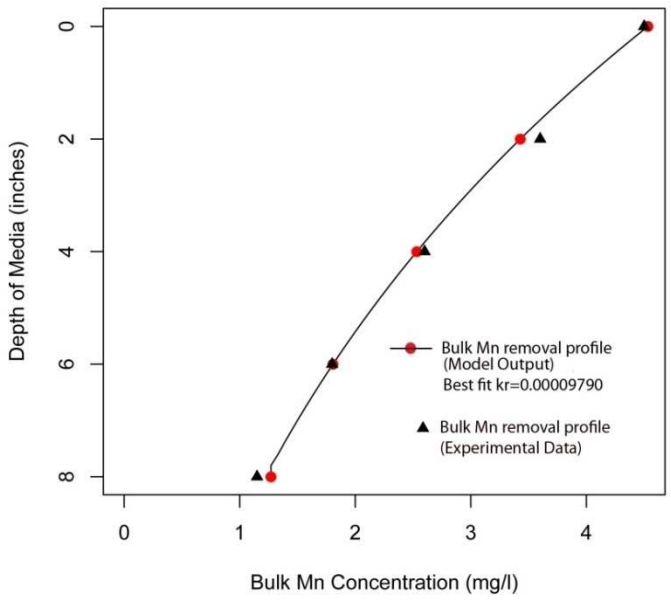

Figure 5.6: Model fit to experimental data of bulk-water Mn profiles in green sand media at a flow rate of 3 ml/min.cm^2

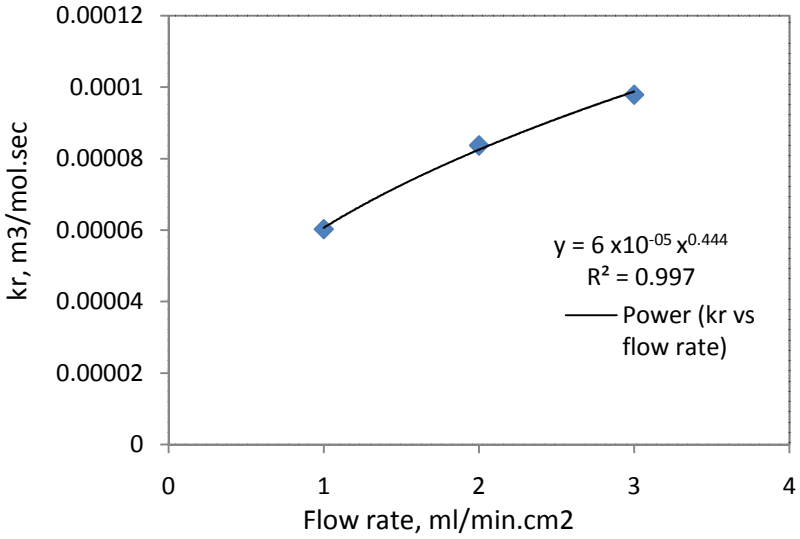

Figure 5.7: Oxidation rate constant, k_r (calculated from model fitting) as a function of flow rate (Initial Mn concentration= 4.2-4.83 mg/l, Alkalinity as $CaCO_3$=254±5 mg/l, pH=7.2±0.1, DO=7.5±0.1, Temp=28 °C)

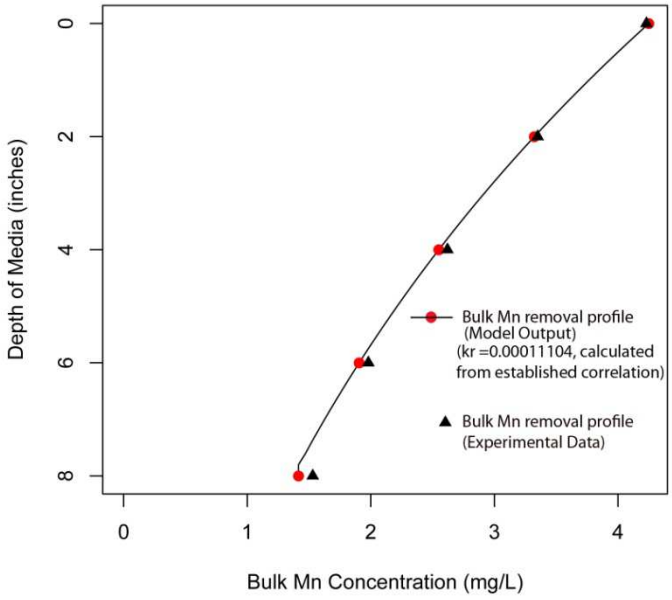

Figure 5.8: Model result (with k_r calculated from established correlation) to experimental data of bulk-water Mn profiles in green sand media at a flow rate of 4 ml/min.cm^2

5.3.3.2 k_r at various initial Mn concentration

Figures 5.9, 5.10 and 5.5 show model fit to experimental data of bulk-water Mn profiles in green sand media at different initial Mn concentrations, keeping the other applied water conditions (noted in Table 4.2) nearly similar. The figures show that the model fitted the experimental Mn profile very well. The results for the best-fit k_r obtained from the model fitting for the above conditions are tabulated in Table 5.4. Based on these results, it was observed that under experimental conditions, the k_r values increased with an increase in initial Mn concentration. This is because higher initial Mn concentration increases the availability of soluble Mn (by increasing liner driving force) to be adsorbed and finally be oxidized. Figure 5.11 illustrates the variation of k_r as a function of initial Mn concentration under experimental condition. The figure shows that under experimental condition, a power equation ($y=2x10^{-05}x^{0.971}$) trend line well predicts the relationship between k_r and flow rate with R^2 value of 0.999.

Table 5.4: Model fit k_r values at various initial Mn concentrations

Initial Mn concentration (mg/l)	Flow rate (ml/(min.cm2))	Alkalinity as $CaCO_3$ (mg/l)	pH	DO (mg/L)	Temp (^oC)	Best fit kr estimated by the model (m^3/(mol.sec)	Standard error
1.15	2	254±5	7.2±0.1	7.5±0.1	28	$2.075x10^{-5}$	$7.133x10^{-07}$
2.31	2	254±5	7.2±0.1	7.5±0.1	28	$4.229x10^{-5}$	$7.183x10^{-07}$
4.83	2	254±5	7.2±0.1	7.5±0.1	28	$8.373x10^{-5}$	$2.589x10^{-06}$

To check the robustness of the model and validity of the established relationship, the value of k_r was calculated by using the established correlation ($y=2x10^{-05}x^{0.971}$) at initial Mn concentration of 11.2 mg/l to generate data for plotting bulk-water Mn profile predicted by model (as shown in figure 5.12). Another bulk-water Mn profile was drawn in the same figure generated by experimental data (as shown in Fig. 4.13(a)) conducted at similar operating conditions used to generate the model data. Figure 5.12 shows that under experimental conditions, both of the soluble Mn profiles (model predicted and experimental) fits very well, indicating that the established relationship of k_r and initial Mn concentration could be effectively used to predict Mn removal profile under experimental condition. However, the applied water conditions studied here were in laminar flow region (Reynolds number, Re< 100); hence, more tests should be run at higher flow rate to validate this relationship in turbulent flow region.

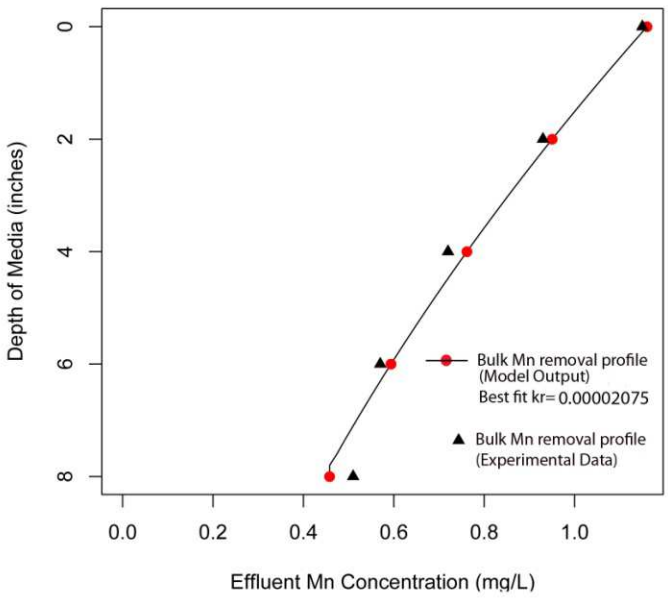

Figure 5.9: Model fit to experimental data of bulk-water Mn profiles in green sand media with Initial Mn concentration of 1.15 mg/l

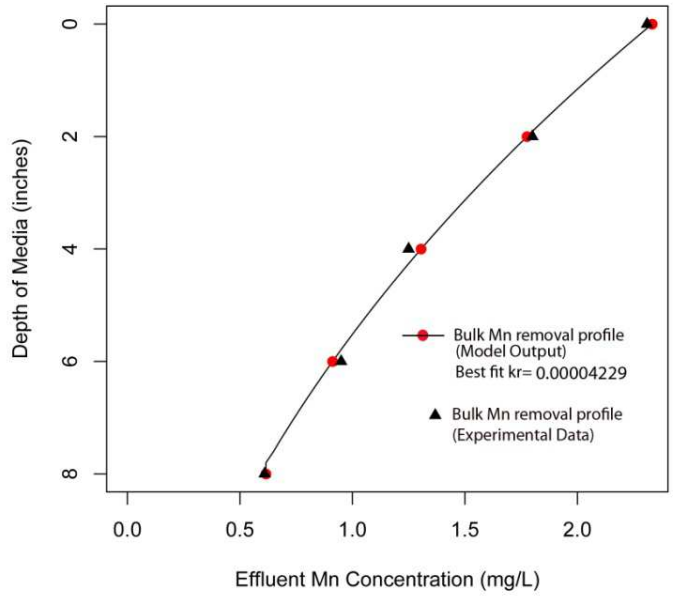

Figure 5.10: Model fit to experimental data of bulk-water Mn profiles in green sand media with initial Mn concentration of 2.31 mg/l

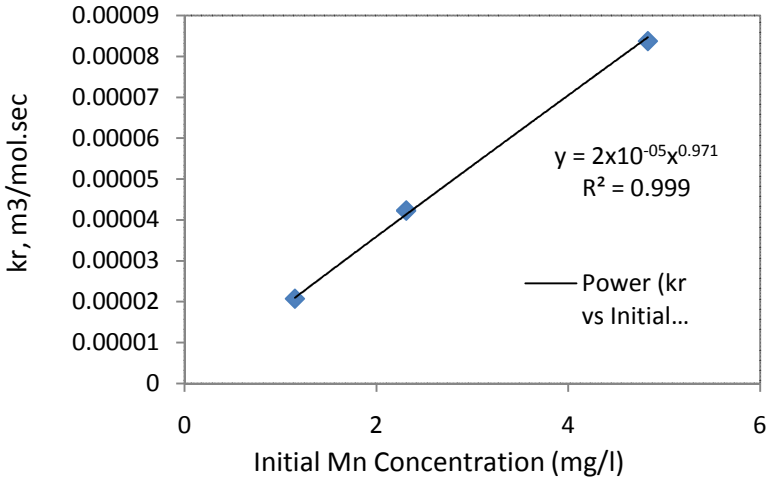

Figure 5.11: Oxidation rate constant, k_r (calculated from model fitting) as a function of initial Mn concentration (Influent water: Flow rate= 2 ml/min.cm^2, Alkalinity as $CaCO_3$=254±5 mg/l, pH=7.2±0.1, DO=7.5±0.1, Temp=28 ^oC)

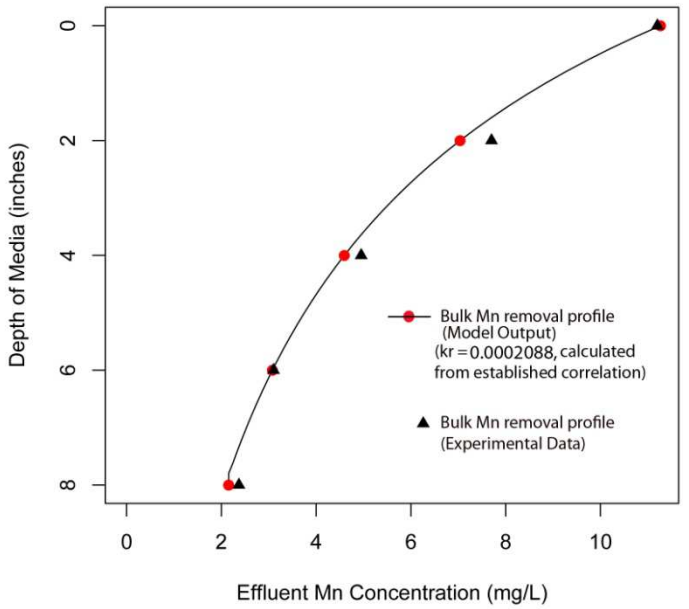

Figure 5.12: Model result (with k_r calculated from established correlation) to experimental data of bulk-water Mn profiles in green sand media with initial Mn concentration of 11.2 mg/l

5.3.3.3 k_r at different pH values

Figures 5.13, 5.5 (discussed earlier) and 5.14 show model fit to experimental data of bulk-water Mn profiles in green sand media at different pH conditions, keeping the other applied

water conditions (noted in Table 4.3) nearly similar. The figures show that the model fitted experiment Mn removal profile well. The results for the best-fit k_r obtained from the model fitting for the above conditions are presented in Table 5.5. Based on these results, it was observed that under experimental conditions, the k_r values increased with an increase in influent water pH. Possibly, this is because alkaline pH promotes adsorption by increasing the amount of available Mn adsorption sites on the Mn oxide coated media (Morgan and Stumm, 1964).

Figure 5.15 shows the variation of k_r as a function of influent water pH under experimental condition. The figure shows that under experimental condition, a power equation ($y = 2E\text{-}07x^{3.091}$) trend line well predicts the relationship between k_r and flow rate with R^2 value of 0.990. However, more experimental data are needed to determine a large number of model fitted k_r values to validate this relationship. Moreover, the applied water conditions studied here were in laminar flow region (Reynolds number, Re< 100); hence, more tests should be run at higher flow rate to validate this relationship in turbulent flow region. It should be noted that the Freundlich isotherm constants determined in solution pH of 7.2±0.1 was used to simulate the model for all influent water with pH of 6.0±0.2, 7.2±0.1 and 8.0±0.1 which would introduce some error in fitted k_r values. Since, Freundlich isotherm constants vary with solution pH so they should be determined for each of type of solution pH by individual experiments.

Table 5.5: Model fit k_r values at various influent water pH

pH	Flow rate (ml/(min.cm2))	Alkalinity as $CaCO_3$ (mg/l)	Initial Mn concentration(mg/l)	DO (mg/L)	Temperature (^oC)	Best fit kr estimated by the model (m^3/(mol.sec)	Standard error
6.0±0.2	2	200±5	5.14	7.5±0.1	28	$5.605x10^{-5}$	$4.121x10^{-06}$
7.2±0.1	2	254±5	4.83	7.5±0.1	28	$8.373x10^{-5}$	$2.589x10^{-06}$
8.0±0.1	2	300±5	4.88	7.5±0.1	28	$1.369x10^{-4}$	$1.174x10^{-05}$

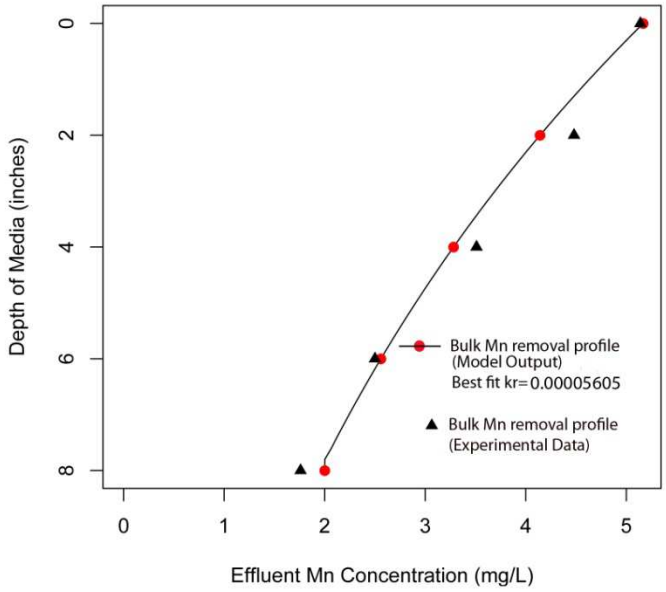

Figure 5.13: Model fit to experimental data of bulk-water Mn profiles in green sand media with influent water pH= 6.0±0.2

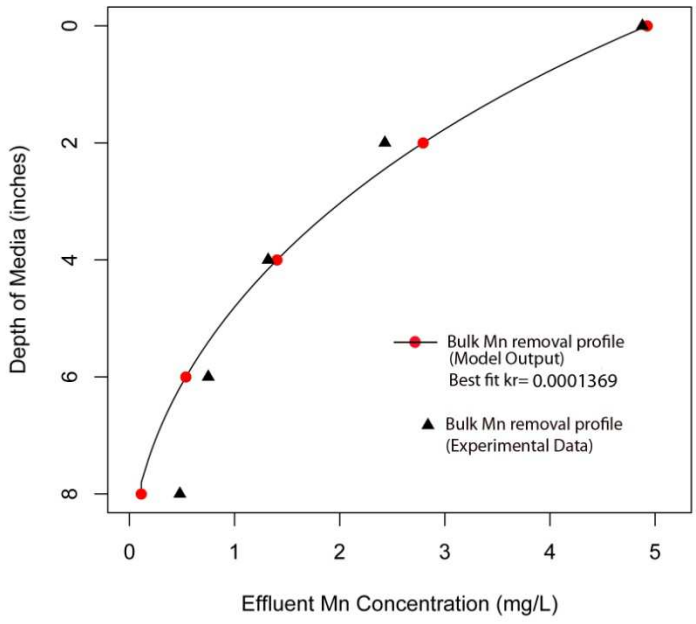

Figure 5.14: Model fit to experimental data of bulk-water Mn profiles in green sand media with influent water pH= 8.0±0.1

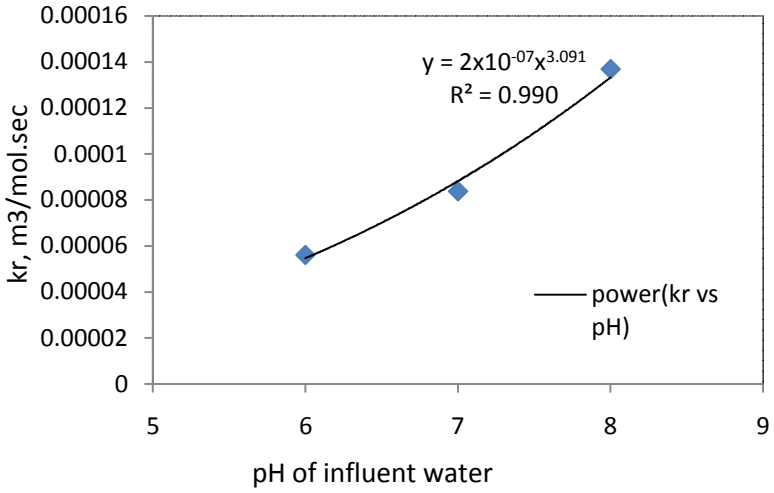

Figure 5.15: Oxidation rate constant, k_r (calculated from model fitting) as a function of pH of influent water (Influent water: Initial Mn concentration= 4.83-5.14 mg/l, HLR=2 ml/min.cm^2, Alkalinity as $CaCO_3$= 200-300 mg/l, DO=7.5±0.1, Temp=28^0 C)

5.4 Sensitivity analysis

Knowledge of sensitivity of parameter of a model is important to gain an insight into the dominant processes and important model parameters. In this study, sensitivity analysis of the model with respect to various operational parameters was performed using the data from operating condition shown in Figure 5.5. For this analysis, the HLR, Freundlich isotherm constants (K, n), oxidation rate constant (k_r), axial dispersion coefficient (D_L), mass transfer coefficient (k_f), and specific surface area of media (A_v) were each varied in turn. Each input parameter was varied by approximately ±50% of the original value used in the model (except specific surface area of media which were varied by ±20%), keeping the other parameters similar. The resulting bulk-water Mn concentration profiles were plotted with the original profile for comparison. The results of the sensitivity analysis are displayed as predicted bulk-water Mn concentration profiles in Figures 5.16 through 5.22.

As shown in Figure 5.16, flow rate (i.e., contact time) has a significant effect on the model predicted bulk-water Mn concentration profile. Removal of Mn increases significantly with decrease in flow rate and vice versa, which is supported by the experimental data presented in Fig.4.10.

Freundlich isotherm constants (i.e., adsorption of Mn onto the media surface), play a vital role, as can be seen in Figures 5.17 and 5.18. As shown in Fig. 5.18, the removal system is extremely sensitive to the Freundlich constant n as clearly shown by the noticeable change in shape of the predicted Mn concentration profiles. Similar effect was found in previous research conducted by Bierlein (2012) who used the model previously developed by Zuravnsky (2006) with modifications. Interestingly, when adjusting K and k_r, the model

changes in a very similar manner (Figures 5.17 and 5.19); in fact, the profiles predicted by adjusting K by ±50% are identical to those predicted by adjusting k_r by ±50%. Similar result was observed by Bierlein (2012) who explained this behavior mathematically by establishing an alternative mathematical form of equation 5.4. Considering the reaction term in that alternative equation, it was clear that adjusting either K or k_r by the same amount will have the exact same effect on model output. Overall, this behavior suggests that as the adsorptive capacity increases the oxidation rate becomes limiting, and as the oxidation rate increases, adsorption becomes limiting.

Axial dispersion coefficient, D_L (Figure 5.20), mass transfer coefficient, k_f (Figure 5.21) and specific surface area of media, A_v (Figure 5.22) did not show any significant effect on the model output. Since, these parameters were estimated by empirical relationships established in Suzuki (1990) and Merkle et al. (1997b), it was important to note that they do not have a significant effect on the model prediction, reducing the amount of error that could be associated with the use of the estimated value from empirical relationship.

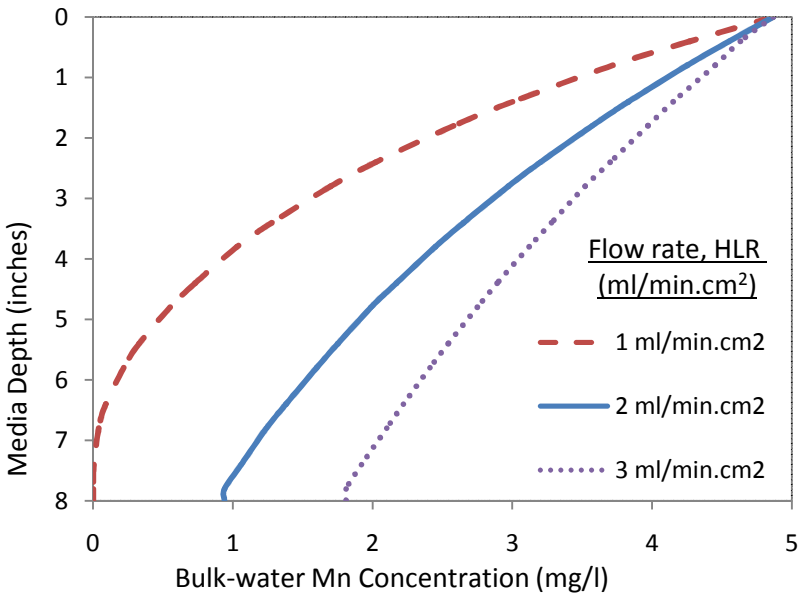

Figure 5.16: Effect of adjusting flow rate (HLR) [unit: ml/min.cm^2] by ±50% on the model predicted bulk-water Mn concentration profile

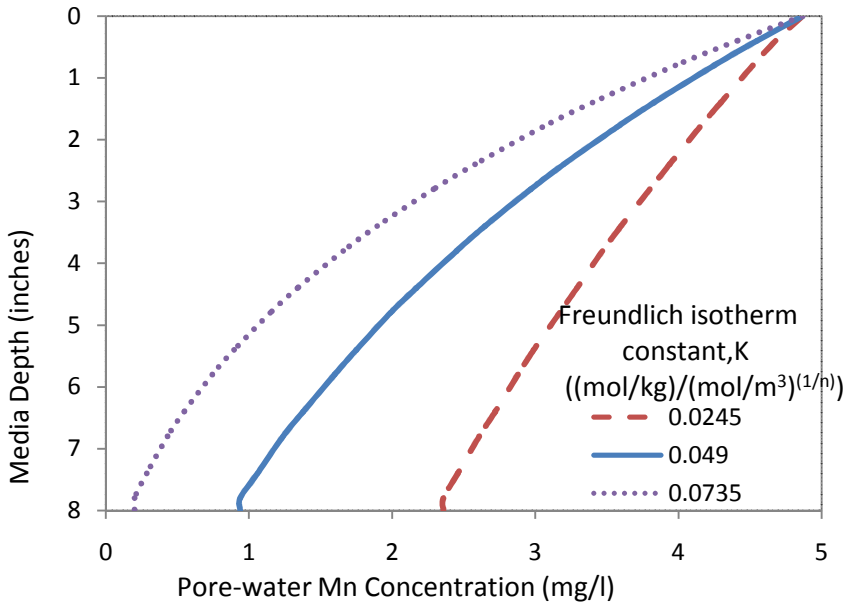

Figure 5.17: Effect of adjusting Freundlich isotherm constant (K) [unit: $(mol.kg^{-1})(mol.m^{-3})^{-(1/n)}$] by ±50% on the model predicted bulk-water Mn concentration profile

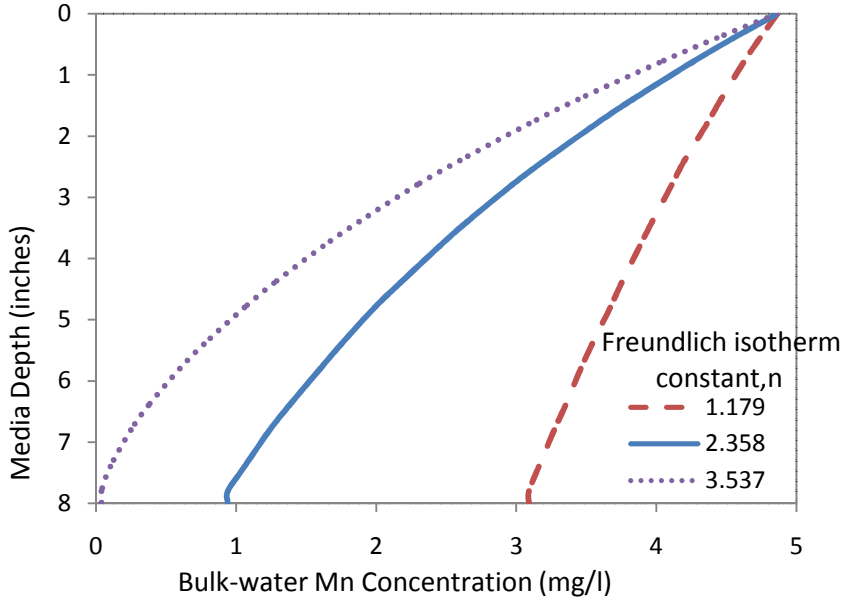

Figure 5.18: Effect of adjusting Freundlich isotherm constant (n) [dimensionless] by ±50% on the model predicted bulk-water Mn concentration profile

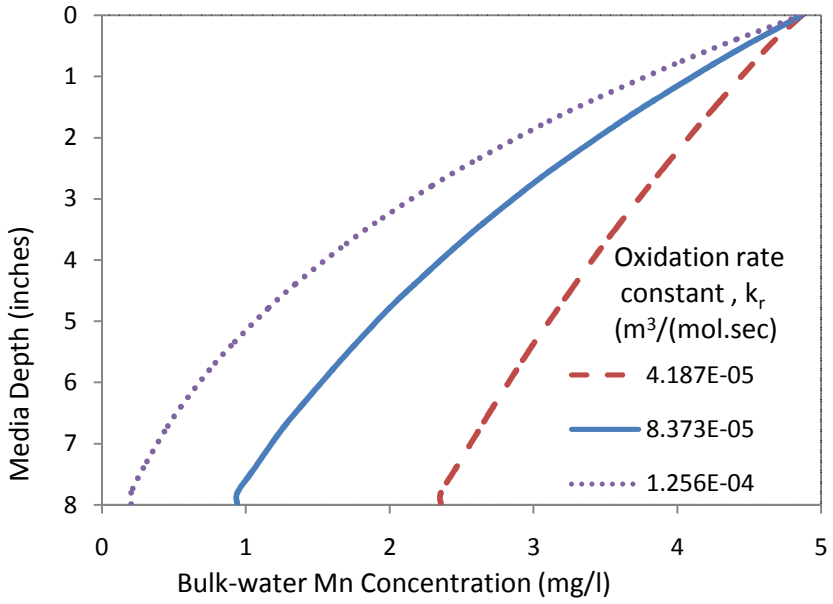

Figure 5.19: Effect of adjusting oxidation rate constant (k_r) [unit: m^3/mol.sec] by ±50% on the model predicted bulk-water Mn concentration profile

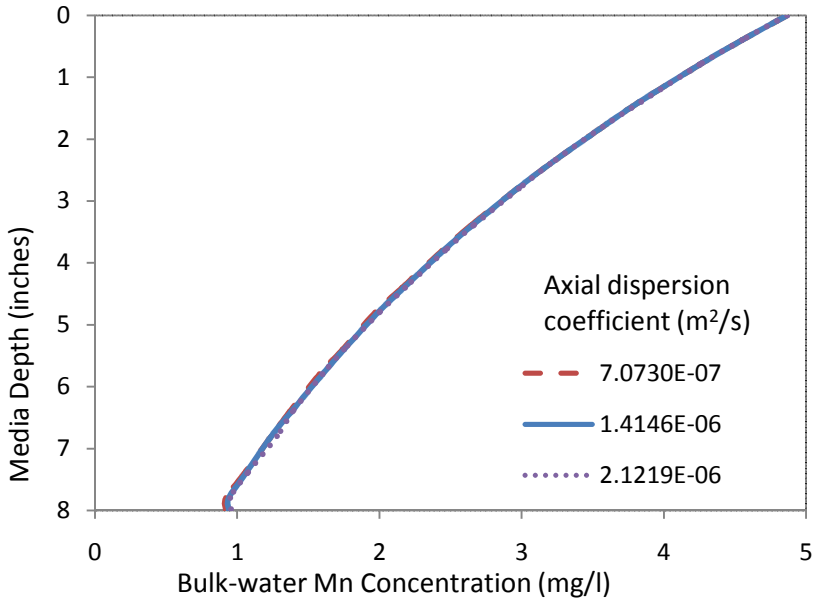

Figure 5.20: Effect of adjusting Axial dispersion coefficient (D_L) [unit: m^2/s] by ±50% on the model predicted bulk-water Mn concentration profile

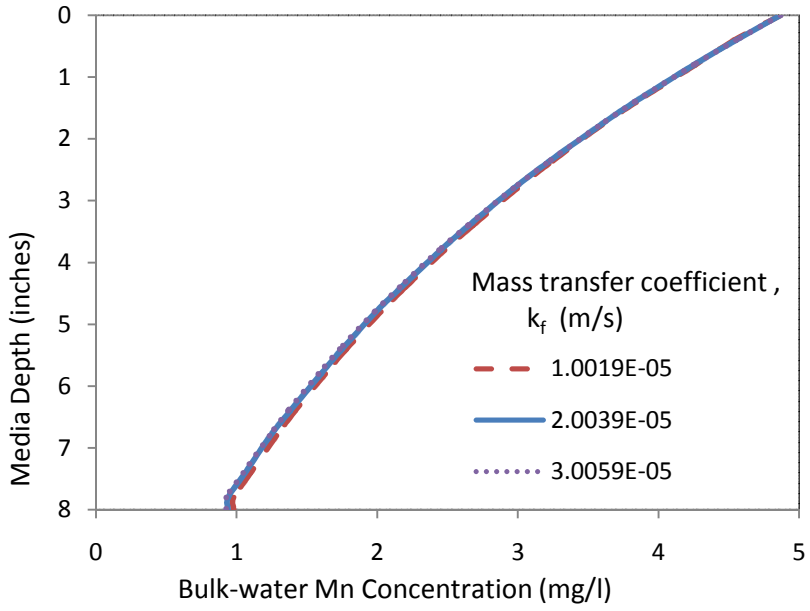

Figure 5.21: Effect of adjusting mass transfer coefficient (k_f) [unit: m/s] by ±50% on the model predicted bulk-water Mn concentration profile

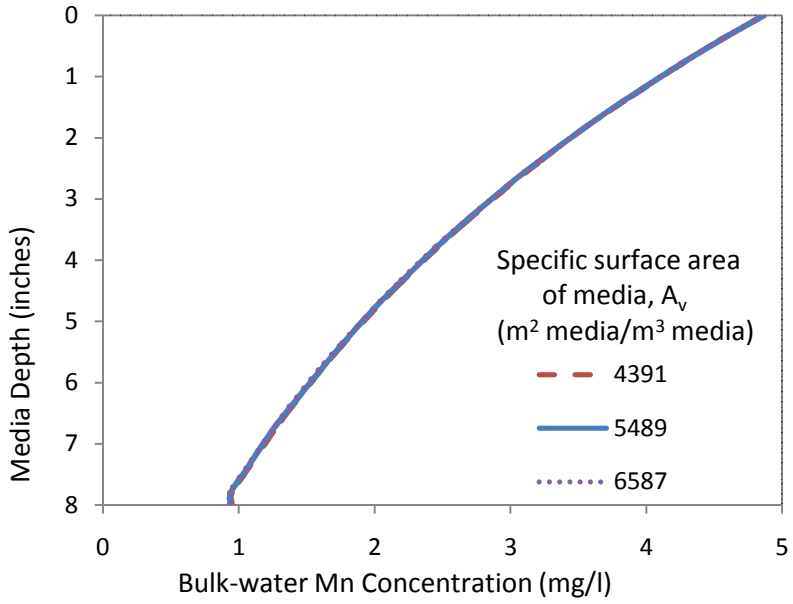

Figure 5.22: Effect of adjusting Specific surface area of media (A_v) [unit: m^2 media/m^3 media] by ±20% on the model predicted bulk-water Mn concentration profile

5. 5 Summary

To predict the soluble Mn removal via adsorption and surface oxidation, a continuous regeneration model previously developed by Zuravnsky (2006) was used in this study with modifications (using DO as oxidant to regenerate the green sand media). The model

equations were solved numerically. All the input parameters (except oxidation rate constant, k_r) to simulate the model were determined using laboratory experiments and empirical relationships. The k_r was the only unknown parameter in this model which was determined by fitting the bulk-water Mn profiles derived from model output with experimental data from the multi-port column study. The model was coded using an open-source statistical software called "R".

The developed model was used to fit experimental data (Mn removal profiles) under different flow rates, pH values, and initial Mn concentrations in order to determine the best-fit estimates of k_r. In each case, the model fitted experimental Mn removal profile well. The k_r values obtained under different experimental conditions were analyzed to develop the relationship of k_r with flow rates, pH values, and initial Mn concentrations:

i. The k_r value was found to increase with increase in flow rate. This is because higher flow rate increases the availability of soluble Mn per unit time (by increasing linear driving force) to be adsorbed and finally be oxidized. A power equation was developed to express the relationship between k_r and flow rate, and the validity of the established relationship and the model was checked estimating k_r value and predicting Mn profile for a flow rate of 4 ml/min.cm^2, and matching the predictions with experimental data.
ii. The k_r values increased with an increase in initial Mn concentration. This is because higher initial Mn concentration increases the availability of soluble Mn (by increasing liner driving force) to be adsorbed and finally be oxidized. A power equation has been proposed to describe the relationship between k_r and initial Mn concentration, and the validity of the established relationship and the model was checked by estimating k_r value and predicting Mn profile for an initial Mn concentration of 11.2 mg/l, and comparing the prediction with experimental data.
iii. The k_r values increased with an increase in influent water pH. Possibly, this is because alkaline pH promotes adsorption by increasing the amount of available Mn adsorption sites on the Mn oxide coated media (Morgan and Stumm, 1964). A power equation was able to relate k_r and with water pH.

Sensitivity analysis of the model with respect to various operational parameters was performed to gain an insight into the dominant processes and important model parameters. Flow rate (i.e., contact time), Freundlich constants and k_r were found to have significant effect on the model predicted bulk-water Mn concentration profile. In contrast, axial dispersion coefficient (D_L), mass transfer coefficient (k_f) and specific surface area of media (A_v) did not show any significant effect on the model output.

CHAPTER 6: CONCLUSIONS

6.1 Introduction

The main objective of this study is to develop better understanding of the Mn removal mechanism from ground water during filtration through Mn oxide coated media, and develop a model to simulate adsorption and surface oxidation of Mn during filtration. This Chapter presents the major conclusions from the present study and provides recommendations for future research.

6.2 Conclusions

Based upon the results obtained in this research, the following major conclusions were drawn:

1. Experimental results suggest that in the absence of bicarbonate in the influent water, the removal of Mn during filtration through a Mn-oxide coated media is characterized by only adsorption, and the system gradually approaches toward the breakthrough point (when effluent Mn concentration becomes equal to the influent Mn concentration). The removal capacity of the media, under such conditions, decreases as the adsorption sites on the media are exhausted with increasing filter run time.

2. In the presence of Bicarbonate in the influent water, Mn removal efficiency of Mn-oxide coated media increases significantly and the system does not approach the breakthrough point. There are two possible reasons for this phenomenon:
   i. Possible surface mediated oxidation (at the surfaces of Mn-oxide coated filter media) of adsorbed Mn by DO in the presence of Bicarbonate, which produces insoluble Mn-oxide and regenerates the exhausted media.
   ii. Possible formation of insoluble $MnCO_3(s)$ in the presence of Bicarbonate which increases removal efficiency by removing Mn within the filter media by precipitation.

3. Results of laboratory column experiments suggest that the dominant mechanism for the removal of Mn(II) is continuous regeneration of Mn-oxide coated media, caused by the surface mediated oxidation of adsorbed Mn by DO in the presence of Bicarbonate, rather than $MnCO_3(s)$ precipitation. Results of multi-port column experiments also support the concept of regeneration of Mn-oxide coated media.

4. Results of laboratory multi-port column experiments provided useful insights on the effects of flow rate, initial Mn concentration and pH on the removal of Mn within the filter media:

i. Mn removal has been found to increase with decreasing flow rate, which promote longer contact time between the filter media and water.
ii. Mn removal capacity of the media has been found to increase with increase in initial Mn concentration of the influent water. This is possibly due to the fact that higher initial Mn concentration increases the linear driving forced (LDF), which increases the soluble Mn mass transfer through the liquid film and hence, removal capacity of the media increases.
iii. The Mn removal capacity has also been found to increase with increase in pH value of influent water; it is well established that Mn oxidation is favored in higher pH range.

5. A model, primarily developed by Zuravnsky (2006), was modified to predict the soluble Mn removal via adsorption and surface oxidation onto Mn-oxide coated media for steady state conditions under continuous media regeneration by DO. The model was calibrated (to find out the value of k_r by curve fitting) using experimental data under various operating conditions (flow rate, initial Mn concentration of influent water, pH of influent water), and subsequently used to predict soluble Mn removal. The model was able to predict Mn removal reasonably well.

6. The sensitivity analysis of the model suggest that flow rate, Freundlich isotherm constants (K, n) and k_r have a significant effect on the model predicted bulk-water Mn concentration profile, while the effects of axial dispersion coefficient (D_L), mass transfer coefficient (k_f) and specific surface area of media (A_v) are not significant.

6.2 Recommendations

1) Effect of DO and Bicarbonate concentration in water on the removal efficiency of green sand media may be investigated by experimental study, and the developed model may be calibrated accordingly.

2) Scanning electron microscope (SEM) analysis of the media surface can be performed to find out the species formed during treatment to reinforce the concept of removal mechanism identified in this study.

3) The experimental conditions applied in this study were in laminar flow region (Reynolds number, Re< 100); hence, more tests can be run at higher flow rate to check the validity of the model in turbulent flow region.

4) Freundlich isotherm constants determined by batch experiment in this study may be slightly different for conditions prevailing in column experiment, since, the linear driving force (caused by the difference between the adsorbate concentration in the bulk solution and the concentration at the external surface of media) gets reduced

with treatment time in batch experiment, while it remains fixed in column experiment. Various combinations of column experiments can be conducted to find out values of Freundlich isotherm constants, and check if this value differs than the batch experiment value determined in current study. In addition, effect of pH, Mn-content of media, and temperature on the Freundlich isotherm constants may be investigated by experimental study.

5) Experimental study can be carried out to assess the effect of washing/ backwashing on physic-chemical characteristics and stability of green sand media.

6) The calibrated model may be simulated to generate the design data for depth of media required to achieve desired removal efficiency at various applied water conditions. Using the design data, a plant can be constructed to study the validity of the developed model to predict Mn removal in bench/pilot-scale treatment system.

REFERENCES

American Water Works Association (AWWA) (1994) *AWWA mainstream,* Denver, Colo.

Bierlein, K.A. (2012) "Modeling Manganese Sorption and Surface Oxidation During Filtration" M.Sc. Engineering Thesis, Civil & Environmental Engineering Department, Virginia Polytechnic Institute and State University.

BGS and DPHE (2001) "Arsenic contamination of groundwater in Bangladesh" Final report, British Geological Survey and Department of Public Health Engineering, February 2001.

BGS and WaterAid (2001) "Groundwater quality: Bangladesh" British Geological Survey and WaterAid Bangladesh.

Bouchard, R. (2005) "Evaluation of Manganese Removal at Aquarion Water Company (AWC) Surface Water Treatment Plants" M.S. in Env. Eng. Thesis, Department of Civil & Environmental Engineering. Amherst, MA, University of Massachusetts.

Bricker, O. (1965) "Some stability relations in the system Mn-O-HO at 25^{o}C and one atmosphere total pressure" *Amer. Mineral.* **50** 1296-1354.

Burns, F. L. (1998) "Case Study: Automatic Reservoir Aeration to Control Manganese in Raw Water Maryborough Town Water Supply Queensland, Australia" *Water Science and Technology* **37**(2) 301-308.

Calne, D.B., Chu, N.S., Huang, C.C., Lu, C.S., Olanow, W. (1994) "Manganism and idiopathic parkinsonism: similarities and differences" *Neurology* **44**(9) 1583–1586.

Cleasby, J.L. (1975) "Iron and manganese removal-a case study" *Journal of the American Water Works Association* **67**(3) 147.

Coffey, B.M., Gallagher, D.L., and Knocke, W.R. (1993) "Modeling soluble manganese removal by oxide-coated filter media." *J. Envir. Engrg. Div.* ASCE **119**(4) 679.

Coughlin, R.W. and Matsui, L. (1976) "Catalytic oxidation of aqueous Mn(II)" *J. Catalysis* **41** 108-123.

Dobson, A.W., Erikson, K.M., Aschner, M. (2004) "Manganese neurotoxicity" *Ann NY Acad Sci.* **1012** 115–128.

Edwards, S.E., McCall, G.B. (1946) "Manganese removal by breakpoint chlorination" *Water & Sewage Works* **93** 303.

Eley, M. and Nicholson, D. (1993) “Chemistry and adsorption-desorption properties of manganese oxides deposited in Forehill Water Treatment Plant” Grampian, Scotland.

Griffin, A.E. (1960). "Significance and removal of manganese in water supplies" *Journal of the American Water Works Association* **52** 1326.

Hargette, A.C. and Knocke, W.R. (2001) “Assessment of Fate of Manganese in Oxide-Coated Filtration Systems” *Journal of Environmental Engineering (ASCE)* **127**(10):1132-1138.

Hem J.D. (1981) “Rates of manganese oxidation in aqueous systems” *Geochim Cosmochim. Acta* **45** 1369-1374.

Hug, S., Gaertner, D., Roberts, L.C., Schimer, M., Ruettimann, T., Rosenberg, T.M., Badruzzaman, A.B.M., and Ali, M.A. (2011) “Avoiding high concentrations of arsenic, manganese and salinity in deep tubewells in Munshiganj District, Bangladesh” *Applied Geochemistry* **26**(7) 1077-1085.

Institute of Medicine Food and Nutrition Board. (2002) Dietary Reference Intakes: Vitamin A, Vitamin K, Arsenic, Boron, Chromium, Copper, Iodine, Iron, Manganese, Molybdenum, Nickel, Silicon, Vanadium and Zinc. Washington DC: National Academy Press.

ITN-BUET (2011) “Removal of manganese and arsenic from groundwater using manganese oxide coated sand”, ITN research series 11, International Training Network (ITN), BUET, Dhaka.

Kessick, M.A. and Morgan, J.J. (1975) “Mechanism of autoxidation of manganese in aqueous solution” *Environ. Sci. Technol*. **9** 157-159.

Knocke, W.R., Hoehn, R.C. and Sinsabaugh, R.L. (1987) “Using Alternative Oxidants to Remova Dissolved Manganese from Waters Laden with Organics” *Journal of the American Water Works Association* **79**(3) 75-79.

Knocke, W.R., Hamon, J.R. and Thompson, C.P. (1988) “Soluble Manganese Removal on Oxide-Coated Filter Media” *Journal of the American Water Works Association* **80**(12) 65-70.

Knocke, W.R., Occiano, S. and Hungate, R. (1990) “Removal of Soluble Manganese from Water by Oxide-Coated Filter Media” *American Water Works Association* Research Foundation.

Knocke, W.R., Occiano, S. and Hungate, R. (1991) “Removal of Soluble Manganese by Oxidecoated Filter Media: Sorption Rate and Removal Mechanism Issues” *Journal of the American Water Works Association* **83**(8) 64-69.

Kozlov, Y.N., Zharmukhamedov, S.K., Tikhonov, K.G, Dasgupta, J., Kazakova, A.A, Dismukes, G.C., and Klimov, V.V. (2004) “Oxidation potentials and electron donation to photosystem II of manganese complexes containing bicarbonate and carboxylate ligands” *Physical Chemistry Chemical Physics* **6** (20) 4905-4911

Merkle, P.B., Knocke, W.R. and Gallagher, D.L. (1997a) “Method for Coating Filter Media with Synthetic Manganese Oxide” *Journal of Environmental Engineering (ASCE)* **123**(7) 642-649.

Merkle, P.B., Knocke, W.R., Gallagher, D.L. and Little, J.C. (1997b) “Dynamic Model for Soluble Mn^{2+} Removal by Oxide-Coated Filter Media” *Journal of Environmental Engineering (ASCE)* **123**(7) 650-658.

Morgan, J.J., Stumm, W. (1964) “Colloid-chemical properties of manganese dioxide” *J. Colloid Sci*. **19** 347– 359.

Murray, J.W., Dillard, J.G., Giovanoli, R., Moers, H. and Stumm, W. (1985) “Oxidation of Mn(II): Initial mineralogy, oxidation state and aging” *Geochim. Cosmochim. Acta* **49** 463-470.

Nakanishi, H. (1967). "Kinetics of continuous removal of manganese in a MnO,-coated sand bed." *Kogyo Kagaku Zasshi*, **70**(4) 407.

Press, W.H., Teukolsky, S.A., Vetterling, W.T. and Flannery, B.P. (2002) *Numerical Recipes in C++, The Art of Scientific Computing 2nd ed., Chapter 15* Cambridge University Press, New York.

Rahman, M.A., Huang, J.Y., Iwakami, Y. and Fujita, K. (2000). “Pursuing the effect of aeration, pH increment, and H2O2 coupled with UV irradiation on the removal efficiency of manganese by microfilter membrane” *Water Science and Technology* 41(10-11):25-31.

Reckhow, D.A., Knocke, W.R., Kearney, M.J. and Parks, C.A. (1991). “Oxidation of Iron and Mangnaese by Ozone” *Ozone Science and Engineering*, **13** 675-695.

Seelig, B., Derickson, R., and Bergsrud, F. (1992) “Iron and Manganese Removal: Treatment Systems for Household Water Supplies” NDSU Extension Service, North Dakota, USA.

Sommerfeld, E.O. (1999) *Iron and Manganese Removal Handbook* Americal Water Work Association, Denver.

Subramaniam, A., (2010) "A Pilot-scale Evaluation of Soluble Manganese Removal Using Pyrolucite Media in a High-Rate Adsorptive Contactor", M.Sc. Engineering Thesis, Civil & Environmental Engineering Department, Virginia Polytechnic Institute and State University.

Suzuki, M. (1990) *Adsorption Engineering* Kodansha Ltd., Tokyo and Elsevier Science Publishers B.V., Amsterdam

Suzuki, T., Watanabe, Y., Ozawa, G. and Ikeda, S. (1998) "Removal of soluble organics and manganese by a hybrid MF hollow fiber membrane system" *Desalination,* **117** 119-130.

Tang, K., Williams, J.C., Allen, J.P., and Ka´lma´n, L. (2009) "Effect of Anions on the Binding and Oxidation of Divalent Manganese and Iron in Modified Bacterial Reaction Centers" *Biophysical Journal* **96** 3295–3304.

Tasneem, K.M. (2010) "Removal of Manganese from Groundwater based on Sorptive Filtration" M.Sc. Engineering Thesis, Department of Civil Engineering, Bangladesh University of Engineering and Technology, Dhaka, Bangladesh.

Trace Inorganic Substances Committee (1987) "Committee Report: Research Needs for the Treatment of Iron and Manganese" *Journal of the American Water Works Association,* **79**(9) 119-122.

Weber, W.J., Jr. (1972) *Physicochemical Processes for Water Quality Control*. John Wiley and Sons, Inc., New York.

WHO (2004) "Guideline for Drinking Water Quality, Health Criteria and Other Supporting Information" 3rd Edition, WHO, Geneva.

Wong, J.M. (1984) "Chlorination-Filtration for Iron and Manganese Removal" *Journal of the American Water Works Association* **76**(1) 76-79.

Worch, E. (2012) *Adsorption Technology in Water Treatment*, Walter de Gruyter GmbH & Co. KG, Berlin.

Yamada, M., Ohno, S., Okayasu, I., Okeda, R., Hatakeyama, S., Watanabe, H. (1986) "Chronic manganese poisoning: a neuropathological study with determination of manganese distribution in the brain" *Acta Neuropathol (Berl)***70**(3–4) 273–278.

Zapffe, C. (1933). "The history of manganese in water supplies and methods for its removal." *Journal of the American Water Works Association* **25**(5) 655.

Zuravnsky, L. (2006). “Development of soluble manganese sorptive contactors for enhancing potable water treatment practices” Master’s Thesis, Virginia Polytechnic Institute and State University, Department of Civil and Environmental Engineering, Blacksburg, VA.

APPENDIX A

This appendix outlines the derivation of mass balance equations (Equations 5.2-5.4, discussed in section 5.2.1) used in the model.

Development of a model to predict soluble Manganese removal via adsorption and oxidation.

Derivation of the mass balance equation for Adsorbate (Mn) (Eqn. 5.2)

To establish a differential material balance, a differential volume element, $dV = A_R dz$, of an adsorber with the cross-sectional area A_R is considered (Figure A1). It can be assumed that the amount of adsorbate that is adsorbed onto the adsorbent or accumulated in the void fraction of the volume element must equal the difference between the input and the output of the volume element. Input and output occurs by advection and axial dispersion. Accordingly, the general material balance is given by Worch (2012).

$$N_{accu} + N_{ads} = N_{disp} + N_{adv} \tag{A1}$$

Where N represents the change of the amount of adsorbate with time, and the indices indicate the processes accumulation, adsorption, dispersion, and advection.

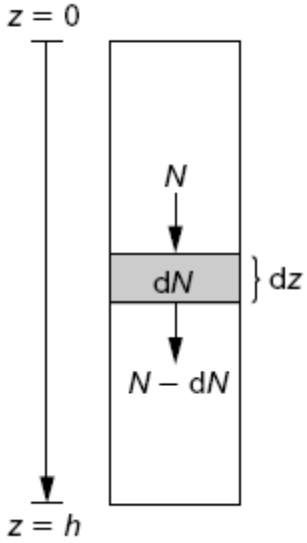

Figure A1: Material balance around a differential volume element of the fixed-bed adsorber.

The accumulation of substance within the void fraction of the volume element, dv, is given by Worch (2012).

$$N_{accu} = \varepsilon_B A_R dz\frac{\partial C_{1b}(t,z)}{\partial t} = \varepsilon_B dv\frac{\partial C_{1b}(t,z)}{\partial t} \quad (A2)$$

where:
ε_B =the bulk (bed) porosity or fractional pore volume (m^3 water/m^3 bed)
A_R=bed cross-sectional area (m^2)
C_{1b} = adsorbate concentration in the bulk solution (mol/m^3)
t=time

The adsorption onto the adsorbent in the volume element can be written as (Worch, 2012)

$$N_{ads}= \rho_b A_R\ dz\frac{\partial q(t,z)}{\partial t} = \rho_b\, dv\frac{\partial q(t,z)}{\partial t} \quad (A3)$$

Where:
ρ_b = bulk density of adsorber (adsorbent) (kg media/m^3 reactor bed)
q = mean adsorbent loading (mol/Kg)
According to Worch (2012), to describe the advection, the difference between the amount of adsorbate fed to and released by the volume element per unit of time has to be considered.

$N_{adv} = v_F A_R C_{1b}(t,z) - v_F A_R C_{1b}(t, z+dz)$

where:
v_F = The linear filter velocity or superficial velocity (m/s)

In differential form, the above Equation becomes

$$N_{adv} = - v_F A_R \frac{\partial C_{1b}(t,z)}{\partial z}dz = - v_F\, dv\frac{\partial C_{1b}(t,z)}{\partial z} \quad (A4)$$

Under the condition that the axial dispersion can be described by Fick's first law, the difference between input and output caused by dispersion is given by Worch (2012).

$$N_{disp} = D_L \varepsilon_B A_R \left[\frac{\partial C_{1b}(t,z)}{\partial z}\right]_{z+dz} - D_L \varepsilon_B A_R \left[\frac{\partial C_{1b}(t,z)}{\partial z}\right]_z$$

Where:
D_L = the axial (longitudinal) dispersion coefficient (m^2/s)

In differential form, this equation becomes

$$N_{disp} = D_L \varepsilon_B A_R \frac{\partial^2 C_{1b}(t,z)}{\partial z^2} dz = D_L \varepsilon_B\, dv\frac{\partial^2 C_{1b}(t,z)}{\partial z^2} \quad (A5)$$

Introducing Equations A2, A3, A4, and A5 into Equation A1 and dividing the resulting equation by dv gives the differential material balance equation in its general form

$$v_F \frac{\partial C_{1b}}{\partial z} + \varepsilon_B \frac{\partial C_{1b}}{\partial t} + \rho_b \frac{\partial q}{\partial t} - D_L \varepsilon_B \frac{\partial^2 C_{1b}}{\partial z^2} = 0 \qquad \text{(A6)}$$

The film diffusion (also referred to as external diffusion) comprises the transport of the adsorbate from the bulk liquid to the external surface of the adsorbent particle (Worch, 2012). As long as the state of equilibrium is not reached, the concentration at the external adsorbent surface is always lower than in the bulk liquid due to the continuing adsorption process. As a consequence, a concentration gradient results that extends over a boundary layer of thickness δ. The difference between the concentration in the bulk solution, C_{1b}, and the concentration at the external surface, C_{1s}, acts as a driving force for the mass transfer through the boundary layer. Merkle *et al.* (1997b) also assumed the soluble adsorbate (Mn) flux to be driven by a linear driving force (LDF), and sorptive equilibrium at the surface with transport through a film or boundary layer region with no internal mass transport resistance. Figure A2 shows the typical concentration profile for the limiting case where the adsorption rate is determined only by film diffusion and the diffusion within the particle is very fast ($q = q_s$, no gradient within the particle). Note that the adsorbent loading, q_s, is the equilibrium loading related to the concentration, C_{1s}, at the external surface of the adsorbent particle.

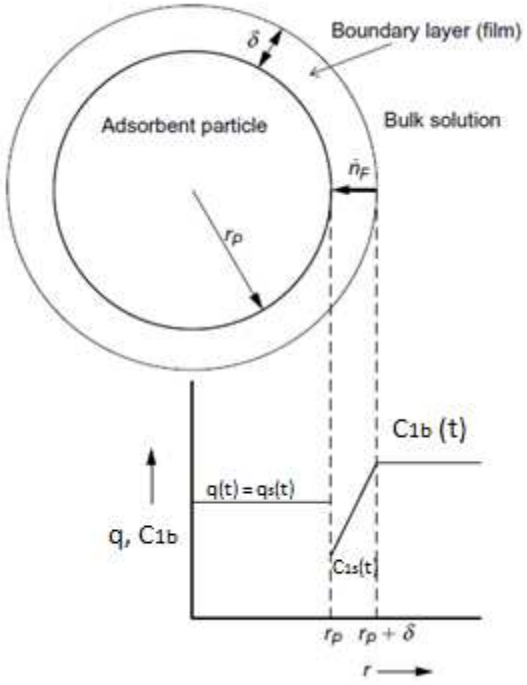

Figure A2: Concentration profiles in the case of rate-limiting film diffusion (no internal mass transfer resistance) (Worch, 2012).

Based on the principle discussed above, the following the mass transfer equation for film diffusion can be established (Merkle *et al.*, 1997b; Worch, 2012)

$$\frac{dq}{dt} = \frac{k_f A_v (1-\varepsilon_B)}{\rho_b} (C_{1b} - C_{1s}) \quad (A7)$$

where:
A_v= Specific surface of the media (adsorbent) (m^2 media/m^3 media)
k_f = liquid to solid mass transfer coefficient (m/s)
C_{1s}= Adsorbate concentration at the external adsorbent surface or liquid-solid interface (mol/m^3)

The Freundlich equilibrium isotherm needs to be applied at the media (adsorbent) surface to describe the relationship between the aqueous-phase soluble adsorbate concentration at the surface and the adsorbed adsorbate concentration on the surface as shown in Equation A8.

$$C_{1s} = (C_{1sa}/K)^n \quad (A8)$$

Where,
C_{1sa} = adsorbed-phase adsorbate concentration on the media surface (mol/kg)
K, n = Freundlich isotherm constants

Substituting the value of C_{1s} from Eqn. A8 in Eqn. A7 gives

$$\frac{dq}{dt} = \frac{k_f A_v (1-\varepsilon_B)}{\rho_b} (C_{1b} - [\frac{C_{1sa}}{K}]^n) \quad (A9)$$

Substituting the differential quotient $\frac{\partial q}{\partial t}$ in Eqn. A6 by the mass transfer equation for film diffusion (Eqn. A9) gives

$$v_F \frac{\partial C_{1b}}{\partial z} + \varepsilon_B \frac{\partial C_{1b}}{\partial t} + \rho_b \frac{k_f A_v (1-\varepsilon_B)}{\rho_b} (C_{1b} - [\frac{C_{1sa}}{K}]^n) - D_L \varepsilon_B \frac{\partial^2 c}{\partial z^2} = 0 \quad (A10)$$

After dividing the both side of the equation by ε_B, material balance equation becomes

$$\frac{\partial C_{1b}}{\partial t} = -U \frac{\partial C_{1B}}{\partial z} + D_L \frac{\partial^2 C_{1B}}{\partial z^2} - k_f A_v \frac{(1-\varepsilon_B)}{\varepsilon_B} (C_{1B} - [\frac{C_{1sa}}{K}]^n) \quad (A11)$$

Where,

U= Effective flow velocity or pore water velocity (m/s) = (v_F/ ε_B)

At steady state

$$\frac{\partial C_{1B}}{\partial t} = 0 = -U\frac{\partial C_{1B}}{\partial z} + D_L\frac{\partial^2 C_{1B}}{\partial z^2} - k_f A_v \frac{(1-\varepsilon_B)}{\varepsilon_B}(C_{1B} - [\frac{C_{1sa}}{K}]^n) \quad (A12)$$

Derivation of the mass balance equation for adsorbed adsorbate (Mn) (Eqn. 5.4)

For a differential volume element, $dv=A_R d_z$ (Figure A1), with continuous oxidation of adsorbed adsorbate by oxidant (i.e., regeneration of adsorbent), it can be assumed that the amount of adsorbate that is adsorbed onto the adsorbent must equal to the amount of adsorbed adsorbate oxidized and not oxidized (that deposits in the surface of adsorbent)

$$N_{ads} = N_{oxid} + N_{dep} \quad (A13)$$

Where N represents the change of the amount of adsorbate with time, and the indices indicate the processes adsorption, oxidation and deposition.

According to Eqn. A9 the adsorption onto the adsorbent in the volume element dv can be written as

$$N_{ads} = \rho_b\, dv \frac{\partial q(t,z)}{\partial t} = \rho_b\, dv\ \frac{k_f A_v (1-\varepsilon_B)}{\rho_b}(C_{1b} - [\frac{C_{1sa}}{K}]^n) \quad (A14)$$

The change in the amount of adsorbed adsorbate oxidized by the oxidant can be written as

$$N_{oxid} = \rho_b\, dv\, \varepsilon_B\, (k_r\, C_{1sa}\, C_{2b}) \quad (A15)$$

Where,

k_r = Oxidation rate constant (m^3bed/mol * s)

C_{2b} = bulk aqueous-phase oxidant concentration (mol/m^3)

The change in the amount of the adsorbed adsorbate not oxidized by the oxidant and therefore, deposition on the adsorbent surface can be written as

$$N_{dep} = \rho_b\, dv \frac{\partial C_{1sa}}{\partial t} \quad (A16)$$

Introducing Equations A14, A15, A16 into Equation A13 and dividing the resulting equation by $\rho_b dV$ gives the differential mass balance equation as

$$\frac{k_f A_v (1-\varepsilon_B)}{\rho_b}(C_{1b} - [\frac{C_{1sa}}{K}]^n) - k_r\, \varepsilon_B\, C_{1sa} C_{2b} = \frac{\partial C_{1sa}}{\partial t} \quad (A17)$$

Assuming steady state condition with complete oxidation of adsorbed adsorbate and also considering no addition species are present that might interfere with adsorption and oxidation (i.e., no increase in media diameter or adsorption capacity due to deposited adsorbate).

$$\frac{\partial C_{1sa}}{\partial t} = 0 \quad \text{(A18)}$$

Introducing Eqn. A18 in Eqn. A17 gives

$$\frac{k_f A_v (1-\varepsilon_B)}{\rho_b} (C_{1b} - [\frac{C_{1sa}}{K}]^n) - k_r \varepsilon_B C_{1sa} C_{2b} = 0 \quad \text{(A19)}$$

Derivation of the mass balance equation for oxidant (Eqn. 5.3)

For a differential volume element, $dV = A_R dz$ (Fig. A1) it can be assumed that the amount of oxidant that take part in oxidation or accumulate in the void fraction of the volume element must equal the difference between the input and the output of the volume element. Input and output occurs by advection and axial dispersion. Accordingly, the general material balance is given by Worch (2012).

$$M_{accu} + M_{oxid} = M_{disp} + M_{adv} \quad \text{(A20)}$$

Where M represents the change of the amount of oxidant with time, and the indices indicate the processes accumulation, oxidation, dispersion, and advection.

The change in the amount of oxidant that takes part in oxidation can be written as

$$M_{oxid} = \rho_b \, dv \, \varepsilon_B \, (k_r \, C_{1sa} \, C_{2b}) \quad \text{(A21)}$$

Where,

k_r = Oxidation rate constant (m^3bed/mol * s)

C_{2b} = bulk aqueous-phase oxidant concentration (mol/m^3)

Based on the similar concept described in previous section, the following relationships can be established

$$M_{accu} = \varepsilon_B A_R \, dz \frac{\partial C_{2b}(t,z)}{\partial t} = \varepsilon_B \, dv \frac{\partial C_{2b}(t,z)}{\partial t} \quad \text{(A22)}$$

$$M_{adv} = - v_F A_R \frac{\partial C_{2b}(t,z)}{\partial z} dz = - v_F \, dv \frac{\partial C_{2b}(t,z)}{\partial z} \quad \text{(A23)}$$

$$M_{disp} = D_L \varepsilon_B A_R \frac{\partial^2 C_{2b}(t,z)}{\partial z^2} dz = D_L \varepsilon_B \, dv \frac{\partial^2 C_{2b}(t,z)}{\partial z^2} \quad \text{(A24)}$$

Introducing Eqns. A21, A22, A23, and A24 into Eqn. A20 and dividing the resulting equation by dv*ε_B gives

$$\rho_b\, k_r\, C_{1sa}\, C_{2b} + \frac{\partial C_{2b}}{\partial t} = -U\,\frac{\partial C_{2b}}{\partial z} + D_L\,\frac{\partial^2 C_{2b}}{\partial z^2} \qquad \text{(A25)}$$

Where,

U= Effective flow velocity or pore water velocity (m/s) = (v_F/ε_B)

At steady state

$$\frac{\partial C_{2b}}{\partial t} = 0 = -U\,\frac{\partial C_{2B}}{\partial z} + D_L\,\frac{\partial^2 C_{2B}}{\partial z^2} - \rho_b\, k_r\, C_{1sa}\, C_{2b} \qquad \text{(A26)}$$

APPENDIX B

Table B1: Batch experiment data for determination of Mn uptake capacity of green sand at pH=7.2±0.1 and temperature of 28°C (Data shows the results of 52 hours of treatment time)

Initial Mn concentration (mg/l)	Green sand (gm)	Sample volume (ml)	Final Mn conc. (mg/l)	Final Mn conc., c(mol/m^3)	mg Mn adsorbed/gm green sand	mol Mn adsorbed/kg green sand, q	C_f/q, kg /m3
3.39	1.0	50	0.06	0.00110091	0.1665	0.00305504	0.36036
3.39	0.7	50	0.2	0.00366972	0.2279	0.00418165	0.877578
3.29	0.4	50	0.52	0.00954128	0.34625	0.00635321	1.501805
12.91	1.0	50	1.24	0.02275229	0.5835	0.01070642	2.125107
5.52	0.4	50	1.25	0.02293578	0.53375	0.00979357	2.34192
12.03	1.0	50	1.4	0.02568807	0.5315	0.00975229	2.634055
12.91	0.5	50	3.6	0.06605504	0.925	0.01697247	3.891892

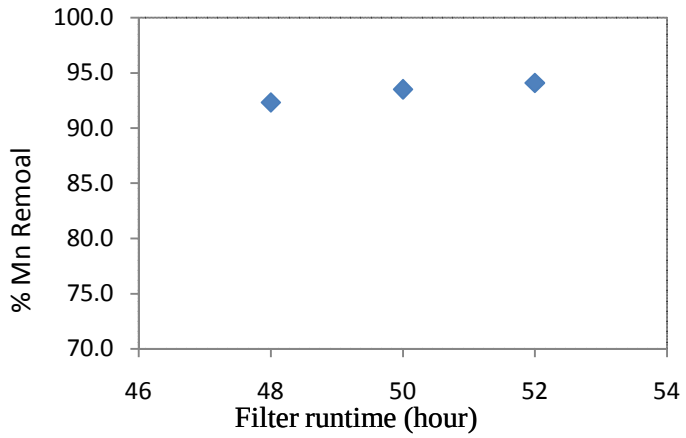

Fig B1: %Mn removal as a function of filter runtime for the batch experiment to determine Mn uptake capacity of green sand [Initial Mn concentration= 3.39 mg/l and green sand= 0.7gm)

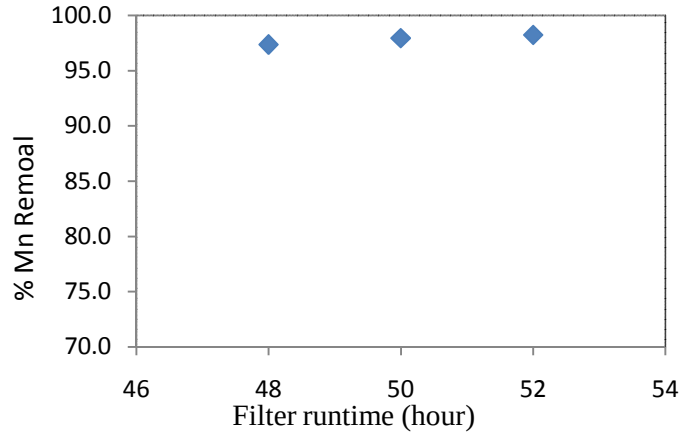

Fig B2: %Mn removal as a function of filter runtime for the batch experiment to determine Mn uptake capacity of green sand [Initial Mn concentration= 3.39 mg/l and green sand= 1 gm)

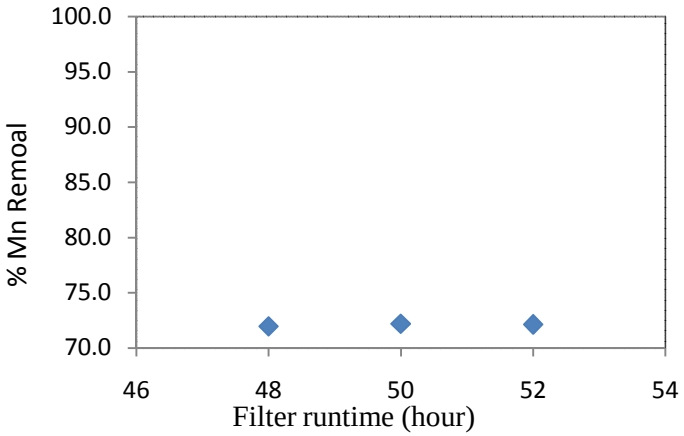

Fig B3: %Mn removal as a function of filter runtime for the batch experiment to determine Mn uptake capacity of green sand [Initial Mn concentration= 12.91 mg/l and green sand= 0.5 gm)

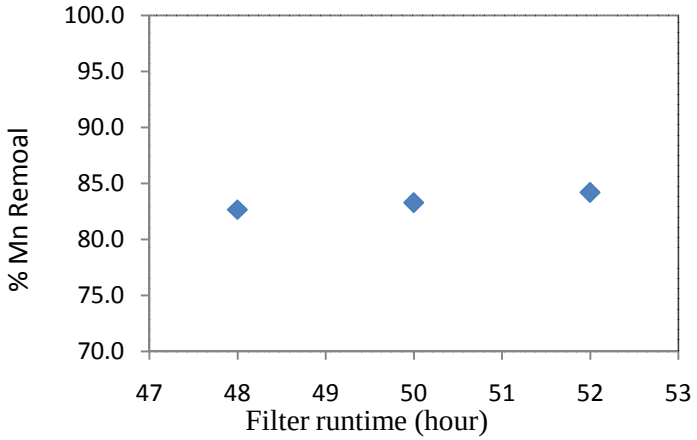

Fig B4: %Mn removal as a function of filter runtime for the batch experiment to determine Mn uptake capacity of green sand [Initial Mn concentration= 3.29 mg/l and green sand= 0.4 gm)

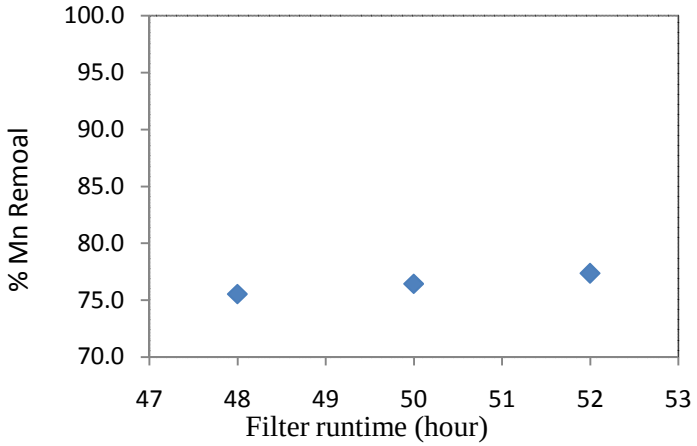

Fig B5: %Mn removal as a function of filter runtime for the batch experiment to determine Mn uptake capacity of green sand [Initial Mn concentration= 5.52 mg/l and green sand= 0.4 gm)

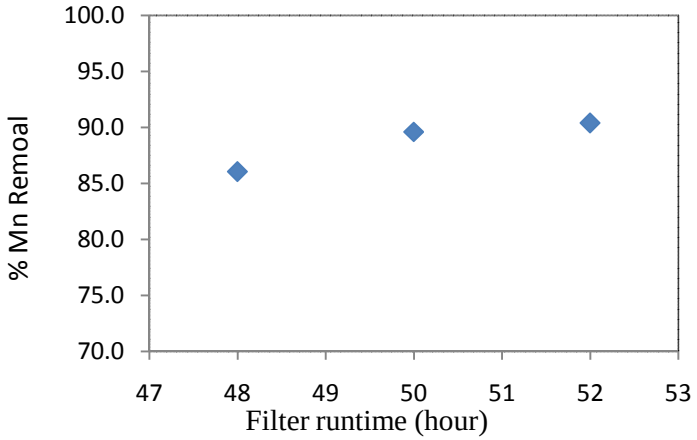

Fig B6: %Mn removal as a function of filter runtime for the batch experiment to determine Mn uptake capacity of green sand [Initial Mn concentration= 12.91 mg/l and green sand= 1 gm)

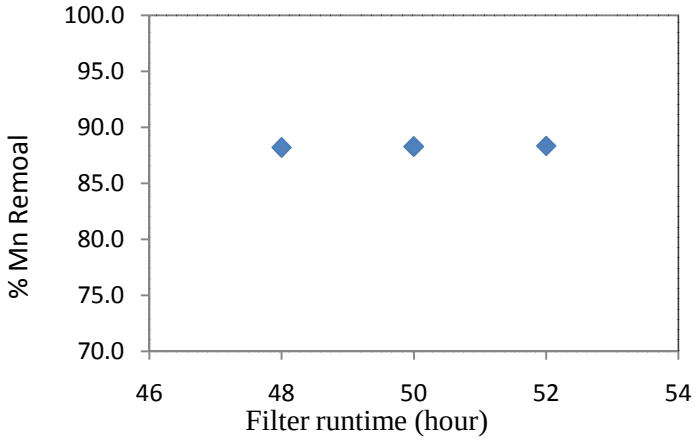

Fig B7: %Mn removal as a function of filter runtime for the batch experiment to determine Mn uptake capacity of green sand [Initial Mn concentration= 12.03 mg/l and green sand= 1 gm)

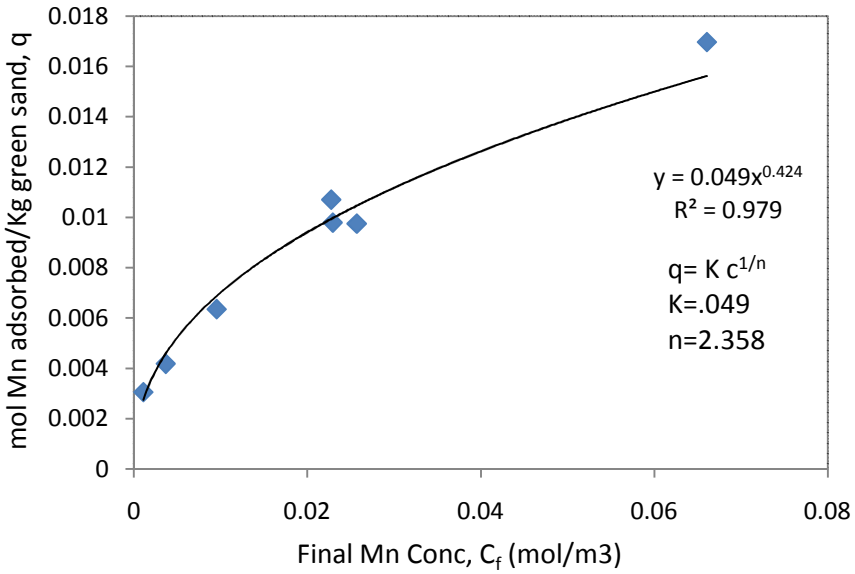

Figure B8: Mn adsorption capacity per weight of green sand at pH=7.2±0.1 over a range of soluble Mn concentrations to determine Freundlich isotherm constants.

Figure B9: Collecting effluent sample from glass burette during laboratory column experiment to calculate Mn concentration

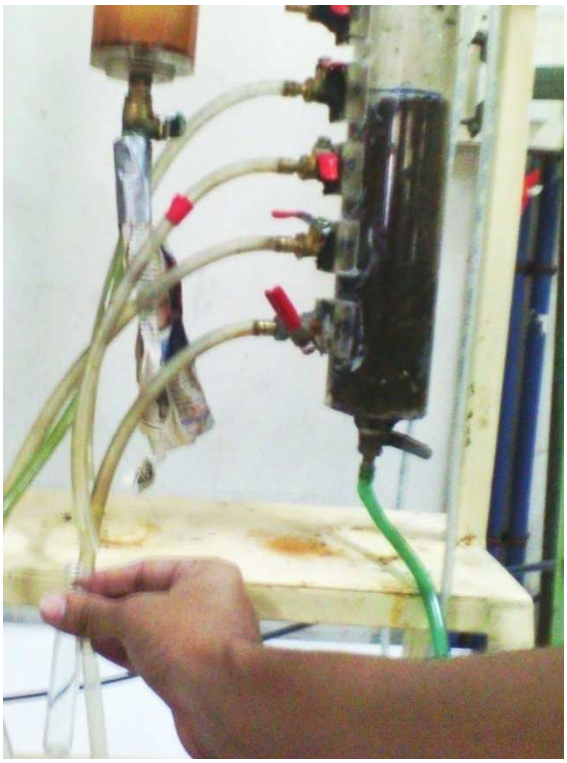

Figure B10: Collecting effluent sample during laboratory multi-port column experiment to calculate Mn concentration.